ALMA MATER STUDIORUM – UNIVERSITÀ DI BOLOGNA

DOTTORATO DI RICERCA IN
INGEGNERIA ELETTRONICA, TELECOMUNICAZIONI E TECNOLOGIE DELL'INFORMAZIONE

CICLO 33
SETTORE CONCORSUALE 09/F2
SETTORE SCIENTIFICO DISCIPLINARE ING-INF/03

THE ROLE OF B5G UAV-AIDED MOBILE NETWORKS

Presentata da
SILVIA MIGNARDI

Coordinatore Dottorato
Prof. ALESSANDRA COSTANZO

Supervisore
Prof. ROBERTO VERDONE

Co-supervisore
Prof. CHIARA BURATTI

ESAME FINALE ANNO 2021

Contents

List of Figures

List of Tables

Acronyms

3GPP 3rd Generation Partnership Project

5G 5th Generation of mobile radio communications

AtG Air-to-Ground

B5G Beyond 5G

BS Base Station

CAPEX capital expenditure

C-V2X Cellular-Vehicle-to-Anything

CAV Connected and Autonomous Vehicle

cdf cumulative distribution function

CQI Channel Quality Indicator

eMBB enhanced Mobile Broadband

FDMA Frequency Division Multiple Access

FSPL Free Space Path Loss

GtA Ground-to-Air

ILP Integer Linear Programming

IoT Internet of Things

KPI Key Performance Indicator

LoS Line of Sight

LTE Long Term Evolution

MBS Macro BS

MCS Modulation and Coding Scheme

MNO Mobile Network Operator

MTC Machine Type Communication

mMTC massive MTC

NB-IoT NarrowBand-IoT

NLoS Non-LoS

NR New Radio

OFDMA Orthogonal Frequency-Division Multiple Access

OP Orienteering Problem

OPEX Operational Expenditure

PL Path Loss

pdf probability density function

PCP Poisson Cluster Process

PPP Poisson Point Process

QoS Quality of Service

RaL Ray Launching

RB Resource Block

REM Radio Environmental Map

RH Rolling Horizon

RRM Radio Resource Management

RSU Road Side Unit

RU Resource Unit

SC Small Cell

SC-FDMA Single Carrier FDMA

SIC Successive Interference Cancellation

SIR Signal-to-Interference Ratio

SNR Signal-to-Noise Ratio

ST Sum Throughput

TBS Terrestrial BS

TCP Thomas Cluster Process

UE User Equipment

UAB Unmanned Aerial BS

UANC UAV Network Controller

UAV Unmmaned Aerial Vehicle

URLLC Ultra-Reliable and Low-Latency Communications

UU Unsatisfied User

Abstract

With the advent of 5G, several novel network paradigms and technologies have been proposed to fulfil the key requirements imposed. Flexibility, efficiency and scalability, along with sustainability and convenience for expenditure have to be addressed in targeting these brand new needs. Among novel paradigms introduced in the scientific literature in recent years, a constant and increasing interest lies in the use of unmanned aerial vehicles (UAVs) as network nodes supporting the legacy terrestrial network for service provision. Their inherent features of moving nodes make them able to be deployed on-demand in real-time. Which, in practical terms, means having them acting as a base station (BS) when and where there is the highest need.

This thesis investigates then the potential role of UAV-aided mobile radio networks, in order to validate the concept of adding an aerial network component and assess the system performance, from early to later stages of its deployment. This study is intended for 5G and beyond systems, to allow time for the technology to mature.

Since advantages can be manyfold, the aerial network component is considered at the network layer under several aspects, from connectivity to radio resource management. A particular emphasis is given to trajectory design, because of the efficiency and flexibility it potentially adds to the infrastructure. Two different frameworks have been proposed, to take into account both a re-adaptable heuristic and an optimal solution. Moreover, diverse use cases are taken under analysis, from mobile broadband to machine and vehicular communications.

The thesis aim is thus to discuss the potential and advantages of UAV-aided systems from a broad perspective. Results demonstrate that the technology has good prospects for diverse scenarios with a few arrangements.

Chapter 1

Introduction

In the recent years, the 5th Generation of mobile radio communications (5G) has seen its initial installation and deployment. The 5G systems have to face a number of challenges, including the ability to respond to high capacity service request with increased flexibility. Even from previous years, there was a general consensus that after 5G deployment, several important issues would remain partly unsolved; among them, the ability of the network to adapt efficiently to traffic demand evolutions in space and time.

5G networks will be characterized by a massive density of nodes, both human-held and machine-type [B1]. As of 5G main families of usage scenarios, services may be of either enhanced Mobile Broadband (eMBB), massive MTC (mMTC), Ultra-Reliable and Low-Latency Communications (URLLC) types [B2]. A larger density and diversity of wireless nodes implies a larger standard deviation in the traffic generation process. Therefore, network planning done based on average, or even peak, traffic predictions as done for previous systems, could bring to results being largely suboptimal. Moreover, the verticals of major interest identified for 5G networks (automotive, health, fabric-of-the-future, media, energy), come with very different requirements and use cases. These networks will handle very heterogeneous traffic scenarios, and the ability of the system to adapt in a scalable manner to service demand evolutions in both space and time is a relevant topic. These requirements, from 5G to Beyond 5G (B5G), force mobile network operators to adopt novel and efficient solutions to shape the network infrastructure.

For the reasons described, 5G and B5G radio networks are expected to be characterised by a degree of network flexibility much higher than in the past: infrastructure nodes must be flexible enough in order to be able to smoothly and autonomously react to the fast temporal/spatial variations of traffic demand. However, there is one main issue in addressing this: hardware location is static and the

offered network capacity on a local scale is fundamentally limited by the density of infrastructure equipment (macro-site and small-cells Base Stations (BSs)) in the area of interest. The solution might be in the sky with flying mobile infrastructure nodes.

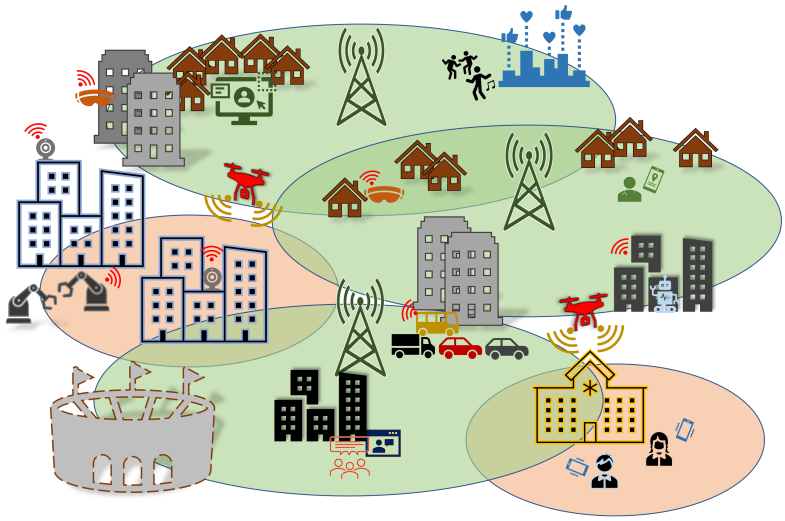

Figure 1.1: UAV-aided future networks illustrative example.

To this purpose, this thesis addresses the topic of Unmmaned Aerial Vehicle (UAV) aided networking. In this vision, new mobile network nodes, namely Unmanned Aerial BSs (UABs), can hover in the sky and provide service to ground terminals on the same area where Terrestrial BSs (TBSs) are deployed. As a matter of fact, UAVs are generally lightweight and small flying objects. Their aerodynamics may be different, classifying them into fixed-wings or rotary-wing aircraft. Contrary to fixed-wing UAVs, rotary-wing drones consist of a number of rotor blades that revolve around a fixed mast, making the aircraft able to hover and a forward movement is not needed to produce lift. Furthermore, they allow higher payload and better maneuvering compared to their counterpart; thanks to these features, in this thesis rotary-wing UAVs are considered [B3]. To carry the payload envisioned hereby, they typically weigh less than 25 kg, and mission flight time is usually no more than 30 minutes (even if higher endurance drones already exist, and their common use is expected to increase in the coming years). The payload refers to all those components not strictly necessary for the UAV to fly, but is carried to accomplish a specific mission. In the case of a UAB, the payload is the BS equipment needed for it to forward/provide the service. A UAB has then to be intended as a UAV carrying radio frequency equipment to act as BS. They might actually be fully functional BSs, or simple relays extending the terrestrial network coverage. Then, if properly equipped with a light-weight and efficient BS antenna

system, UABs are asked to increase coverage and capacity where the TBSs can not adequately serve the underlying users. The scenario suggested in the thesis is the one envisioned for recent and future networks (i.e. 5G and beyond), where an heterogeneous system gathers a few kind of network components to increase coverage, spectrum efficiency and Quality of Service (QoS). The different components, being either aerial platforms, macro or small/micro cells, are referred to as *network tiers*. Figure 1.1 pictures an example scenario of the kind, where UABs provide service *where* and *when* needed. The UABs have then to be able to fly along trajectories devised in agreement with the terrestrial network. It is assumed that UABs keep a direct Line of Sight (LoS) link (i.e. in free-space path loss condition) with the closest TBS to forward the traffic to the Core Network. This is feasible, since almost no obstacle is found on air. Backhaul links could exploit millimeter waves or Visible Light Communication, which are assumed to maintain a separate carrier frequency with respect to UAB-user or TBS-user links to avoid interference issues. The focus of this thesis is mainly on the service provided to ground users (or User Equipment (UE)), being either human-held, Internet of Things (IoT) devices or vehicles.

The main scope of this thesis is then to evaluate the network performance of a UAV-aided networking under different aspects. The relevance of the achieved result will raise the discussion on the role of B5G UAV-aided networks. Network Key Performance Indicators (KPIs) are computed at network level to have a high level view of the several and different elements building the system. The aspects considered are:

- a feasible network architecture that binds all system components together to properly cooperate;
- an appropriate channel modelling, that accounts for the different features playing a role when service is provided from a platform moving in the sky;
- the design of a dynamic trajectory to enhance both coverage and system capacity, from a heuristic to an optimized approach;
- conformance with the standardization protocols and procedures;
- application to different possible scenarios, with both broadband and IoT services.

The network performance is simulated with dynamic network simulators built on purpose. Among different research activities some system parameters may change (e.g. carrier frequency, bandwidth availability constraints, and similar), due to the

progress of the standardization from Long Term Evolution (LTE) to 5G made by the 3rd Generation Partnership Project (3GPP) standardization body.

The thesis is organized as follows. Chapter 2 introduces the current state of literature in UAV-aided networking and related issues. In Chapter 3, the system architecture proposed in the thesis and referenced throughout the activities is described. The particular channel modeling to be accounted for UABs is studied in Chapter 4, and Chapter 5 discusses different frameworks and possible solutions related to the additional aerial component of the network. Then, emphasis is given to 3GPP procedures, protocols and use cases in Chapter 6, where the network model is proposed in different perspectives for different scenarios. Finally, Chapter 7 summarizes the main thesis findings and achievements.

Chapter 2

State of the Art

When dealing with a flying BS node added to an already complex network structure, a number of elements have to be taken into account. For this reason, research activities in the field of aerial communications have investigated and discussed aspects related to link and network level views, positioning and trajectories, energy consumption and capacity improvement, to name a few. Such a quite recent topic is still rising new intriguing challenges, making the research field still highly active and continuously proposing novel solutions.

2.1 Channel Modelling and System Integration

The first element that makes a UAB different from a legacy BS is its altitude from the ground. In principle, this leads to less obstacles encountered when trying to establish a link, and a different propagation model with respect to the commonly known channel for terrestrial nodes to be investigated when planning network design. In fact, most of the research field targeting UAVs at the early stages addressed the coverage problem looking at how Path Loss (PL) for the so-called Air-to-Ground (AtG) channel can be modelled [B4, B5, B6]. Thanks to these analyses, the elevation angle of the UAV established with a single target and, consequently, the drone height above the ground, were shown to have a non negligible impact on mean PL and shadowing formulation. In [B5, B6] the AtG channel is subject to LoS or Non-LoS (NLoS) conditions under a certain probability based on the environment and the elevation angle from ground.

In some cases, it is however preferred to have a precise and highly accurate channel modelling for a given urban environment. In this way, PL samples are known *a priori* as a sort of *radio map* with a given precision to drive UAVs [B7, B8]. Radio maps may then be exploited as environment information to tune network

parameters and performance as desired.

Once the problem is addressed at the link level, network issues start to be considered with increasing details on the different aspects. For example, activities in this direction discussed the trade-off in UAV networks between connectivity issues and area coverage [B9], or start to study the integration of drones in the next generation networks [B10]. Moreover, UAVs are considered jointly with a cellular network in [B11], where a delay-optimal cell association for ground users is proposed through optimal transport theory. In [B12] UAVs mount a Pico Cell radio equipment and their efficiency in placement is compared to the static infrastructure counterpart. Other examples of integrating drones as supplement in present cellular infrastructure can be found in [B13], where Authors considered the maximization of the downlink coverage of drone small cells (DSCs) by computing the optimal height and minimizing the used transmit power. The impact of interference on deployment of multiple DCSs was discussed along with the desired distance between the DCSs that can improve coverage performance. In [B14], UAVs were used as relays. The model uses density and cost functions to calculate areas with higher demands and multiple UAVs are deployed depending on these functions.

Studies about the integration of terrestrial infrastructure and aerial platforms assume a wider perspective in [B15], where aspects such as radio access, backhaul links and coverage of multiple drone-cells are introduced. However, they mainly focus on uplink machine type communication and do not consider a joint system resource management that includes trajectory design. Furthermore, the Authors in [B16] consider to offload traffic from the terrestrial network through a proactive deployment of drone-cells; it depends on three types of traffic and there is no interference between the ground network and the UABs.

2.2 Applications and Use Cases

Some specific applications have been identified in the early stages of UAV-communications research, being public safety and delay-tolerant services [B17, B18, B19]. In [B17] public safety problems are addressed by using Monte Carlo simulations to evaluate capacity and throughput coverage. Then, [B18] investigates if drone mounted femtocell base stations can be a solution to provide coverage in a disaster scenario, when the existing infrastructure is no longer available.

The IoT world includes many interesting possible applications for moving aerial nodes. Because of the time spent in flying, delay-tolerant applications are one of the first kind to be investigated [B19]: clearly, UABs are the *mules* that carry data from one node to another (e.g. the gateway). Another important issue, especially

for machine-type communications, is the energy consumption. Industry 4.0 and low power nodes apply a number of technques to stay on idle or sleep mode when possible to keep a lifetime in the order of years. Dynamic trajectories in 3D space are studied in [B20] with the purpose to connect IoT devices at their activation time. They jointly optimize the transmission power of machine nodes, the overall energy spent in movement and the choice of the next stop of each UAV.

2.3 Deployment of UAVs

At early stages in UAV-networks research activities, few papers address the optimal design of UAV paths. The reason lies in the complexity of the topic; in fact, the dynamic trajectory of UAVs should be defined according to a number of factors, including the position of candidate UEs on the ground, their traffic requirements, the energy available on the UAV, and so on. On the opposite, the optimal static placement of a UAV can be more easily computed, once the terminals positions are known, accounting for the link quality of all links established. For this reason, the following works study the static deployment of UAVs.

In [B21], the optimal 3D placement of multiple UAVs was addressed to optimize the downlink coverage measurements in terms of antenna gain and altitude. The circle pack-theory was used to handle the interference of the overlapping coverage areas of the UAVs, while minimizing the transmit power. However, this is done without considering an underlay operating cellular network. The work [B22] considers multiple UAVs having the aim to maintain an overall network connectivity in a 3D scenario with several ground nodes. The optimal position of drones acting as relays is found through the particle swarm optimization, following three different analyzed metrics; through this method, UAVs may change their paths dynamically maximizing system performance while minimizing communication links and costs. Furthermore, clusterization algorithms for UABs placement and trajectories are introduced.

Other more focused activities with UAV maintaining a fixed position can be found in [B23, B12]; the former has the purpose to achieve the minimum energy consumption with exactly one UAV per cluster in an uplink IoT scenario, and the latter focuses on finding a single point with 2D coordinates (height fixed) for the UAV-mounted access point to serve the highest possible number of users.

2.4 Resource Management and Interference in UAV networks

Interference issues are analyzed and modelled in [B24]. The interferers are other UABs, each transmitting towards a ground node. However, the presence of the mobile network is not considered.

As for RRM, [B25] investigates optimal resource allocation mechanisms in an IoT environment for cluster heads and UAV links with the goal of minimizing the transmission power while meeting the rate requirements of IoT devices. Moreover, [B26] studies user scheduling in the terrestrial network for non-orthogonal transmission in UAV relay networks. Potential interference is analyzed for both backhaul and UAV-UE link with the terrestrial network, and an interference avoidance solution is proposed. In [B27] issues of scheduling for UAV networks are addressed, with the aim of achieving the maximum system performance in terms of encounter rate and energy efficiency; in particular drones behave as small cells and optimal beaconing periodicity is sought following a game theory model in order to have cooperation among UAVs. [B28] minimises the number of flying base stations needed to provide coverage to a group of UEs.

Generally, the joint operation of the aerial and terrestrial network has not been properly investigated. Indeed, a joint management of the available resources would improve the spectrum reuse, the solution flexibility and the model efficiency, resulting in one effective tradeoff between costs and service quality.

2.5 UAV Trajectories with Energy or User Rate Optimization

More recently, mathematical modelling and optimization techniques have been pursued to improve the measurable metrics present in UAV-communications. Usually, because of the tools applicability, the joint operation of UAVs with the terrestrial network is not considered. For example, the optimal placement in UABs network is studied pursuing the energy efficiency [B29, B30] by minimizing the energy consumption. Also, a trajectory can be identified by maximizing the minimum user rate, to achieve user fairness [B31, B32]. Clearly, being these highly complex models requiring computation times in the order of hours or days (sometimes even with powerful machines), optimization problems generally include a number of strong assumptions. In fact, though achieving a final optimal or suboptimal solution, small input instances (e.g. less than 10 users active in the service area), highly

discretized environments or rather unrealistic scenarios (e.g. always LoS conditions or no consideration of delay) are used to extract performance. Furthermore, the traffic demand is usually assumed to be known a priori. Despite the problem difficulties, the quality of literature advancements is always increasing.

All the papers described above have been published approximately in the same timeframe of the activities carried out in this thesis. The interest and relevance in literature related to UAV-networks and UAV support in heterogeneous networks increased drastically in the last few years, and the works complexity and completeness improved as well. In this thesis, a detailed description from simpler heuristics to advanced optimization techniques and integration with 5G systems is present.

Chapter 3

Network Architecture

A system that wishes to integrate an aerial and a terrestrial network tier needs to be built on top of a robust architecture and well-defined structure. The two tiers must be allowed to efficiently operate together to sustain the network costs on capital expenditure (CAPEX) and Operational Expenditure (OPEX). In simple words, this means that each network node (being either a BS or an UAB) has to allocate resources and provide service without adding severe interference that may degrade network performance. The foreseen increased service demand coming with 5G allows an initial investment for CAPEX in flexible and scalable new network nodes (i.e. UABs), and their efficient management covers the periodical costs on OPEX. The meaning of network *efficiency*, being it related to spectrum and resource management or flight times and trajectory design and other system parameters, will be discussed thoroughly across the thesis.

Since the main focus of the thesis is the definition of the UABs trajectories given the network status and conditions of the links UAB-UE and TBS-UE, some initial assumptions are made. First, channel state information is assumed to be available at both UAB and TBS side. Second, a backhaul/fronthaul link exists between a single UAB to a nearby TBS, in order to connect it to the rest of the network. In fact, it must receive a minimum requirement of 60-100 kbps [B33] in the command and control link for navigation purposes, but the link capacity needs to be much larger if it wants to accommodate also network services. However, since UABs fly in the sky which is naturally free of obstacles, the backhaul connection can be assumed to be provided through high capacity LoS wireless links (e.g., by using millimetre-wave or visible light communication). This assumption is commonly implicit in the literature, but it will become increasingly practical with B5G systems. In this way, it will not represent a bottleneck for UABs service provision and can be considered beyond the scope of this thesis.

An efficient system has a proper design on where intelligence and management lies. As such, the placement of a control mechanism, where decisions on operating procedures are taken, has to be defined. Usually, two solutions may become viable, being:

- *Centralized control*, where a central entity with a broad system knowledge is in charge of selecting the optimal network behaviour;
- *Distributed control*, where the responsibility of making decisions is dislocated on the single network nodes having limited information on its surroundings and other network nodes.

A distributed control does not make an efficient solution because it does not guarantee sufficient awareness of other network nodes needs as poor link conditions, temporal traffic overload or lack of good QoS provision. On the contrary, a centralized structure allows an increased awareness of the network status since decisions are taken by a central entity, having general knowledge on the different network components. In fact, it is able to collect control plane information about link conditions of different users on different tiers, and it might instruct a more flexible node as the UAB to supply service in a specific position in real-time. This becomes feasible in 5G systems where network functions are governed by an *orchestrator* node. Figure 3.1 shows the hierarchical centralized structure envisioned for this thesis' activities.

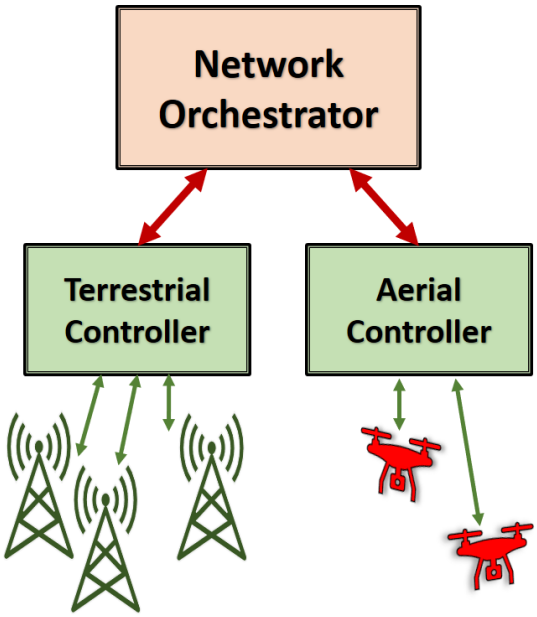

Figure 3.1: Reference network architecture with terrestrial and network tiers.

5G network architectures will then rely on approaches based on SDN (Software Defined Networking) and virtualization of networking functions (also known as NFV). The orchestrator will be responsible, among others, of the global management of network resources; SDN controllers will locally manage resources made available by the physical network. One can generally assume that a general, standardized management and orchestration framework (e.g., the MANO framework proposed by ETSI [B34]) will include an interface towards a UAV Network Controller (UANC) that will be responsible for both managing the radio resources assigned by UABs, and defining their missions and trajectories. Through this interface, the UANC will be aware of all information related to the ground user traffic demand, and how the TBSs are serving it. In particular, a common assumption made in scientific literature is that the UABs are aware of the positions of the ground users they have to serve. Similarly, in this thesis, the UANC is assumed to have real-time information on the performance indicators and the resources exploited in all links between TBSs and UEs. Figure 3.1 shows specifically the interface with the aerial controller (or UANC), being the thesis main topic. The MANO will be later referred to as simply *orchestrator* or even *network controller*, to emphasize the centralized infrastructure.

Given the envisioned scheme able to govern UABs operation, its efficiency relies on the use of feedback signals from the UANC to the network functions controlling the TBSs. Three main cases may occur:

1. UABs and TBSs are deployed in orthogonal spectrum bands, and feedback signals to the orchestrator have little impact;

2. UABs and TBSs are deployed in the same spectrum band, but the TBSs controller is working independently and the MANO gives instructions only to the UANC;

3. UABs and TBSs are deployed in the same spectrum band, the MANO receives feedback signalling from both TBSs controllers and the UANC, and instructs both on the best way to operate together.

The first case is quite trivial and definitely not cost-efficient, and therefore will be subject to only an introductory work (see Sect. 5.1.1). In the second and third cases, the two network tiers are sharing network resources (later referred to as Resource Blocks (RBs)), making their operation more cost-efficient when properly planned. Here, the central architecture plays a (possibly) critical role by taking decisions on how to manage resources. In fact, the presence and use of feedback signals from TBSs to UABs sharing control information (i.e. where the MANO

communicates with the UANC and TBSs controller) determines the system higher or lower efficiency. Improved efficiency and adaptability can be found when a joint operation between aerial and terrestrial tiers are set in place. A thorough discussion follows in Sec. 5.1.4. For completeness, the architecture of Fig. 3.1 has thus been proposed for all the activities presented in this thesis from the simplest to the most efficient use case of the three presented above.

Chapter 4

The Air to Ground Channel

One of the main advantages of a UAB is its ability to provide a connection from the sky. As generally known, channel impairments due to ground obstacles such as trees and buildings give a power loss that is quite higher with respect to LoS links. On the contrary, LoS visibility is much more likely in the sky, allowing higher probability to achieve a Free Space Path Loss (FSPL) link computed through the Friis formula with propagation exponent equal to 2. The exact formulation is given in the following.

However, when a link has to be established between a UAB and a user on the ground (that is the UE as per 3GPP terminology, having a height of 1.5 m) obstacles on the ground may still impair the link quality, and the propagation cannot be easily computed as in LoS links. This is especially true in urban scenarios, where broadband service is provided to a higher number of users (for e.g. events, meetings, work, and so on). Still, the increased height from the ground with respect to traditional TBSs, allows a UAB to keep a lower transmit power and channel conditions decrease less rapidly with distance. To emphasize these differences, this particular channel is denoted as AtG channel. For the remainder of the thesis, the propagation model detailed in the following and fairly known in the literature for experts in the field is employed.

Nonetheless, it is not guaranteed that this model perfectly applies in all scenarios for the very diverse metropolitan areas of the world. When it comes to accurate prediction of a link loss given the exact coordinates of an urban area, Ray Launching (RaL) is an interesting solution. RaL is a technique that, extending ray tracing, is able to evaluate link losses from a single transmitter to multiple receivers located all over a given area. Thus, in this thesis, a channel model comparison made via a network simulator is considered. In fact, since the scope of the thesis remains on network-level evaluation, the comparison is made on the impact that a statistical

model or a coverage map makes on the network performance.

To have a complete view on the channel modelling used throughout the thesis, here it is given the channel loss happening between a TBS and a UE. Usual impairments of urban environments have fluctuations like fading and shadowing, superimposed to a power loss that is much larger than what would be found in free space; typically, power loss depends on distance through an exponent β_{env} between 3 and 4. For the sake of simplicity, only a shadowing component is considered. Then, the propagation or channel loss of the link TBS b to UE u can be computed as

$$L_{b,u}(t) = 20 \log \left(\frac{4\pi f_c}{c} \right) + 10\beta_{\text{env}} \log(d_{u,b}(t)) + \Sigma_{\text{env}}(t), \tag{4.1}$$

where f_c is the carrier frequency, c the speed of light, β_{env} the propagation exponent and $d_{u,b}(t)$ the distance between UE u and TBS b. However, users may be pedestrians or vehicles and move, which makes the distance $d_{u,b}(t)$ change along the time axis (where time steps are denoted by t). Also, $\Sigma_{\text{env}}(t)$ is the shadowing component that fluctuates over time t, and it is normally distributed as $\Sigma_{\text{env}} \sim \mathcal{N}(0, \sigma_{\text{env}})$.

On the opposite, the UABs, owing to their position at a considerable height (typical values are in the range 50-200 m), can serve users on the ground through a LoS link, with power loss exponent equal to 2 and channel fluctuations kept to a minimum. Most papers in scientific literature use the so-called AtG channel model (see e.g. [B11, B20]) that describes the radio propagation through a two-state model, where LoS and Non-LoS states are considered. The probability of a link to be in LoS, p_{LoS}, depends on the angle between the ground and a straight line connecting the UE to the UAB (also referred to as elevation angle). The larger is the angle, the closer to one is p_{LoS} (see later Eq. (4.2)).

4.1 A Literature-based Propagation Loss

Probably the first and most used propagation model for aerial platforms is the one investigated in [B5, B6], where the AtG channel PL is mentioned. This can be considered a statistical model, and because it's widely known and more suitable than others, it is chosen as the reference propagation model for the AtG channel in the thesis. Note that, these studies do not consider a possible UAB operation during harsh weather conditions, which may alter attenuation and fast-fading. This section describes more details related to this model.

The AtG channel can then be calculated link-by-link through the following steps.

1. Choose one of the environment types specified in ITU Rec. P.1410 and consider the related parameters a_{atg}, b_{atg}, g_{atg}. Values are shown in Table 4.1.

2. Compute the S-curve parameters α_{atg} and β_{atg}, as described in [B6], based on the selected a_{atg}, b_{atg}, g_{atg}.

3. Pick randomly through the probability p_{LoS} a propagation group, ξ, where ξ indicates wheter the link UAB-UE u is in LoS or NLoS; the probability of LoS, p_{LoS}, is computed as in [B6] (Eq. 4.2):

$$p_{\text{LoS}}(\theta_u(t)) = \frac{1}{1 + \alpha_{\text{atg}} \exp(-\beta_{\text{atg}}[\theta_u(t) - a])}, \tag{4.2}$$

   where $\theta_u(t)$ represents the elevation angle in degrees from the ground terminal u to the UAV. The notation underlines that the angle $\theta_u(t)$ depends on the UE u position at time step t if user mobility is considered.

4. Pick a sample of the Gaussian random variable representing the excessive path loss, η_ξ, having different mean and standard deviation depending on ξ. This is independent from the shadowing of TBSs, and it can be denoted as:

$$\eta_\xi(\theta_u(t)) \sim \mathcal{N}(\mu_\xi(\theta_u(t)), \sigma_\xi(\theta_u(t))), \tag{4.3}$$

   where the dependency of the excessive loss $\eta_\xi(\theta_u(t))$ on the angle $\theta_u(t)$ is emphasized.

5. Depending on the resulting propagation group ξ, compute the AtG PL as in Eq. (4.5).

Finally, the AtG channel loss, $L_{u,a}(t)$, will then depend on the u-th receiver position w.r.t. UAB a, FSPL, ξ, and η_ξ:

$$L_{u,a}(t) = FSPL_u(t) + \eta_\xi(\theta_u(t)), \tag{4.4}$$

$$FSPL_u(t) = 20 \log \left(\frac{4\pi f_c d_{u,a}(t)}{c} \right), \tag{4.5}$$

where $d_{u,a}(t)$ is the 3D distance from the UAB a to terminal u.

4.2 Comparison between Statistical Models with Given Databases

As previously mentioned, an intriguing feature of aerial platforms allows UAVs to stand out against the urban layout more than terrestrial BSs, thus benefitting from

Table 4.1: Radio Resources parameters and requirements.

	Suburban	Urban	Dense Urban	Highrise Urban
a_{atg}	0.1	0.3	0.5	0.5
b_{atg}	750	500	300	300
g_{atg}	8	15	20	50

better overall propagation conditions for both the access link toward the ground users and the backhaul. This was, in fact, one of the first literature interests bound to the use of UAV-aided networks, that mainly focused on the link-level and PL characterization [B4, B5, B6]. In contrast with these studies, the activity related to channel modelling of this thesis is not focused on providing a better link-level consideration, but rather on comparing possible existing solutions at the network-level view. Several other significant factors may come into play. When considering system planning, it is relevant to know if the shape of the terrain/urban environment is highly affecting performance results. Furthermore, another element of discussion is about how the speed and height of UAVs are influenced by radio channel parameters. A number of simulations are performed to test the robustness of the method and discuss the feasibility of the different solutions.

As in relation to literature, many works related to UABs assume FSPL propagation environment [B29, B31]. This is a quite simplistic assumption since the channel model may vary significantly depending on the task location and especially in urban environments. Existing AtG models try to capture this channel variations from typical UABs heights but are rarely tested and compared in practical scenarios. In this regard, an exception relevant to mention is [B7], since it proposes a method to reconstruct a radio map of the considered environment with UABs. Through the proposed approach, it is possible to let a UAV fly offline to reconstruct and store in its memory (or in a centralized database) the radio map.

Through this activity, a database of coverage maps of an urban environment using a self-developed RaL software is introduced. This is different from [P4], where radio maps are just emulated based on the AtG statistical channel model. Here, the goal is to convert a more realistic and RaL-based database of PL samples into inputs for the network simulator. Then, the channel loss impact on system performance is compared with the one achieved through the statistical model from a network level view [P8]. Figure 4.1 gives a schematic example of the network scenario with Radio Environmental Map (REM) usage, where Q_d represents the current position of the UAB.

To include proper RaL estimations in this model, one need to consider a real

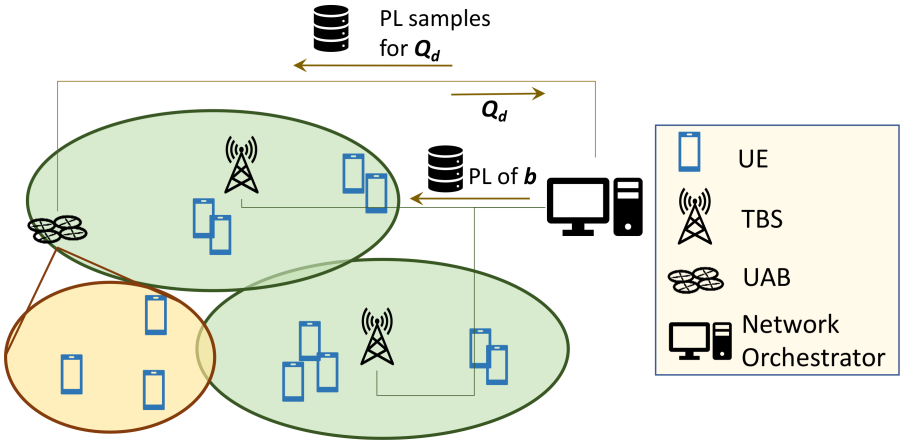

Figure 4.1: Schematic example of a REM database usage in aerial-terrestrial heterogeneous networks. Q_d represents the current UAB location and $b \in \mathcal{B}$ represent a terrestrial BS. Both BS types receive the respective coverage map.

map of an urban city as the service area. In this case, the city centre of Bologna, Italy, was selected, and a map in UTM coordinates is used as reference system over an area of around 6.5 km^2. Fig. 4.2 serves as a reference for the map used. The TBSs locations are emulated starting from the actual network service deployment of a city operator (UMTS/LTE bands). The UABs are initially parked in one of the TBSs, that becomes the starting point of their flight. Both BS types operate as a 5G network system with carrier frequency $f_c = 3.5$ GHz, and radio resources correspond to the RBs of LTE.

To comply with RaL simulations, users are randomly distributed in the outdoor space of the city centre (white spaces in Fig. 4.2). The network parameters used as reference for the network level simulations are taken from the simulator described in Sec. 5.1.

Deterministic Channel Model through Ray Launching

The Discrete Environment-Driven RaL model (DEDRL), has been introduced for the first time in [B35]. The software relies on a digitalised urban model of the city where each building is a polygon with a defined shape, material, position, and height; this is the same map as it can be seen in Fig. 4.2. The model is discrete, i.e. the building walls are properly discretized into tiles with a predetermined size. In addition to seamless space tessellation, other advanced features have been implemented to achieve very high accuracy while drastically reducing computation time. The main advantage of discretization is that the tile centres can be assumed as fixed points, therefore all the visibility relations among the tiles can be pre-computed

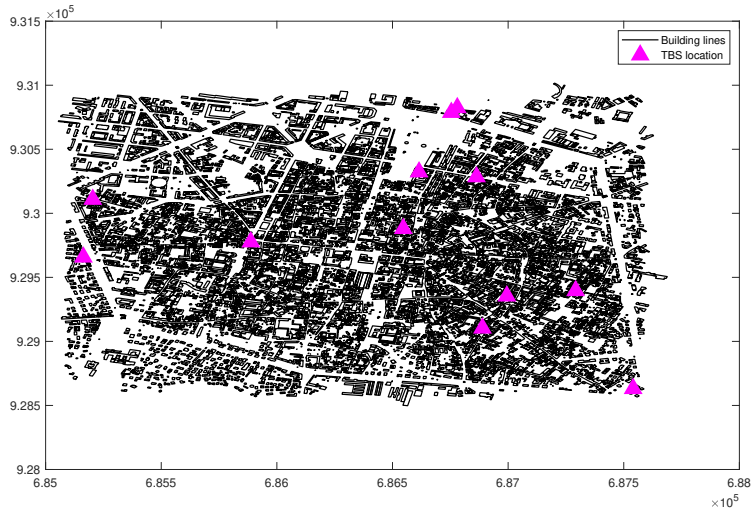

Figure 4.2: Bologna city center map given for ray launching simulations in UTM coordinates. TBSs' location sites are included [P8].

and properly stored into a visibility matrix. This visibility pre-processing is carried out only once, for a single simulation scenario. Of paramount relevance is the fact that both the visibility pre-processing and the bouncing of the ray tubes in RaL, are suitable to be parallelized into Graphical Processing Units (GPUs) and can be thus run using Nvidia cards. Typical computation times for complete predictions range from a few seconds to tens of minutes, depending on the size of the urban scenario and the characteristics of the transmitting site. Based on the outcomes in [P4] and [B36], this activity exploits in a realistic manner coverage maps, where coverage is computed via a complete set of fast RaL simulations made available a priori to the system. The RaL simulation parameters, set accordingly with the network simulator, are shown in Table 4.2. Simulations run on a commercial workstation, equipped with an Intel(R) Xeon(R) CPU E5-2620 v4 2.10 GHz [8c/16t] and 48 Gb RAM. Simulations were boosted employing Nvidia Titan Xp card, configured for GPU computing acceleration.

A Network Level Performance Comparison

Subsequently, performance is computed to study the difference between channel estimation through known models and retrieving a previously calculated value of PL over a REM database. Specifically, each PL sample of one REM file is taken on squared ground tiles having a 10 meters side, resulting in more than 170000 tiles covering the entire area. Thus, one REM file size may need a few MB. Also, the entire database is made of a set of REMs calculated on each of the 1156 drone

Table 4.2: Ray launching simulator parameters [P8].

Parameter	**Value**
Frequency	3.5 GHz
Altitude	{50, 75, 100} m AGL
UAV (i.e. transmitter) position	distributed square grid of 1156 points
Number of interactions	5 bounces, 5 reflections, 2 diffractions, 1 scatter
Number of combined interactions	3 among reflections and diffractions(max) 3 among diffractions and scatter(max)
Scattering coefficient	0.4
Relative permittivity	5
Wall conductivity	0.01 S/m

positions, as stated before in Table 4.2. This leads to an average distance of around 70 m between each consecutive drone position, enhancing the accuracy of the database on one hand, but increasing the complexity on the other hand. Actually, PL evaluations influence not only the channel gain for each user but also the UABs' trajectory design through sum throughput estimation; this is better described later in Sec. 5.1.3, as it is not the main focus of this work. The system performance is evaluated in terms of the throughput gain, G, introduced by the UABs over terrestrial network throughput. Figures 4.3 and 4.4 simulate a traffic load where an average number of more than 3000 users are asking for service. They compare the performance by varying different parameters of the UABs:

- UAB altitude, between 50 m and 100 m, where the propagation environment is more critical, especially in an urban scenario;
- antenna radiation angle (and consequently the transmission gain), increasing from 60 to 100 degrees;
- the number of UABs providing service to users in the urban area.

These pictures include two curves representing the simulation results for the different channel models. Fig. 4.3 shows the network performance in terms of throughput gain, while Fig. 4.4 in terms of the percentage of served users within the service area when both TBSs and drones are available. In general, Fig. 4.3 is the set of plots proving a higher difference in performance between the two channel propagation computations. In particular, up to 1.5% throughput gain improvement is shown in network performance while varying both aperture angle and UAB height. Moreover, in the case of multiple UABs, the gap between the two model results

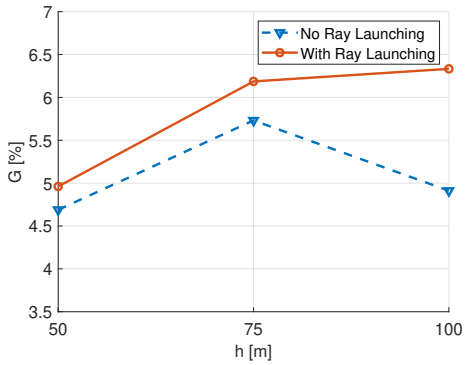

(a) Gain varying UAB altitude.

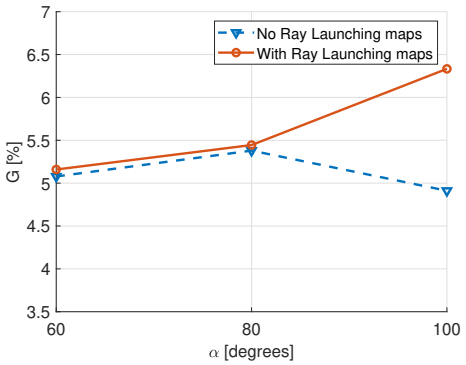

(b) Gain varying aperture angle.

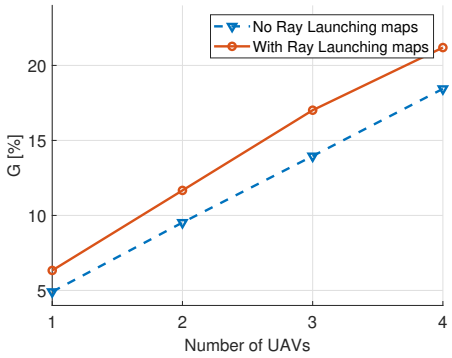

(c) Gain varying number of UABs providing service.

Figure 4.3: Ray Launching. Throughput gain of a flying UAB while varying system parameters [P8].

increases the gain of up to 5%. This is reasonable because the increased number of links in the network due to more aerial stations sharpens the difference.

Having the same network trend also proves the implementation accuracy, as a similar network behaviour was anticipated. One may also note the maximum created by simulation with statistical models in Figs. 4.3b and 4.3a. While a maximum for the altitude was expected because of the trade-off between distance and LoS probability, one for the aperture angle was not. In this case, statistical models indicate an optimal trade-off in choosing both the altitude and the radiation angle, that the RaL model shows it is not applicable for the scenario of Bologna city centre. In this case, the results from statistical models may be misleading and alter the network planning made by a mobile operator. However, please note that the metric analysed here is in terms of overall network throughput, which is not a fairness metric among different users, but helps in understanding the efficacy of the system model versus applied costs.

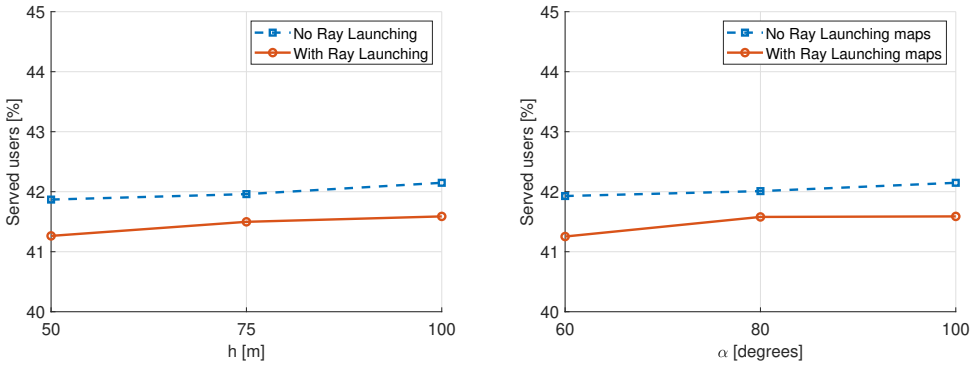

(a) Percentage of served users varying altitude.

(b) Percentage of served users varying aperture angle.

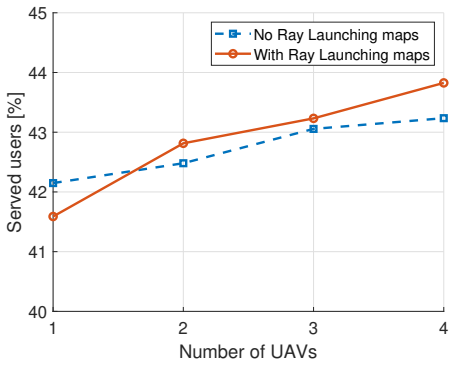

(c) Percentage of served users varying number of UABs providing service.

Figure 4.4: Ray Launching. Percentage of served users while varying system parameters [P8].

In summary, in this work, a RaL simulator is introduced to investigate the impact in network performance of statistical channel modelling and city-based PL samples. The activity is a further advancement of the emulation in [P4], where the main focus was on the system design and UAB path instead, and the concept of REMs was introduced. However, the activity in [P4] mainly focuses on the UAB path planning and network design itself and will be therefore discussed later. As expected, results show the presence of a difference between simulations with RaL and statistical models. The gap can demonstrate the significance of having RaL accuracy in a realistic scenario, where the use of resources changes based on how strong is the AtG link. Clearly, the precision of RaL strongly depends on the space discretization of the possible drone positions. If the REM database contains a small number of files (i.e. PL samples per UAB position), the simulations are no longer capable of capturing the true propagation loss. Though the additional accuracy

given by RaL PL sample may result in network performance modifications, if there is no database storage availability, statistical models might still provide satisfactory results.

Chapter 5

LTE and 5G Networks with UAV Support

As mentioned previously, the support of an aerial component to the network (e.g. the UABs) may increase significantly the network performance and efficiency. In fact, it adds the flexibility and scalability to the service it offers by directing flying nodes *where* and *when* the demand arises. Many use cases can take advantage of this potential, a few examples including occasional and crowded events, as concerts or sport matches at the stadium, connected vehicles, massive machine-type communications for Industry 4.0, enhanced media download, virtual reality and gaming. Due to the structure of the proposed system, the target of this activity lays on the provision of high throughput services to ground UEs having non-stringent delay constraints. In fact, services with stringent delay requirements cannot benefit from the aerial component of the network owing to the limited speed of UAVs. UABs can thus cooperate with TBSs to enhance service supply and offload the ground network from additional demand.

Some macrocell BSs, located on rooftops or towers, can act as UAV *homes*. UAVs might be normally parked in any home (where batteries can be charged), and leave it only when required by the central controller to fly along trajectories optimized to traffic needs. Ground terminals asking for service supply are hereafter denoted simply as *users* to generically indicate the person or UEs, as per 3GPP terminology. In summary, the advantages of using UABs are manyfold. As such, i) UABs can fly **where** TBSs cannot offer good coverage and capacity, ii) with a proper trajectory planned, the UABs can satisfy traffic demand **when** needed, and iii) Line of Sight (LoS) conditions are easy to achieve both in the backhaul and in the radio access link toward the ground users.

In this Chapter, different approaches are thoroughly discussed to properly de-

sign the UAB trajectory so that the system model is validated and the network improvement by the aerial component becomes significant. As will be discussed, every framework has been implemented by a dynamic simulator built on purpose. Since the main thesis' target is an analysis at network-level, the simulator building blocks have been developed accordingly. For example, the numerology and time-frequency resource structure of the protocol subject to the study (either LTE/4G, 5G or NB-IoT) have been implemented, while the physical layer and control signalling have been strongly simplified. Though this may simplify the performance results in absolute terms, this work is not intended to provide exact design parameters but rather to investigate qualitatively the impact of the many factors affecting the role of UAV-aided networks for 5G and beyond. In fact, the main performance metric investigated is a percentage gain.

5.1 Heuristic Approach

The first framework discussed in this thesis targets a heuristic approach, where different levels of the system flexibility and scalability can be analyzed without a drastic increase in computational effort. As a starting point, the model needs to be validated by considering relevant KPIs for Mobile Network Operators (MNOs), as network throughput and outage rates. In this thesis, a first simple approach is introduced only for the scope of running a validation test. It is called *static* approach because the path planning is decided a priori and not on-the-fly. Then, another significant aspect as spectrum sharing and resource usage is considered to make the system efficient. In this way, there are no additional bandwidth costs, but the same *pool* or set of radio resources (e.g. RBs) is used for providing enhanced service. Hence, approaches to interference for interference avoidance from UABs to the legacy terrestrial network and more advanced techniques of joint Radio Resource Management (RRM) are investigated thoroughly. Please note that all the above-mentioned studies are carried out for a massive presence of nodes in the service area, as envisioned for 5G deployment. Ground users are usually in the order of several hundred per km^2 (scaling proportionally for larger areas). In fact, the heuristic approach has the advantage of allowing focused tests and simulations without requiring a huge computational effort. This section proposes highly scalable models from the area size to the algorithmic point of view. The number of active users for one input instance is probably the parameter having the highest impact on computational resources.

5.1.1 Initial Static Approach

An heterogeneous environment is most likely to take place in a future network's scenario. Advanced technologies will be employed for a plethora of diverse use cases, for which a number of BSs will shape cells of different sizes. To start with, an initial static approach is proposed in [P2].

Heterogeneous Network Scenario

Here, the network scenario has a set of TBSs $\mathcal{B}$ comprising both Macro BSs (MBSs), set $\mathcal{C}_M$, and Small Cells (SCs), set $\mathcal{C}_S$, where $\mathcal{B} = \mathcal{C}_M \cup \mathcal{C}_S$. Users present in the scenario are considered part of the user set $\mathcal{U}$. Each MBS is positioned on its mast, being located on a specific *site*. The considered scenario is a square area with side L_a and spacing between sites Δd_site. A squared layout is assumed for the base station sites. Each base station site consists of four TBSs, each having a quadri-sectorial directional antenna. Furthermore, N_{SC} SCs are uniformly and randomly distributed over the area. The parameters concerning the environment and MBSs characteristics are shown in Table 5.1. The users arrive in the area according to a Poisson process with arrival rate λ_u per second per km^2. The users can either move or not during a simulation. The movement of the users is simulated through a Random Way Point model, which selects a random direction to be travelled with a given speed $v_u \sim \mathcal{U}[0, 1.5]$ m/s. The users are requesting to download a video through a streaming service, requiring a minimum throughput, and accept a maximum delay to start downloads. All parameters related to the user traffic are shown in Table 5.1.

A user is assumed to be *served* or *satisfied*, only as long as the entire video requested is downloaded. Since accurate terrestrial network modelling is out of the scope of this thesis, the closest BS to a UE is denoted as its *serving* BS or cell. The variable $\xi_{u,b} = 1$ denotes BS $b \in \mathcal{B}$ as u's serving BS: it holds $\xi_{u,b_n} = 0 \quad \forall b_n \neq b \in \mathcal{B}$. The user or UE u is said to be *camping* on BS b for which $\xi_{u,b} = 1$ during inactivity periods.

TBSs serve ground users through a radio channel affected by the typical impairments of urban environments, like fading and shadowing. The channel model affecting the TBS-UE link is described in Sec. 4.1, where $L_{b,u}(t)$ defines the loss between $b \in \mathcal{B}$, being either a MBS or a SC, and $u \in \mathcal{U}$ at instant t. Then, the PL model and channel conditions follow an exponential decay with link distance having propagation exponent β_env. Also, they are affected by shadowing fluctuations, assumed to be zero-mean normally distributed with standard deviation (in dB) σ_env. The time axis is discretized in time steps t having a small snapshot interval

of Δt seconds. A time horizon T_{h} is considered to capture the dynamic behaviour of the system through time. Throughput computation for UE u follows Eq. (5.4):

$$X_{u,b}(t) = \min\left(\gamma_{u,b}(t), \gamma^{\mathrm{I}}_{u,b}(t)\right) \tag{5.1}$$

$$\gamma^{\mathrm{I}}_{u,b}(t) = \frac{Pr_{u,b}(t)}{\sum_{i=1}^{|\mathcal{C}_M|} Pr_{u,i}(t)} \tag{5.2}$$

$$\gamma_{u,b}(t) = \frac{Pr_{u,b}(t)}{2 \cdot N_0 \cdot B_{\mathrm{subc}}} \tag{5.3}$$

$$C_{u,b}(t) = \sum_{b \in \mathcal{B}} \xi_{u,b} \frac{B_{\mathrm{c}}}{N} \sum_{n=1}^{N_{\mathrm{sbc}}} c_{u,n}(t) \log_2(1 + X_{u,b}(t)) \tag{5.4}$$

where $c_{u,n}(t)$ equals 1 or 0 depending on whether RB n is assigned to UE u at time instant t. N_{sbc} is the total amount of subcarriers and B_{c} the whole bandwidth. Here, $Pr_{u,b}$ represents the useful power received at terminal u from TBS $b \in \mathcal{B}$. To reduce computation time, received power is independent of the subcarrier set. N_0 is the noise spectral density depending on the noise figure and B_{subc} the equivalent bandwidth of one RB. Similarly, $Pr_{u,i}$ is the interfering power coming from interferer i, which sums up to the total $|\mathcal{C}_M|$ MBSs interfering in the same carrier frequency. The reuse factor indicating which is the RBs reuse distance between neighbouring cells is chosen equal to 1 for keeping higher spectrum efficiency. To simplify notations and algorithms clarity, subscripts will just refer to the user $u \in \mathcal{U}$ and TBS $b \in \mathcal{B}$ or UAB $a \in \mathcal{A}$ to indicate the link between u and b or a, indipendently of the set n of RBs assigned to u.

Radio Access and Scheduling

To simplify the integration with the 3GPP standard and procedures, throughout the thesis the operating carrier frequencies, available bandwidth, access procedure and numerology is set as in LTE or 5G NR [B37, B38] and reported here in Table 5.2. Therefore, the channel access undergoes Orthogonal Frequency-Division Multiple Access (OFDMA) scheme in downlink and Single Carrier FDMA (SC-FDMA) in uplink, where the minimum amount of radio resources that can be assigned to a user corresponds to a Physical Resource Block (PRB), which is simply referred to as RB. One RB is composed of 12 subcarriers [P2] with a fixed sub-carrier spacing, Δf, that equals 15 kHz, for a total 180 kHz of bandwidth occupation. Then, each terminal requires from the network a minimum amount of throughput (see Table 5.1) that generally corresponds to more than one RBs to be assigned.

MBSs and SCs have the role to supply this traffic demand by looking at the link conditions and applying scheduling techniques. In this case, each RB available

Table 5.1: Mobile network parameters set [P2].

Parameter Definition	**Notation**	**Value**
Squared area side	L_{a}	6000 m
Distance between MBSs' site	Δd_{site}	2000 m
Arrival requests per second	λ_u	10 arrivals/s
Range of speed for walking users	v_u	0 - 1.5 m/s
Simulation time	T_{h}	30 min
Total amount of SCs	N_{SC}	50
MBSs transmit power	$P_{\mathrm{tx,MBS}}$	43 dBm
SCs transmit power	$P_{\mathrm{tx,SC}}$	33 dBm
UAB transmit power	$P_{\mathrm{tx,UAB}}$	0 dBm
MBSs transmit gain	$G_{\mathrm{tx,MBS}}$	12 dBi
UAB transmit gain	$G_{\mathrm{tx,UAB}}$	0 dBi
UEs receiver gain	$G_{\mathrm{rx},u}$	3 dBi
UEs' noise figure	F_{N}	10 dB
SCs coverage radius	r_{SC}	100 m
Carrier frequency of MBSs	$f_{\mathrm{c,MBS}}$	800 MHz
Carrier frequency of SCs	$f_{\mathrm{c,SC}}$	10 GHz
Carrier frequency of UAB	$f_{\mathrm{c,UAB}}$	2600 MHz
Bit rate per subcarrier	$R_{b,mn}$	30 kb/s
Minimum SNR requested	γ_{min}	10 dB
Minimum SIR requested	$\gamma^{\mathrm{I}}_{\mathrm{min}}$	3 dB
Minimum throughput requested	R_{min}	10 Mb/s
Traffic demand size per UE	D_u	25 MB
Maximum link capacity	C_{max}	100 Mb/s
Maximum accepted waiting time	ΔT_{w}	24 s
Shadowing standard deviation	σ_{env}	6 dB
Propagation exponent	β_{env}	3.8
UAB speed	v	12 m/s
UAB height	h	80 m

at BSs, either macro or small, will be assigned to get maximum exploitation of resources. Interference level with Signal-to-Interference Ratio (SIR) is thus computed as in Eq. (5.2). Signal-to-Noise Ratio (SNR) instead follows Eq. (5.3). A first-come first-served Round Robin and Proportional Fair scheduling algorithms are implemented successively until last RB available. The first aims at allocating

Table 5.2: Access interface based on LTE numerology.

Definition	**Value**
Subcarrier spacing	15 kHz
Number of subcarriers per RB	12
Time slot interval	0.5 ms
Frame time duration	10 ms
Bandwidth of macro BS, B_c	20 MHz
Bandwidth of small cells	1.74 MHz

resources up to the minimum requested to the first UEs becoming active in the network, while the second one comes into play if more RBs are still available to enhance the perceived quality. If resources are not sufficient to satisfy the QoS instead, a user will remain unserved because of BS overload.

Due to the scenario characteristics, several users at borders remain unsatisfied on their traffic requests. At this moment, the network should ask the UAB for support, choosing which inputs to give it to maximize its efficiency. Figure 5.1 shows a snapshot of the environment of the status of the terrestrial connections, as fed to the trajectory design algorithm. Due to the system structure, three different categories of nodes remain out of network service, as highlighted in Fig. 5.1:

- UEs having a link with low SNR on serving BS b, $\gamma_{u,b} < \gamma_{\min}$;
- UEs having a link with low SIR on serving BS b, $\gamma^{\mathrm{I}}_{u,b} < \gamma^{\mathrm{I}}_{\min}$;
- UEs blocked due to an overload on the BS b they are currently camping on (lack of available RBs).

Nodes with these characteristics are defined *unserved* or *unsatisfied* from the terrestrial network, and therefore denoted as Unsatisfied Users (UUs). As for mathematical notation, the set $\bar{\mathcal{U}}$ is defined to collect all UUs for which one or more of the categories above applies. However, not all these types of nodes can be *seen* by the terrestrial network. If it is not aware of the presence of a user, its terminal cannot be considered in the clusterization algorithm. Clearly, blocked terminals are known and the system can account of them. Almost the same happens to terminals suffering only from interference: the network knows they are asking for service but the link quality is not enough to provide a stable connection with the required QoS. The opposite is true for nodes without sufficient SNR to establish a communication link with BSs: the network is unaware of them.

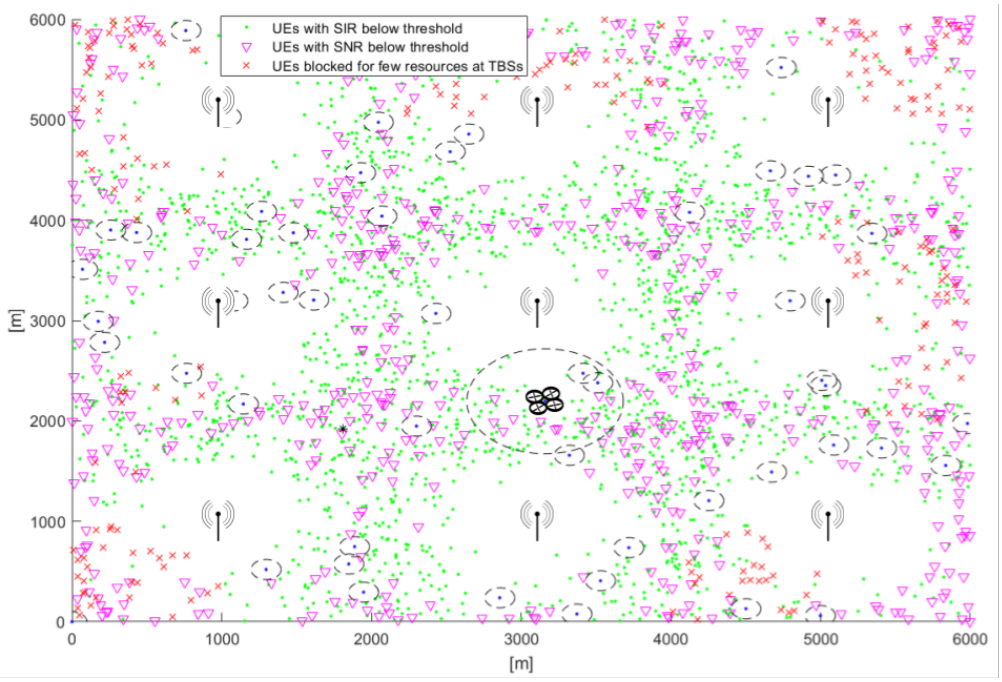

Figure 5.1: Heuristic simulator's network; uncovered nodes plotted with MBSs and SCs locations [P2].

Aerial Network Introduction

In most cases, the UUs are confined at the cell edges where normally SIR and SNR are smaller. Therefore, the spatial distribution of UUs is not uniform and UAB trajectories will privilege cell borders. This is a fair motivation for the development of a static trajectory defined prior to the UAB starts its flight. Fig. 5.1 shows an instance of the traffic distribution of UUs, obtained through the LTE-like simulator implementing the network scenario described above [P2].

An initial approach to trajectory design based on the environment is to group the UUs in a certain number of different logical clusters, which are identified based on users current location [P2]. In this way, the UAB path will follow an approach aimed at serving groups of UEs, not individual users. The total amount of clusters needed for optimizing the path trajectory is subject to a discussion later. Additionally, the work targets the trajectory design aspect by properly accounting for the information the UAB may have. Based on the categories of nodes introduced before, the system is able to clusterize the unsatisfied nodes except for the first type (i.e. UEs having low SNR). This proposal sees the clusters as a mean to drive the UAB towards the unserved users in the network. Please note that this

Algorithm 1: Heuristic. Static trajectory through clusterization and nearest neighbour algorithm.

Data: User positions, $\forall u \in \mathcal{U}$
Result: $\bar{\mathcal{U}}$ first snapshots clusterization, and static trajectory set $\mathcal{F}$
Initialize unserved users set $\bar{\mathcal{U}}$ and cluster set $\mathcal{K}$;
for *each user* $u \in \mathcal{U}$ **do**
  if *u is not served (hence falls under the UU category)* & $\gamma_{u,b} > \gamma_{\min}$ **then**
    add u to $\bar{\mathcal{U}}$;
  end
end
run *centroid-linkage (UPGMC)* clusterization algorithm for the set $\bar{\mathcal{U}}$ to find $K = |\mathcal{K}|$ clusters;
initialize $\bar{\mathcal{K}} = \mathcal{K}$ and flight segments ordered set $\mathcal{F}$;
initialize Home position k_0 and add k_0 to $\bar{\mathcal{K}}$;
set $k = k_0$;
while $\bar{\mathcal{K}} \neq \varnothing \bigvee j = k_0$ **do**
  compute cluster centroid k distance to each centroid $i \in \bar{\mathcal{K}}$, $\forall i \in \bar{\mathcal{K}}$, $d_{k,i}$;
  Find nearest neighbor j, having $d_{k,j} = \min\{d_{k,i}\}$, $\forall i \in \bar{\mathcal{K}}$;
  $\bar{\mathcal{K}} = \bar{\mathcal{K}} - j$;
  add j to the ordered set $\mathcal{F}$;
  $k = j$;
end

approach is fundamental if the goal is to serve a large area like a city centre, where thousands of users are asking for service. The static trajectory heuristic algorithm is capable of driving the UAB among clusters' centroids, using a nearest neighbor algorithm [P2]. The UAB flies from the current position over a straight line towards the nearest centroid, serving in the meanwhile all users with whom connectivity is established. The latter condition is met if the throughput is larger than the minimum required according to Eq. (5.4) and Table 5.1. Algorithm 1 describes this static approach through nearest neighbor cluster selection, and Fig. 5.2 shows a pictorial example of the above described approach.

For the sake of simplicity, this approach sees the trajectory computed just once when the UAB starts moving. Still, it works fair without adapting it to the dynamic behaviour of clusters, as discussed later. On the other hand, unserved nodes tend to be always placed at cell edges. Of course, the definition of a more dynamic

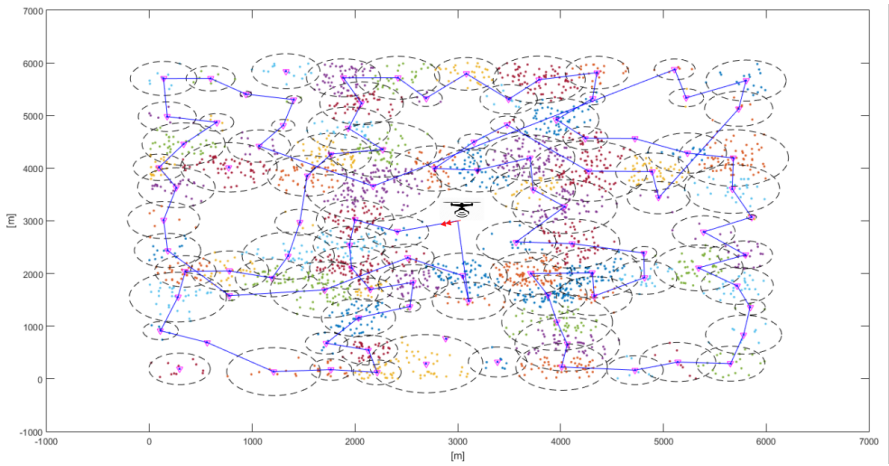

Figure 5.2: Static heuristic. A clustering example is shown along with the path selection according to the nearest neighbor algorithm [P2].

trajectory design would lead to a more efficient UAB operation. This will be the object of study in Sec. 5.1.2. In any case, this basic approach captures the main idea that the UAB never stops in any centroid and is continuously serving the underlying UEs.

Initial Assessment and Validation

To assess the advantage of a UAV-aided network, sum throughput, satisfaction rate and outage rate are computed by varying some key parameters like the transmit power from the UAB, the number of clusters and the UAB speed. Sum throughput (or network throughput), S_N, is defined as the sum of throughputs perceived by all links in the network, then averaged in time. It may also be referred to as Sum Throughput (ST), or STh. To validate the system model, the idea is to show its increase achieved thanks to the UAB. Moreover, other two metrics are computed, which correspond to the satisfaction and outage rates. The total outage rate R_{out} is the ratio between the number of UEs N_{out} remaining unserved and the total number of UEs N_{tot} present in the service area. On the other hand, the satisfaction rate is considered as the ratio between the UEs number having the request fulfilled, N_{sat}, and the ones currently present on the area, N_{tot}. These values are taken for every discrete time step t and averaged over the entire UAB flight, T_{h}. These metrics are

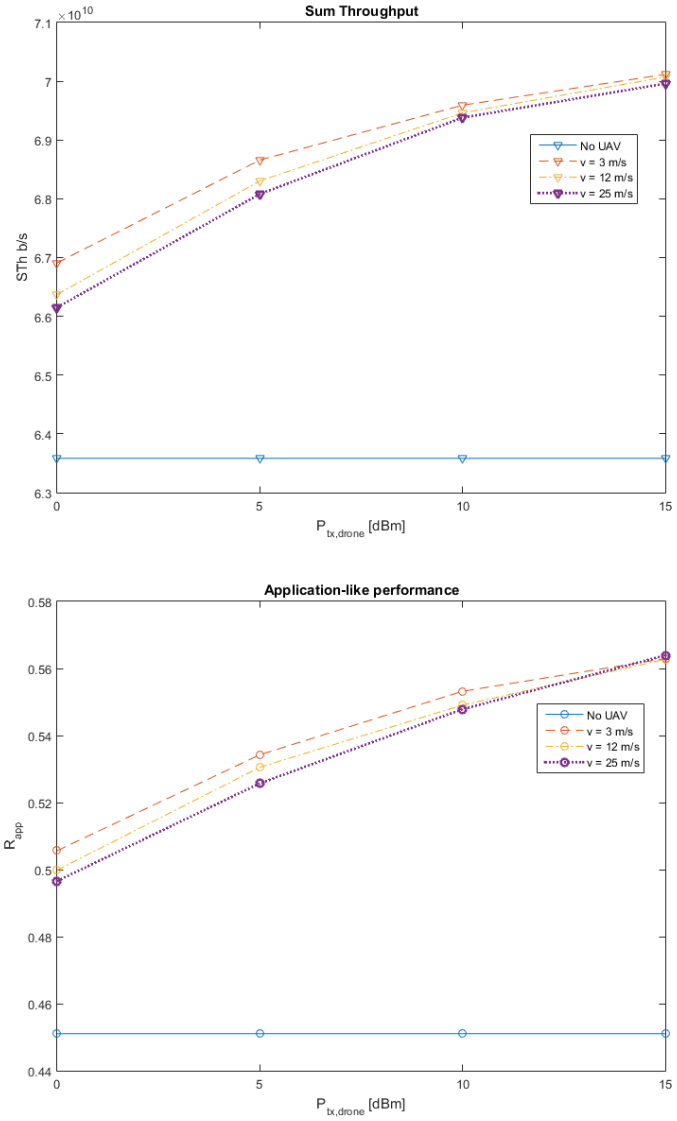

Figure 5.3: Static heuristic. System KPIs by varying UAB speed [P2].

computed following Eqs. (5.5).

$$S_N = \frac{1}{T_\mathrm{h}} \sum_{t=0}^{T_\mathrm{h}} \sum_{u \in \mathcal{U}} C_{u,b}(t_i) \tag{5.5a}$$

$$R_\mathrm{app} = \frac{1}{T_\mathrm{h}} \sum_{t=0}^{T_\mathrm{h}} \frac{N_\mathrm{sat}(t)}{N_\mathrm{tot}(t)} \tag{5.5b}$$

$$R_\mathrm{out} = \frac{1}{T_\mathrm{h}} \sum_{t=0}^{T_\mathrm{h}} \frac{N_\mathrm{out}(t)}{N_\mathrm{tot}(t)} \tag{5.5c}$$

Results are given where a total of $|\mathcal{K}| = 100$ clusters has been chosen. The value of $|\mathcal{K}|$ can be referred to as the cluster cardinality. The above metrics are

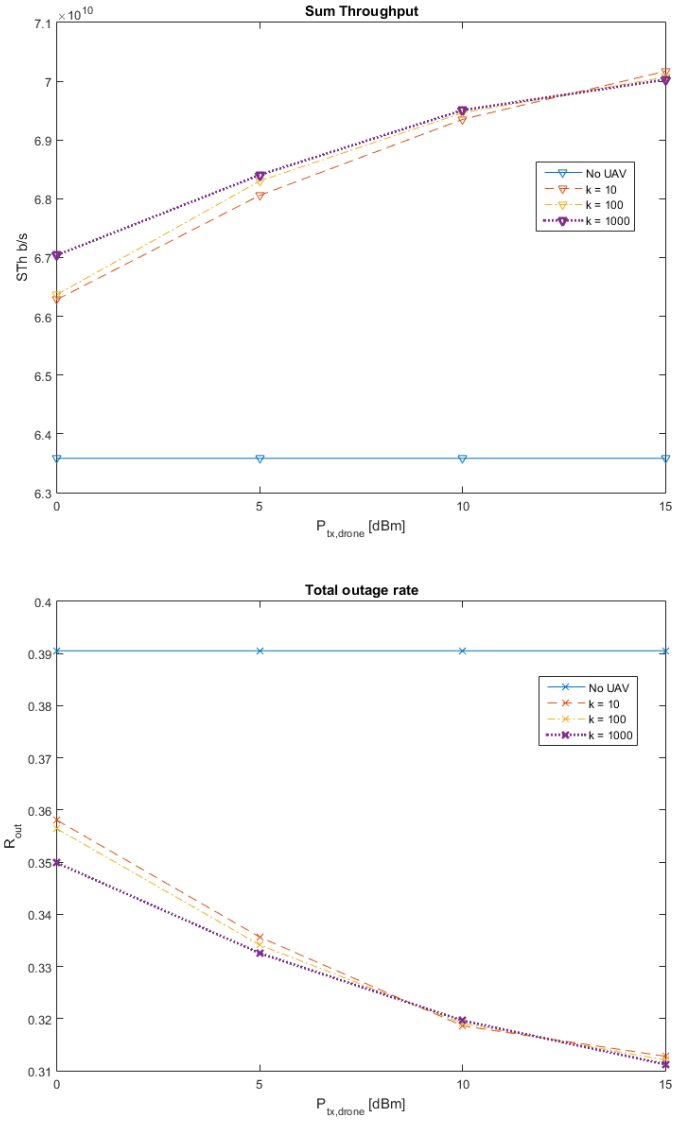

Figure 5.4: Static heuristic. System KPIs by varying the cluster cardinality K [P2].

plotted against the power transmitted by the drone in Figs. 5.3. The curves are obtained by varying the UAB speed, and show that when the drone coverage area is smaller (smaller transmit power) the speed should decrease to achieve better system performance. On the contrary, when the UAB coverage area is larger, the speed has no relevant impact. A UAB can fly faster where it is needed, but might not serve sufficiently well the UEs due to the short time period spent in providing the service.

Figs. 5.4 show performance improvements in adding the UAB as a function of the number of clusters used in the clusterization. Both figures show that the impact of such parameter on performance improvements is very low. This proves

the stability of the approach, as performance is not significantly impacted by the (a priori) choice of the parameter value.

To summarize, this work gives a glimpse of UABs potentials in future generation mobile networks by assessing a significant improvement in network performance even when only one drone is serving an area covered by many BS sites. Thus, it first validates the proposed system model. As anticipated, the approach in this initial part is oversimplified, since radio resources are orthogonal between the different tiers and the UAB trajectory is designed at flight start and not dynamically. Still, these results paved the way for interesting further advancements that are analyzed in the following sections.

5.1.2 Interference Management

In this section, the design of the UAB path is enhanced by introducing spectrum efficiency and the ability to adapt direction on-the-fly based on actual service demand. The new element of this path planning is the fact that it is event-driven, meaning that once a UAB arrives in a certain cluster, it is possible to define its next target cluster on-the-go. This allows the aerial component to respond to the very dynamically and quickly changing user traffic in future wireless networks. The activity is based on the paper [P1]. Both approaches are applied to an urban environment where users move and request video downloads with a minimum throughput. The aim of this activity is to introduce the concept of dynamic trajectory discovery in a mobile network scenario with TBSs and thousands of ground nodes that can potentially remain unsatisfied dependently on the network behaviour. The novelty of the model lies on the dynamic trajectory discovery, the continuous availability of service while flying and the approach of handling interference. In fact, the impact of the path and system performance are analysed for the case of a single carrier usage for both TBSs and the UAB.

The scenario taken as reference corresponds to the one described above in Sec. 5.1.1 and [P2]. Then, the main parameters related to the scenario and mobile networks are listed in Table 5.1. One significant difference from Table 5.1 is the value of the UAB carrier frequency, which is updated to $f_{\mathrm{c,UAB}} = f_{\mathrm{c,MBS}} = f_{\mathrm{c}} = 800MHz$, allowing then a closer look on efficient RBs reuse. The starting point for the UAB flight is the center of the area.

Design of the Dynamic Trajectory

The trajectory of the UAB is based on the clustering of the UUs, defined by the set $\bar{\mathcal{U}}$. The UAB will fly from centroid to centroid of these clusters. As before,

Algorithm 2: Dynamic UAB trajectory algorithm through clustering.

Data: $Q_a(t)$, user positions, $\forall u \in \mathcal{U}$, and data-rate demand, D_u
Result: Next trajectory point
Create unserved users set $\bar{\mathcal{U}}$, create cluster set $\mathcal{K}$, create cost function vector $\mathbf{C}$;
initialize time instant $t = t_0$;
initialize Q_k as UAB home;
while $t \geq T_{\mathrm{h}}$ **do**
  if $Q_a(t) == Q_k$ **then**
    check UE $u \in \mathcal{U}$ data-rate demand;
    for *each UE* $u \in \mathcal{U}$ *in the scenario* **do**
      if u *is not served* **then**
        add u to $\bar{\mathcal{U}}$;
      end
    end
    run *centroid-linkage (UPGMC)* clusterization algorithm for the set $\bar{\mathcal{U}}$ to find $K = |\mathcal{K}|$ clusters;
    for *each cluster* $i = \{1, ..., K\}$ **do**
      compute the centroid point of cluster i;
      compute the cost factors selected for cluster i;
    end
    normalize the cost factors computed at previous step, $\forall i = \{1, ..., K\}$;
    for *each cluster* $i = \{1, ..., K\}$ **do**
      compute cost function C_i;
      add C_i to $\mathbf{C}$;
    end
    $C_k = \min(\mathbf{C})$, $k \in \mathcal{K}$;
    select centroid of cluster k, as next path step and update next UAB destination Q_k;
    $t = t + d_k/s$;
  end
end

the clustering algorithm for the unsatisfied users is the hierarchical *centroid-linkage (UPGMC)*. However, user demand evolves in a highly dynamic way, and defining the complete path of the UAB at the start might not be very useful. People may already have left the area or withdrawn their request when the UAB arrives at their cluster. Therefore, the newly proposed UAB's trajectory becomes more dynamic as well. Now, when the UAB arrives at one centroid, the clustering algorithm is computed again just to decide which cluster centroid has to be visited next. In this way, the UAB builds its trajectory dynamically on a step by step base. Algorithm 2 describes the complete procedure in better details. In short,

1. the network orchestrator groups the UEs that are unsatisfied in $|\mathcal{K}|$ clusters [P2];
2. for each cluster ($i = 1, \ldots, K$), its centroid is computed starting from the knowledge of UE positions;
3. for each centroid ($i = 1, \ldots, K$), a cost function, C_i, is computed;
4. the centroid with the smallest cost function is identified (its distance from the current position is denoted as d_k);
5. the UAB starts flying in the direction of the chosen centroid. It keeps the same direction till when the centroid is reached, after a time d_k/v, where v is the UAV speed. During its flight, the UAB serves all UUs encountered;
6. as soon as the selected cluster is reached, the procedure is repeated again. The algorithm stops at the end of the flight.

Then, for each of the clusters identified, a visiting cost is calculated, and the cluster having the smallest one is chosen as next direction. The cost C_i for cluster i is determined as follows:

$$C_i = \left(\frac{d_i}{d_{\text{th}}(K)} + W(K) \cdot \frac{\delta}{\delta_{\max}} \right) \cdot (1 + A(L)) \tag{5.6}$$

The first fraction in Eq. (5.6) i.e., $\frac{d_i}{d_{\text{th}}(K)}$, represents the fly distance to the cluster, while the second fraction i.e., $\frac{\delta}{\delta_{\max}}$, represents the user density within the cluster. These factors are normalized. The different parameters and functions are defined as follows [P1]:

- K: the cluster cardinality,
- d_i: the distance between the UAB's current position and the centroid of cluster i as shown in Fig. 5.5,

- $d_{\text{th}}(K)$: a threshold distance depending on K. Whenever the fly distance is larger than the threshold distance i.e., $d_i > d_{\text{th}}$, the corresponding cluster is not eligible as next cluster. The more clusters K present, the lower this threshold will be. The function is obtained through spline interpolation from:

$$d_{\text{th}}(K) \begin{cases} 2500 & K = 10 \\ 2000 & K = 20 \\ 1500 & K = 50 \\ 1000 & K = 100 \end{cases}$$

  For $K > 100$, $d_{\text{th}}(K) = 1000$.

- $W(K)$: a function depending on K to give the same weight to the fly distance as to the user the density. It is obtained through *spline* interpolation from:

$$W(K) \begin{cases} 1 & K = 100 \\ 1.18 & K = 500 \\ 1.27 & K = 1000 \end{cases}$$

  $W(K)$ is considered to be 1 for $K < 100$.

- δ: the mean distance inside the i-th cluster between the UEs and the centroid (with $\delta > 0$). If $\delta = 0$, the cluster is composed only by one node, and is for this reason discarded.

- $\delta_{\max}$: $= \max(\delta_1, \delta_2, ..., \delta_n)$, δ_n the distance between the n-th UE and the centroid of its cluster as shown in Fig. 5.5,

- L: half of the length of the size of the square with as center the current position of the UAB as shown in Fig. 5.5,

- $A(L)$: a function accounting for the past direction as a function of L. If the centroid of cluster i lays in the square with size $2{\cdot}L$ around the current position of the UAB, an extra cost is added to avoid that the UAB is moving back and forward between two positions. This additional cost depends on how close the cluster i is located compared to the current position of the UAB.

The functions $d_{\text{th}}(K), W(K)$ and $A(L)$ and their arbitrary values are studied and designed in order to give the same weight to each component of the cost function and to ensure a minimum spatial fairness. To obtain them, several simulations were performed; from the cumulative distribution function (cdf) of the different elements in the cost function and the resulting trajectory of the drone. The functions are obtained heuristically.

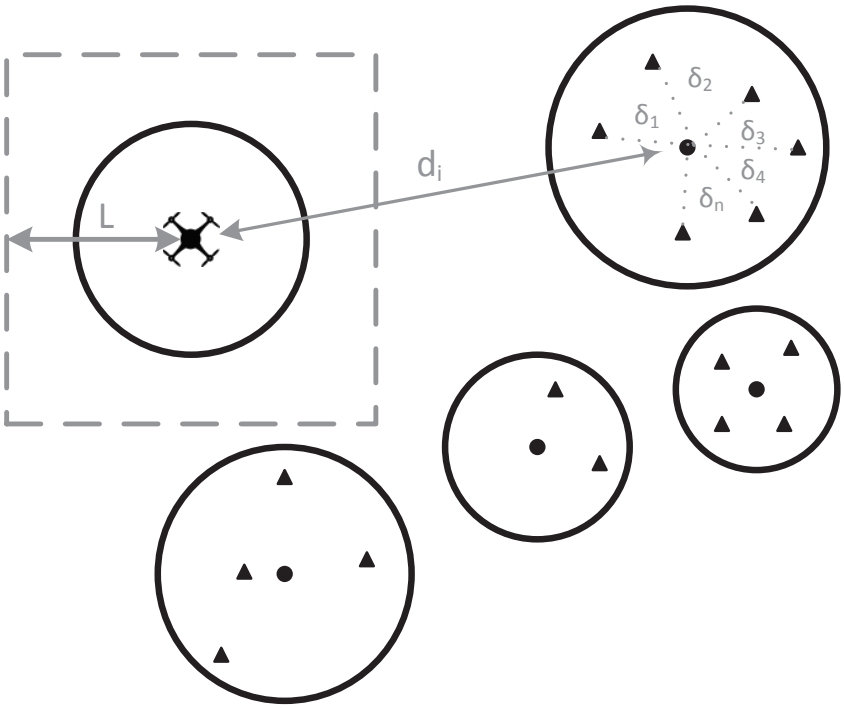

Figure 5.5: Dynamic heuristic. Identifying the different parameters for the cost-function to determine the next cluster to visit. The triangles represent the unsatisfied users [P1].

So far, the emphasis has been given to the trajectory becoming dynamic, and the fact that the UAB introduces interference to the terrestrial network when operating in the same frequency band is discussed next. The approach to interference avoidance is mainly based on the RBs assignment to the users. As done previously, the TBSs and SCs assign resources first by considering the link conditions and applying the same scheduling techniques (i.e Round Robin and Proportional Fair) to allow maximum exploitation of resources [P2, P1]. Next, the UAB assigns resources. Since both the terrestrial network and the UAB are operating in the same frequency band, they both have access to the same pool of RBs. Therefore, to avoid interference with the terrestrial network, there is the necessity to limit the pool of RBs available for the UAB. To this end, the *footprint* of the UAB is determined as shown in Fig. 5.6. The footprint of the UAB is here defined as the projection of a cone with as centre the UAB, a height of h_{fly} (i.e, the fly height of the UAB), and a radius of $h_{\text{fly}} \cdot \cot \frac{\pi}{12}$. In simple words, the UAB footprint corresponds to its coverage area on the 2D ground plane. An angle of $\frac{\pi}{12}$ corresponds to 15°, which is the maximum angle under which there is no more coverage according to the AtG propagation model in Sec. 4.1. Lower elevation angles have a limited

probability of receiving any signal from the UAB [B5]. Furthermore, the selected simulation setup of [B5] can only produce results for down to about 15° only. The RBs that are assigned from the terrestrial network to the users present within the footprint of the UAB are then excluded from the UAB's pool of radio resources as shown in Fig. 5.6. The coverage area denoted for RB re-usage can also be referred to as *safety range*. The UAB can now start assigning RBs to the unsatisfied users it is targeting by using the terrestrial network's scheduling techniques.

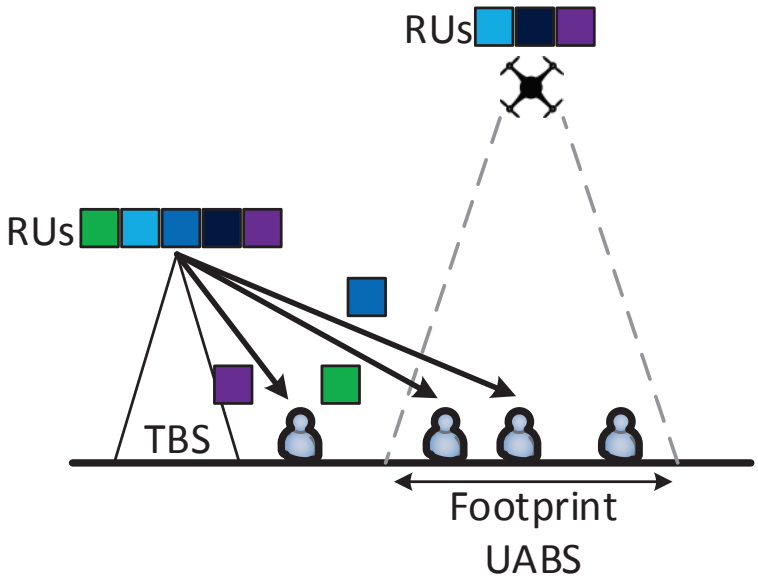

Figure 5.6: Dynamic heuristic. Radio resource assignment to avoid interference from the UAB to the terrestrial network [P1].

Dynamic Trajectory with Interference Avoidance Assessment

To assess the performance of the proposed algorithms and approaches, the following metrics are evaluated: the sum throughput, the user outage rate, and the number of used RBs. Each of these performance metrics are evaluated by varying some key parameters such as the UAB's speed, its height or transmit power. To show the effective improvement of having one or more UABs in the scenario, a further metric called *throughput gain*, G (or $G[\%]$ if considered it in percentage), is introduced. G, can be computed following Eq. (5.7):

$$G = \frac{\frac{1}{T_\mathrm{h}} \sum_{t=0}^{T_\mathrm{h}} \sum_{u \in U, b \in \mathcal{A}} R_{u,b}(t)}{\frac{1}{T_\mathrm{h}} \sum_{t=0}^{T_\mathrm{h}} \sum_{u \in U, b \in \mathcal{A} \cup \mathcal{B}} R_{u,b}(t)}, \tag{5.7}$$

where the two dividend and divisor represent the average sum throughput achieved by the aerial component only, and by the overall network, respectively. When analysing values assumed by G, it has to be taken into account which is the scenario, how wide is the area, approximately how many users are present and how big or small is the ratio between the number of aerial and terrestrial network elements in the service area.

Fig. 5.7a shows the percentage throughput gain when varying UAB speed and cluster cardinality. It can be seen once again that introducing a UAB in the network combined with the proposed dynamic trajectory design has a positive influence on the network's performance. Depending on the considered speed and cluster cardinality, the sum throughput increases between 0.8% to almost 1.6% (sum throughput without UAB equals 65.9 Gbps). One might argue this improvement is rather limited. However, this is the result of introducing just one UAB in a quite large area. Increasing the number of UAVs will of course increase the benefit. Further investigation is required to determine if the effect will be linear or not, and this was actually already verified in Fig. 4.3c. Nevertheless, even the earnings of introducing a single UAB are an interesting addendum for an operator, since it allows to satisfy 1% of the users that were unsatisfied by the terrestrial network for only a limited investment (about 8000 euro per drone).

Furthermore, the higher the cluster cardinality, the higher the sum throughput, but to a limited extent. When increasing the cardinality from 50 to 1000, the sum throughput gain, G, grows up to 0.4%. Using a larger amount of clusters makes the users in these clusters closer to the centroid. Because of this, the UAB is able to cover more users when it flies over the centroid. However, the cluster cardinality should never be as high as the number of UEs in the area, or they will be targeted singularly. To keep the cardinality value under control, in the following activities it will be computed in relation to the expected number of users per cluster and the spectral efficiency (see later, e.g. Sec. 6.2). The impact of the UAB speed on the sum throughput is limited. An improvement between 0.2% and 0.7% is noticed when the UAV accelerates from 5 to 25 m/s. When the UAB flies faster, a larger number of clusters is visited and the waiting time of each user is reduced, resulting in a higher success rate and sum throughput. The network's performance with the interference avoidance strategy proposed is investigated in the following. Fig. 5.7b shows the improvement percentage of the sum throughput compared to the scenario without a UAB for varying height and speed. Note that the cluster cardinality K equals 1000 as the results discussed above show the best performance for this value. Furthermore, unless mentioned otherwise, the transmit power of the UAB is increased to 9 dBm. This increase is necessary because with a transmit

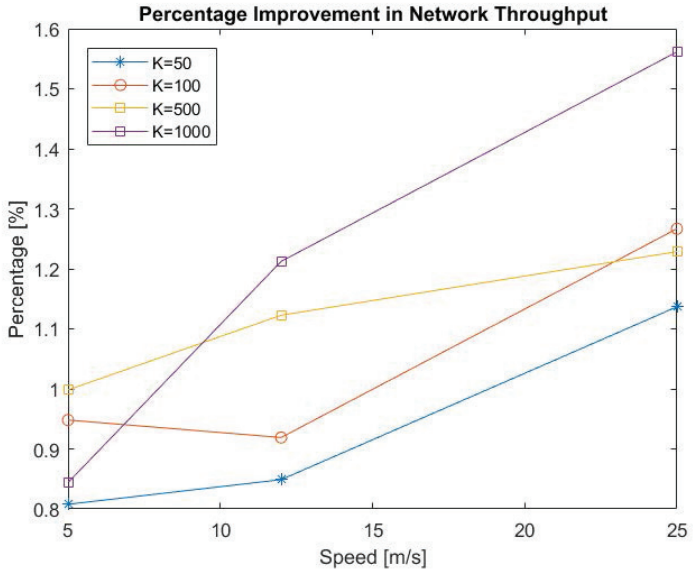

(a) Gain with varying UAB speed and different cluster cardinalities [P1].

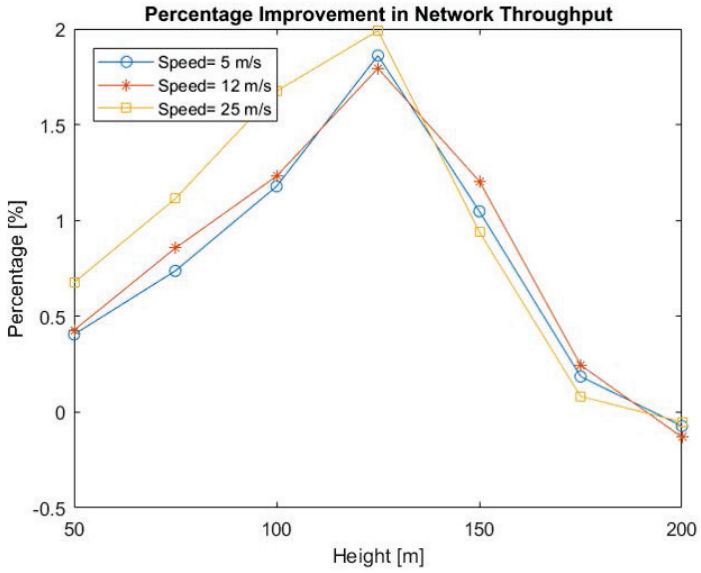

(b) Gain with varying UAB height and speed ($K = 1000$) [P1].

Figure 5.7: Interference avoidance. Sum throughput gain, G, obtained by varying different system parameters [P1].

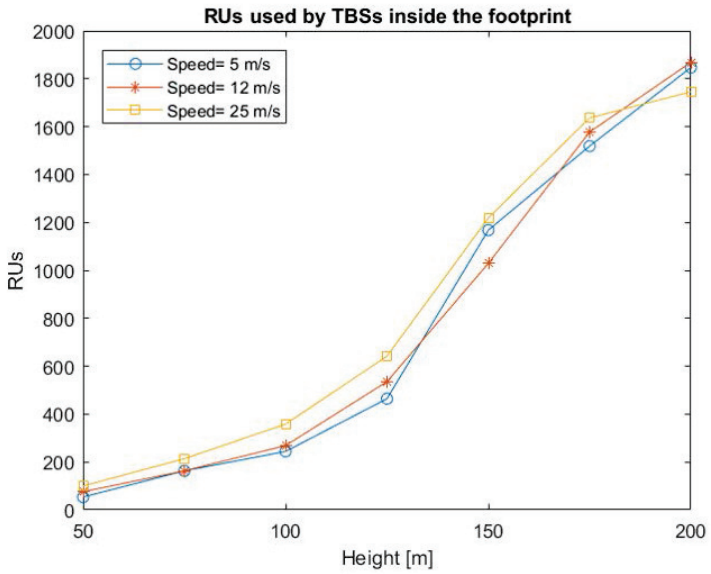

Figure 5.8: Interference avoidance. Number of RBs used by TBSs inside the footprint of the UAV for varying UAB height and speed ($K = 1000$) [P1].

power of 0 dBm, the transmit power of the UAB becomes too low with respect to the 43 dBm transmit power of the TBS.

As one might expect, introducing an interference avoidance approach reduces the sum throughput gain obtained by using the UAB. About 0.3% of the sum throughput improvement is lost compared to when interference is not accounted for (Fig. 5.7b versus Fig. 5.7a for a height of 50 m). However, interference cannot be neglected and results show an improvement of at least 0.5% and even up to 2% when using a height of 125 m and a speed of 25 m/s.

Nonetheless, the positive effect of the fly height on the sum throughput is not unlimited. When flying higher than 125 m, the sum throughput decreases again and drops even below the performance of the scenario without a UAB for a height of 200 m. The main reason for this behaviour is the pool of available RBs that can be assigned by the UAB. When the fly height increases, the coverage range of the UAB, and thus its footprint, becomes larger. The larger this footprint and safety range, the more users are present within it and the more RBs are already assigned by other TBSs. Due to this, the pool of the RBs available to the UAB is restrained and the UAB has not enough RBs available to serve all the unsatisfied users in the cluster. Fig. 5.8 shows the influence of the UAB's fly height on the amount of RBs used by TBSs inside the UAB's footprint. For a height of 150 m, more than 1000 RBs are already assigned, which is about half of the available RBs. For a height of 200 m, almost all RBs are assigned by the TBSs.

Besides the fly height, also the transmit power of the UAB has an influence on its footprint. Table 5.3 show the gain percentage of this sum throughput and outage ratio when varying the transmit power of the UAB for a height of 100 m, a speed of 12 m/s and a cluster cardinality of 1000. Doubling the transmit power can improve the sum throughput up to 0.2% (9 dBm transmit power). A higher transmit power corresponds to a larger coverage range of the UAB. Due to this, the UAB can cover a higher number of UUs when visiting a cluster. As expected, the user outage ratio due to SIR reduces when increasing the transmit power from 3 dBm to 9 dBm and results in an 11% reduction of user outage due to SIR. This is simply due to enhanced coverage achieved through higher transmit powers. Clearly, due to the UAB characteristics and costs, the transmit power is not increased significantly but kept lower than the one of legacy TBSs.

Table 5.3: Interference avoidance. Improvement percentage of the sum throughput and user outage ratio due to SIR for varying $P_{\text{tx,UAB}}$ ($K = 1000$, $v = 12$ m/s, $h = 100$ m).

	$P_{\text{tx,UAB}} = 3$ dBm	$P_{\text{tx,UAB}} = 6$ dBm	$P_{\text{tx,UAB}} = 9$ dBm
G [%]	1.02	1.14	1.36
R_{tot} [%]	53.5	49.0	43.0

In conclusion, this dynamic trajectory design improves the sum throughput up to almost 1.6% compared to the scenario without the UAB. Also, the cluster cardinality should be set according to the scenario size. Furthermore, when introducing an interference avoidance approach, one expects that the sum throughput improvement obtained by using a UAB will deteriorate. However, the decrease in sum throughput is limited to only 0.3%. An improvement of up to 2% can still be obtained compared to the network without the UAB depending on the assumed cluster cardinality, the UAB's transmit power, fly height, and speed. This study comes from in [P1].

5.1.3 Radio Environmental Data

One of the most immediate improvements from the above activities is to enhance further the path selection and trajectory cost function. However, due to the large number of factors playing major and minor roles in this heterogeneous system, it is not a trivial task.

To start with, the environment is naturally an element having a possibly large effect on propagation links. If the ground or AtG connections undergo severe interference or propagation impairments, the sum throughput decreases significantly

as well. An interesting factor to be included in the UAB path selection is thus rich information of the environment in the targeted service area. Since terrestrial bases cannot move, the UABs are the ones that potentially take a huge advantage on this knowledge. If a set of 3D locations provide a high propagation loss with respect to the others, these points might be simply avoided. The environmental information constitutes the entire *radio coverage maps* that build a large database of path-loss samples given transmitter and receiver positions, as discussed in Sec. 4.2. When this knowledge is exploited for network-level algorithms (e.g. related to RRM), it can be referred to as REM.

Secondly, another parameter possibly having a negative effect on the UAV flight is its endurance on flight time, and therefore how much the UAV consumes from going to one centroid to another. The energy consumed should be kept to a minimum, such that if the UAV is about to run out of battery, it can stop at a close-by recharge station and replace batteries.

Finally, to enhance the AtG links, a study on the radiation angle of an antenna system on-board UABs is introduced. As for the frequencies used, from this activity onwards, the carrier frequency f_c of both aerial and network tiers is set to the 3.6 GHz band, candidate for 5G services in cities. Therefore, the system model and parameters correspond to the heuristic scenario in Table 5.1, but having $f_{c,UAB} = f_{c,MBS} = 3.6$ GHz. The carrier frequency value has been chosen to purposefully cover spectrum bands envisioned for 5G. From this activity onwards, the UAB trajectory design is kept dynamic as introduced in [P1], to maintain a responsive and more efficient system. This enables a better reaction to traffic demand from the aerial network side.

Directive Antenna System Introduction

To include a more accurate transmission scheme, antenna systems with precise parameters are considered. These elements can provide an additional directivity property. In previous activities a transmit gain similar to a TBS was considered for the UAB, which is a simple assumption but not practical. From this activity onwards the assumption is dropped and the transmit gain of the UAB will depend on its employed antenna system. Hence this work improves the propagation considerations making it more realistic. Each antenna system mounted on the UAB generates a different UAB footprint on the ground, resulting in a different coverage area. The smaller is the radiation angle the smaller it is the coverage range beneath the drone. However, a directive antenna has the advantage to bring a higher gain with respect to the omnidirectional antenna case. The parameter G_α is this antenna gain, which supports ground terminals by increasing both SNR and SIR.

The gain as a function of the radiation angle is approximated as Eq.(5.8) [B21], to be summed then to the omnidirectional gain assumed:

$$G_\alpha = \frac{29000}{\alpha^2} \tag{5.8}$$

A 3 dB gain is added to Eq. (5.8), to account for a minimum level of gain even when α is very large. The angle α strongly affects the UAB coverage area, because it increases the link budget of the UAB with UE. For this reason, the best triad (h, α, v) featuring the UAB is investigated, with h defined as the UAB height. By decreasing α, the coverage area and the number of users served decrease, but the availability of RBs and transmitter gain per user increase. In contrast, by increasing α the possibility of interference with the cellular network increases and the RBs available for UEs on the UAB decrease. This modelling is simplified because an accurate antenna design is out of the scope of this work. Then, assuming an ideal antenna without side lobes and with constant gain, the area covered by the BS carried by the UAV, the UAB footprint, under uniform propagation conditions is a circle of radius $r = h \cdot \tan\alpha$. It is worth noting that, the larger is the UAV height, the larger is the footprint and the number of UUs that can be served by the UAB; however, the potential interference generated on other users on the ground, is also larger. Fixing h, the larger is α, the larger is the footprint and the smaller is the antenna gain. The considerations on variations of h and α do not change in a real case when channel fluctuations give a non-circular footprint shape. In fact, simulations with the statistical channel have this trend, shown also in [P4], and reported later in the activity results. This fact gives space to the introduction of an enhanced RRM, to be created on purpose in the following. The same assumptions as above are valid for the remained of the chapter.

The AtG channel model is one of the aspects influencing the most the performance of a UAB. However, previous studies with the AtG propagation implemented link by link have some limitations in wide-area predictions. Thus, thanks to recent advancements in processing and storage capability in embedded devices, the UAB is assumed hereby to be able to exploit REM information. These data of PL can be collected a priori and the values saved in a database accessible by the central unit. In this way, from PL samples, it can be extracted the SNR, $\gamma_{u,a}$, one would get from a user $u \in \mathcal{U}$ in a certain position with a certain granularity in space. This method allows the UAB to avoid expensive on-board computations each time a PL evaluation is needed, which drain much faster the UAB battery capability (if done on-board) or introduce unwanted latency for command and control (if done at network edge). Instead, it creates a site-specific database on PL samples once, and this can be re-used. The propagation data gathered can thus create several

maps of the same area, each one being different based on the 3D coordinates of the drone transmitter. PL information allows the network to know the received power of the u-th UE links with both TBSs and UABs (see Chapter 4) and thus to compute the SNR as for Eq. (5.3).

Radio Map Knowledge for Path Planning

This activity, differently from [P8], emulates the PL samples by reproducing the channel behaviour expressed in [B5] and Sec. 4.1 for simplicity. Channel model accuracy or comparison is out of the scope of this particular activity and the focus lies on how the PL database is exploited. Then, the radio maps are obtained as samples of the AtG statistical channel. Still, radio maps introduce a relevant new aspect to the model in [P1], since a database of PL samples is available a priori. Now, the UAB follows the procedure (similar to Sec. 4.2 and Fig. 4.1):

1. the drone stores Pr samples from the REM. These values depend on the user distance and UAB height, with 5 m definition steps,
2. current terminal locations are frozen at run time,
3. the values of Pr are read from the stored data for each UE that is inside the i-th cluster with $d_i < d_{\text{th}}$,
4. SNR is computed from the values of Pr for each link,
5. from SNR values, the UAB can estimate the throughput it would achieve by hovering on each found centroid a priori, and thus weigh the choice on the next centroid to visit.

Next, the modifications to the cost function including also the energy aspect are introduced. By using the above notation, the flight segment i for flying from one centroid to another is weighed by a cost, C_i, which is here further improved. As before, the flight segment with lowest cost is selected and followed by the UAB during its flight. The new cost function is thus defined as:

$$C_i^{(\text{REM})} = \left(\frac{d_i}{d_{\text{th}}(k)} + W(k) \cdot \frac{\delta}{\delta_{\max}} \right) \cdot (1 + A(L)) \frac{E_i}{E_{\max}} \cdot \frac{1}{\sum_{u \in \mathcal{K}_i} S_u} \tag{5.9}$$

$$E_i = \frac{d_i}{v} \left(c_1 \cdot v^3 + \frac{c_2}{v} \right) \tag{5.10}$$

The fraction $\frac{d_i}{d_{\text{th}}(k)}$ represents the flight distance to the cluster, while $\frac{\delta}{\delta_{\max}}$ represents the user density within the cluster. The term $(1 + A(L))$ introduces spatial fairness in the path choice. Then, $\frac{E_i}{E_{\max}}$ and Eq. (5.10) represent the normalized equation

accounting for the UAB's energy consumed to reach cluster i at constant speed v [B29]. This is the factor allowing the UAB to keep the energy consumption to a minimum value. Finally, the last factor denotes the i-th cost dependence on the throughput, S_u, computed for each user u belonging to cluster i. In this way, the larger is the i-th sum throughput, the lower is the cost for reaching cluster i. In particular, the definition of other parameters equal the one of Sec. 5.1.2 and [P1].

As anticipated, another term weighting the cost is added to control the energy spent during flight, as computed in [B29]. In particular, c_1 and c_2 are two parameters featuring the drone's mechanical characteristics, which are set as $c_1 = 9.26{\cdot}10^{-4}$ and $c_2 = 2250$, and $E_{\max}$ is the maximum energy that can be consumed in reaching the different centroids, used as normalization factor. Note that this makes the cost function to consider the UAB limited lifetime, in an attempt to save energy. However, the simulated scenario takes into account a time of operation of $T_{\mathrm{h}} = 30$ minutes, and professional drones having this endurance already exist. It is expected that in the coming years the available technology for UAVs improves further.

REM Emulation Assessment

Once more, G is the performance metric of the UAB's effect on the system. In

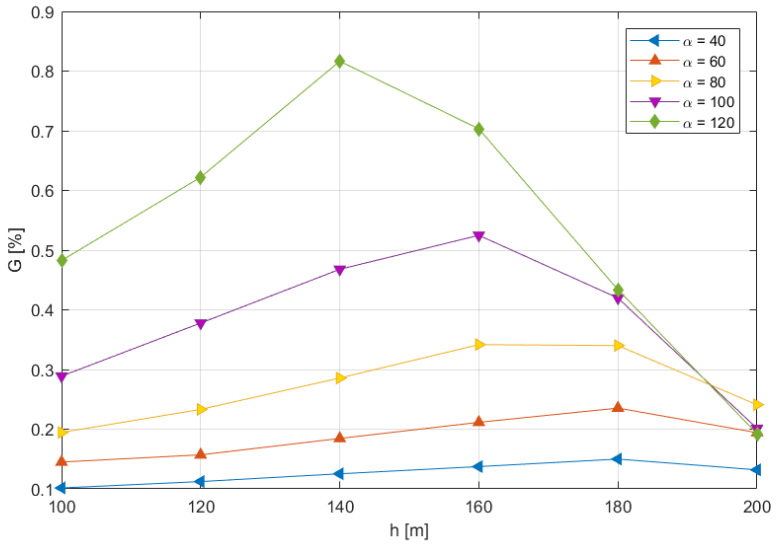

Figure 5.9: REM emulation. Throughput gain as a function of drone height [P4].

Fig. 5.9 it is shown the dependency of G in percentage from different heights, with constant speed, v, equal to 10 m/s. A number of curves are obtained by varying the radiation angle α. Each curve has a maximum of throughput gain for a specific altitude value. With small height values, the coverage footprint remains small

and less users are served. In contrast, with increasing altitudes, the RB availability decreases and the UAB provides service to less users. Larger covered areas result in higher offered traffic and possibly lack of RB availability. In fact, the RRM chosen for the model implies soft capacity at the drone side, so that resource availability depends on the number of underlying users [P1]. In particular, increasing the flying height means decreasing the RBs pool of the UAB. Therefore, as it was for [P1], a maximum in performance is obtained when a trade-off between coverage and RBs availability is reached.

Also, G decreases with α, highlighting the fact that smaller angles (i.e. narrower beams) give more antenna gain but decrease the covered range. The peak performance for each setting is obtained by properly weighting parameters as height and angle to find the best coverage. The maximum achieved gain decreases for narrower beams because the safety range is not a function of the radiation angle, but a constant which depends on the AtG model footprint.

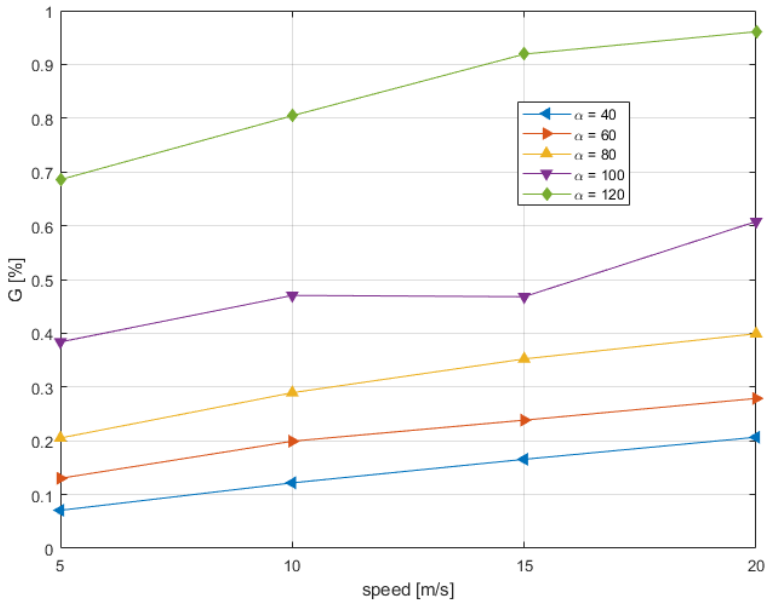

Figure 5.10: REM emulation. Throughput gain as a function of drone speed [P4].

Fig. 5.10 shows the impact of speed at different radiation angles on the throughput gain, G, with a fixed drone height of 140 m. This value was chosen because it presented the highest peak of about 0.8% of throughput gain. The plot shows that speed does not impact the fact that large radiation angles provide the best performance. Therefore, speed and radiation angle are two independent parameters. However, each curve has a slight increase in throughput when increasing the UAB velocity: greater speed allows the UAB to cover a larger area and to provide service

to a higher number of users. Therefore, a high value of drone speed is preferable, like 15 or 20 m/s.

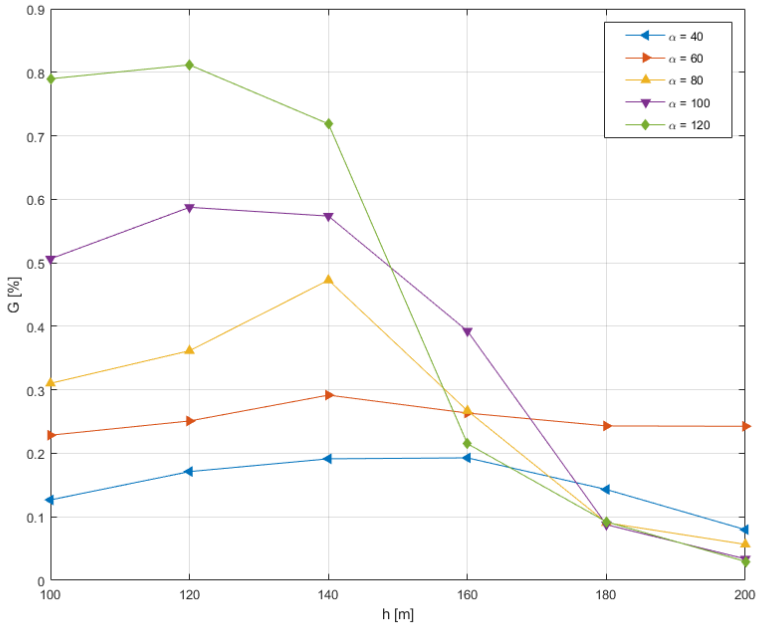

Figure 5.11: REM emulation. Throughput gain as a function of drone height with double the offered traffic [P4].

In Fig. 5.11, performance curves with an increased offered traffic, that is doubling the value $\lambda_u = 20$ arrivals/s, are presented. As expected, when more users demanding for service are present the directive gain is impacting more strongly the performance. The obtained gain in percentage drops more quickly than previously in the case of lower directivity, reaching less than 0.1% for 200 m of height. On average, all the most directive antennas bring an increase in the throughput gain of 0.1% when doubling the offered traffic. However, the maximum throughput is still around 0.8%. This fact is compliant with what analyzed before, since each curve decreases when the RRM is not able to satisfy each user efficiently. As a consequence, the maximum achieved in throughput gain is obtained with lower height of the UAB.

Figure 5.12 represents the throughput gain as a function of the radiation angle. Different curves are obtained by varying the number of clusters, K, as input to the clusterization technique. Simulations are repeated for two cases, being i) using the cost function C_i (Eq. (5.6)) in the algorithm for centroid selection (dashed lines) and then ii) $C_i^{(\mathrm{REM})}$ (Eq. (5.9)) (continuous lines). Thus, the plot compares two sets of curves: one of a system not having REM knowledge and the other of a

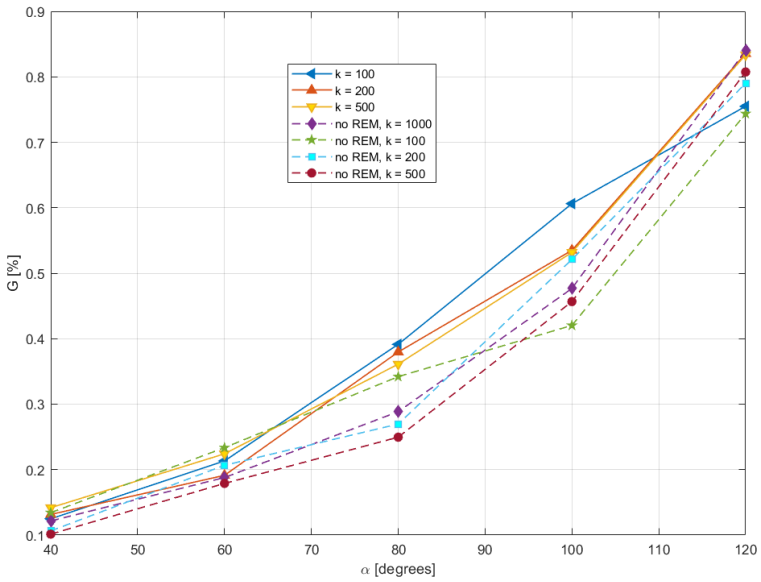

Figure 5.12: REM emulation. Throughput gain as a function of the radiation angle [P4].

system taking it into account. Although less evident with smaller beams, the set of curves representing no REM usage is below the others in performance. In fact, it is expected that estimating the throughput in advance better helps the network to direct the UAB in more useful locations (applied also for [P8]). Even if the REM in this particular case is just emulated, the advantage of this knowledge to the new cost function can still be appreciated. Thus, a system that can predict sum throughput does improve performance, especially if it includes a flexible solution able to answer user needs on-demand and in real-time.

These heuristic analyses highlight optimal working parameters for the chosen scenario settings. In particular, high speed, large beams and low-medium altitude give better results in a wide network. Furthermore, the discussion on results has brought more general conclusions:

- different antenna gains have to be balanced with different drone heights. In particular, an increase in the flying height may require a decrease in the radiation angle to improve performance and depends on the traffic load;
- high speeds let the UAB provide service to more users, thus making the solution more efficient;
- knowledge of REMs can be exploited to estimate ST in advance and devise trajectories able to improve the system flexibility and efficiency.

Please note that, however, the throughput gain improvement for higher speed is obtained with a given user traffic request. It may happen that, with more demanding requirements, too high speeds deteriorate system performance. Performance improvements shown can be up to 0.9% or 1% through the whole set of simulations. These results are still relevant because the network throughput is in the order of magnitude of 10^9 bit/s and just one UAB is flying over the wide area. The different trends in simulation results shown help in setting and planning a similar system in a different scenario, which can have other requirements or constraints.

5.1.4 Joint Radio Resource Management

A significant aspect to investigate next is related to the efficiency of RBs assignment over time, which is hereafter considered under the umbrella of RRM. It is worth noting that the real-time identification of the optimal route of the UABs in a dynamic context, is a problem that should be addressed jointly with RRM [P6]. In fact, the UAV position, being a degree of freedom, can be seen as an additional dimension in the resource pool to be administered by L2 and L3 radio resource assignment algorithms. Network simulations provide results that support this discussion and became the main achievements of [P6].

Generally, UABs are equipped with a fixed directional antenna (or fixed coverage range) pointed towards the ground, with an angle of aperture of α degrees (see e.g. [B14, B15]). For a more efficient exploit of the UAB *footprint* introduced in the interference Section 5.1.2, the transmission gain based on the aperture angle α, G_α, is considered. Assumptions about G_α are introduced in Sec. 5.1.3.

Here, the main idea is to introduce a novel concept in the RRM scheme, to be added on top of the heuristic approach of the previous sections for the UAB trajectory design. In this activity the system architecture is recalled, fundamental for RRM considerations. It is the network controller the one in charge of sending the updated information on UUs, their traffic demand, and radio resources assigned by TBSs, to the UANC (see Chapter 3). Based on this information, clusterization and flight segments definition is computed at each flying step as detailed in Algorithm 2. The cost function is re-adapted for this activity as Eq. (5.11) below.

$$C_i = \left[\frac{d_i}{F_1} + \frac{\delta_i}{F_2}\right] \cdot \left[\frac{E_i}{F_3}\right] \cdot \left[\frac{1}{S_i^{(\mathrm{cl})}}\right] \cdot F \tag{5.11}$$

where:

– δ_i is the mean distance between UEs in cluster i, and its centroid (it measures the cluster compactness and is smaller for more compact clusters),

- E_i is the energy consumed to reach the i-th centroid, computed as in [B29, P4],
- $S_i^{(\mathrm{cl})}$ is the sum throughput that would be obtained from users when the drone is at the i-th centroid,
- F is a factor accounting for spatial fairness, avoiding sudden U-turns (as in [P1]),
- F_1, F_2, F_3 are normalizing factors (see [P4]).

From the viewpoint of the RBs pool used by the aerial network component to serve the ground users, there are several options. The simplest approach is to assume that UABs serve the UEs using a different frequency band with respect to the TBSs. Of course, this excludes the presence of interference. On the other hand, the overall spectral network efficiency is not optimized. Initial papers in the scientific literature implicitly assume the UABs do not interfere with the TBSs because of separate pools of radio resources (see e.g. [B16, B14]). In this section, this simplistic assumption is not considered, and further improved by two steps.

Let us assume the TBSs and UABs use the same radio resource pool. The UANC is made aware of the RBs set used by any TBS to serve any UE both for the uplink and downlink. The UAB, while serving ground users, should choose the set of RBs that will minimize or avoid any interference with the underlying terrestrial network. It is worth noting that this approach (equal to the one presented in Sec. 5.1.2) is not based on a joint management of resources. The UAB assigns RBs in order to keep interference under control, while leaving to the terrestrial network the power to choose freely what resources to assign in any link with the TBSs. In other words, the assignment of RBs happens first at TBSs, then on the UAB.

Let us consider downlink streams first. The solution proposed in [P4] and [P1] represents the optimal choice under this scenario. Assuming that the UAV determines a footprint whose area depends on h and α as described earlier, the UAV will use at any instant only those RBs that are unused by the UEs contained in its current footprint (known by the UANC). Under the assumption of an ideally directive antenna, the UAV transmission will have no impact on any other ground receiver outside its footprint; inside it, no UE is using the RBs used by the UAB. Interference is neglected, while in fact the UAB is (re-)using some of the RBs used by the terrestrial cell. In such situation, there is no negative contribution to the overall network throughput, while there might be positive contributions as long as some RBs are available for serving unsatisfied UEs in the safety range. The larger the UAB footprint, the larger the potential set of UEs to be served, while

Algorithm 3: Radio resource scheduling for joint RRM.

Data: UAB and TBSs positions, users positions and data-rate demand D, β_{env}, σ_{env}, AtG channel, γ_{min}, $\gamma^{\text{I}}_{\text{min}}$, TBSs and UAB resource pool capacity

Result: Sets of served and unserved users

for *each RRM interval* **do**
  for *each user* $u \in \mathcal{U}$ **do**
    compute SNR and SIR of u to closest TBS $b \in \mathcal{B}$, $\gamma_{u,b}$ and $\gamma^{\text{I}}_{u,b}$;
    compute SNR and SIR of u to the UAB $a \in \mathcal{A}$ if in the coverage range, $\gamma_{u,a}$ and $\gamma^{\text{I}}_{u,a}$;
    if $\gamma_{u,a} > \gamma_{min}$ *AND* $\gamma^{\text{I}}_{u,a} > \gamma^{\text{I}}_{min}$ *AND RBs required* $<$ *pool capacity* **then**
      if $\gamma_{u,b} > \gamma_{u,a}$ **then**
        u is scheduled by TBS b;
      else
        u is scheduled by the UAB a;
      end
    else
      if $\gamma_{u,b} > \gamma_{min}$ *AND* $\gamma^{\text{I}}_{u,b} > \gamma^{\text{I}}_{min}$ *AND RBs required* $<$ *pool capacity* **then**
        u is scheduled by the TBS b;
      else
        u is not served;
      end
    end
  end
  compute Round Robin algorithm for scheduling at the TBS b;
  compute Round Robin and Proportional Fair algorithm for scheduling at the UAB a;
end

the number of available RBs will be small. Clearly, there is an optimal footprint value to be found as tradeoff [P4].

Let us now consider the uplink and the same RRM strategy as above. For the UE-UAB link, there is no interference generated by UEs, because the UAB assigns orthogonally to its served UEs only RBs unused in the footprint, and other uplink sources outside it do not contribute with received power at the UAB. However, the transmitted signals generated by UEs served by the UAB, might interfere at the TBSs with other UE transmissions in the cell. This effect can be minimized by using a reduced level of transmit power at the UEs served by the UABs, and because of the high chance that they will be located at cell edge.

However, there is margin for further improvement [P6]. Let us now assume that RRM is performed simultaneously and jointly at the UAB and TBSs. For any UE that can be served by both the terrestrial network and the UAB, an optimal choice can be made. The advantage in this case with respect to the previous one is that there might be situations where a UE in the footprint of the drone will be served with much higher SNR by the UAB, even though it might have been also served (but with lower throughput) by the TBS. An overall increase in terms of sum throughput is expected in this case. To provide an estimation of such advantage, let us consider a TBS serving a macrocell of radius $r_{\mathrm{T}} = 200$ m, and a UAB covering in its trajectory a circular area of radius r (equal to its footprint range) internal to the macrocell, adjacent to its border. Assume free space conditions for the UAV-UE link, while the TBS serves the UE at distance d with a propagation exponent equal to 3.5 typical of urban environments. The SNR can be computed for the two links, and the Shannon capacities compared. Figure 5.13 shows the percentage gain, G, in terms of link throughput, using the UAB instead of the TBS to serve the UE, for all distances covered by the UAB (d ranging from $r_{\mathrm{T}} - 2r$ to r_{T}). The gain is large, and would be much larger for larger values of r_{T}. This simple example demonstrates that a joint RRM would allow the UE to get a better service from the UAB instead of the TBS.

A further consideration is related to latency. The separate RRM does not include any sort of feedback to the terrestrial network, therefore the TBS scheduler activity is not delayed or impacted by the UAB operation. The situation may be different when using joint RRM, but only for those UEs that change the serving node: in fact, in this case the network may issue an handover in favour of the UAB to serve the selected users. Handovers of this kind are investigated in the next chapter.

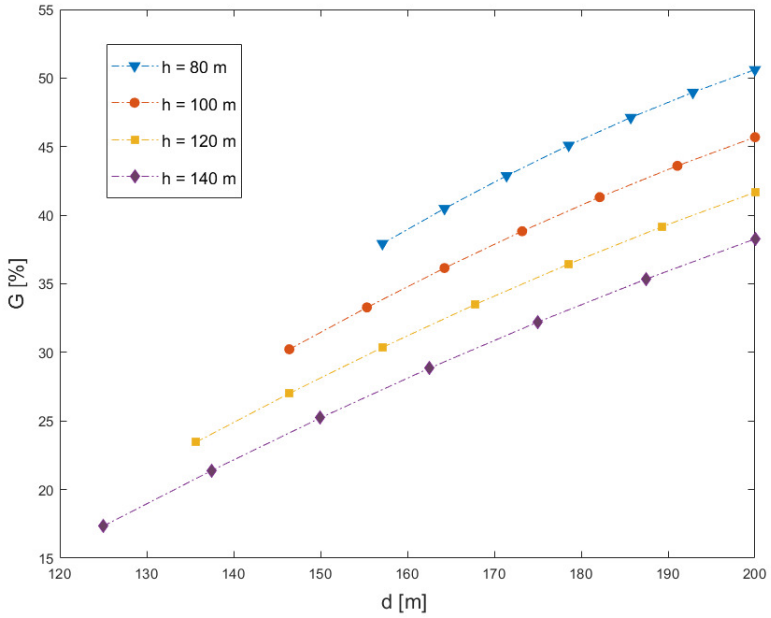

Figure 5.13: Average throughput gain using the UAB instead of the TBS, as a function of the UE distance d; $r_{\mathrm{T}} = 200$ m; $\alpha = 30$ degrees; $v = 10$ m/s; transmitted powers at TBS $P_{\mathrm{tx,TBS}} = 40$ dBm and UAB $P_{\mathrm{tx,UAB}} = 20$ dBm; transmission gains at TBS $G_{\mathrm{tx,TBS}} = 100$ and UAV $G_{\mathrm{tx,UAB}} = 60$; propagation exponent for aerial links $\beta_{\mathrm{env}} = 2$ [P6].

Joint RRM Assessment

Results obtained through the LTE-like dynamic network simulator are described hereafter. The simulated area has side $L_{\mathrm{a}} = 6000$ m. Metric's results are averaged over time (with a time horizon, T_{h}) and 10 simulation runs.

Let us first analyze the impact on performance of the system parameters that determine the footprint size: h and α. Then, the RRM strategy is considered. Figure 5.14 shows the throughput gain, G, in percentage, for different radiation angles α. The speed, v, is constant, its value equal to 10 m/s. A number of curves are obtained by varying the drone height, h. Every curve has an important antenna-dependent effect: a maximum in throughput gain for an UAV height value. In fact, small altitude values generate small footprints and less served users. In contrast, increased heights give less RB availability and therefore the UAB provides service to a lower number of users; larger coverage results in higher offered traffic and possibly lack of resources. Thus, a maximum in performance is obtained when a trade-off between coverage and RB availability is reached, as it was observed before. In this case, $h = 140$ m and large values of α seem to represent the optimal

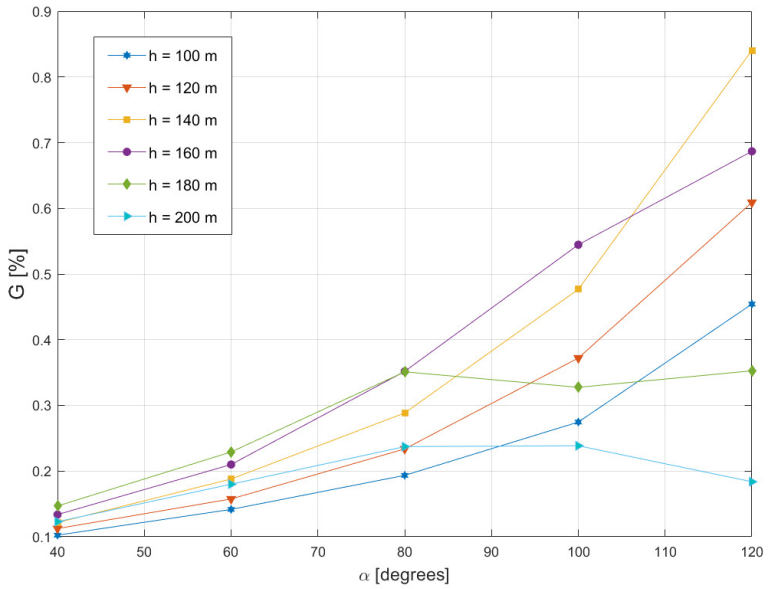

Figure 5.14: Average throughput gain as a function of α [P6].

choice. Though, this is slightly different from previous results because the scenario and UAB parameters changed, the main trend remains. The analysis is limited to $\alpha = 120°$, as traditional trisectorial antennas. Figure 5.15 highlights the effect of the previously mentioned joint RRM technique, with fixed height $h = 140$ m. Two curves compare different throughput gains at varying radiation angles, α. The trend clearly shows that for each chosen α, the joint RRM algorithm introduces a notable performance enhancement with respect to the separate RRM case.

To summarize, this activity has studied the potential advantages of the integration between the terrestrial and aerial components of a B5G UAV-aided mobile radio network, from the view point of RRM. Simulation results with a single UAB show that, by properly optimizing the system parameters related to the drone flight, a single UAB can bring an improvement in terms of network throughput of up to 1%. Using multiple UABs, the performance increase can be much larger and is studied later. In particular, it has been proved that by using a joint RRM approach, where the UAB and the TBSs schedule the assignment of radio resources in a coordinated way, notable advantages are found with respect to the implementation of separate RRM algorithms.

However, there is one further step of potential improvement still to be discussed. As mentioned, the design of the UAB trajectory might be included among the set of degrees of freedom used by the joint RRM strategies implemented in the network. Indeed, the UAB position at any instant represents a resource to be

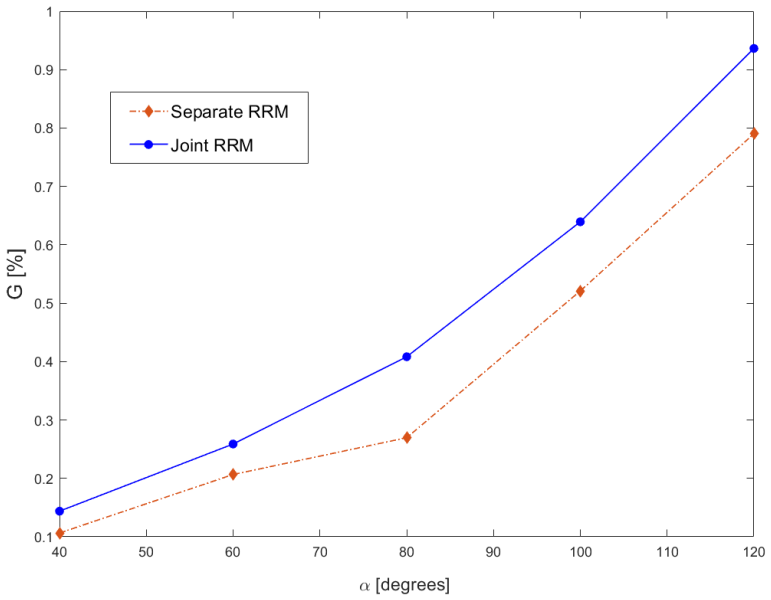

Figure 5.15: Comparison of average throughput gains with separate and joint RRM [P6].

optimally used in order to achieve the target of an higher network throughput. In this activity, the choice of UAB trajectory does not account for the number of radio resources that the UAB will be allowed to exploit in the region it is going to visit next. The inclusion of this consideration in the cost function might bring to further improvements. Therefore, a thorough analysis of the cost function factors and impact on the path planning by adding this parameter are investigated next. Nonetheless, it is important that the joint RRM algorithms running at the network layer of the protocol stack in the control plane, should also take part in shaping the UAB trajectory. The inputs needed to define the drone path and their time evolution, are compatible with usual RRM algorithms.

5.1.5 Analysis of the Cost Factors

In the following, the activity in [P5] is reported. It shows an important analysis that discusses in more details the impact of the cost function factors selected for the UAB path planning. This section concludes the studies on this heuristic approach to RRM and UAB trajectory design, and it deepens the analysis on the impact of the cost function factors.

The cost function is hereby further improved and studied. It is now based on the normalized factors introduced before, plus one. For the reader's convenience and to simplify the following analysis, Eq. 5.12 defines the cost function in a simpler

manner via emphasizing the meaning of each term.

$$C_i = F_d \cdot F_\delta \cdot F_W \cdot F_S \cdot F_E \cdot (1 + B) \tag{5.12}$$

where:

- $F_d = \frac{d_i}{d_{\max}}$; d_i is the distance between Q and the i-th centroid, $d_{\max}$ is the maximum of all values of d_i;
- $F_\delta = \frac{\delta_i}{\delta_{\max}}$; δ_i is the average distance between UUs in cluster i and its centroid, $\delta_{\max}$ is the maximum of all values of δ_i over all clusters;
- $F_W = \frac{W_i}{W_{\max}}$; W_i is the number of RBs already used by the TBSs inside the UAB footprint when the UAB is above the i-th centroid, and $W_{\max}$ is the maximum among all values of W_i;
- $F_S = \frac{S_{\min}^{(\mathrm{cl})}}{S_i^{(\mathrm{cl})}}$ considers the estimated sum throughput that will be obtained when the UAV will be above centroid i, $S_i^{(\mathrm{cl})}$ (see later); $S_{\min}^{(\mathrm{cl})}$ is the minimum sum throughput achievable in the current set of K clusters;
- $F_E = \frac{E_i}{E_{\max}}$; E_i is the energy that the UAB will spend to reach the i-th centroid at constant speed v [B29], computed as $E_i = \frac{d_i}{v}(c_1 \cdot v^3 + \frac{c_2}{v})$, and $E_{\max}$ is the maximum among all values of E_i;
- the term $(1 + B)$ provides spatial fairness.

In summary, apart from the term $(1 + B)$, the cost function introduced in this and previous sections, is the product of a number of factors taking values between 0 and 1. These factors were chosen to jointly reduce energy consumption and improve efficiently sum throughput. As before, the UAB will take the direction identified by the lowest among all evaluated costs; as long as the listed factors are closer to zero, the i-th centroid has higher chance to be chosen.

As far as the radio resource pool used by the aerial network component to serve the ground users is concerned, the joint RRM option is chosen here and in the remainder of the thesis.

It is worth noting that the choice of the cost function reported above, includes the consideration of the expected number of radio resources that will be available in the cluster to be visited next, through the factor F_W. According to the RRM technique used here, the number of RBs available in each cluster is variable depending on how many UEs are served by the TBSs in the UAB footprint. Therefore, the design of the UAB trajectory is performed accounting for the specific type of

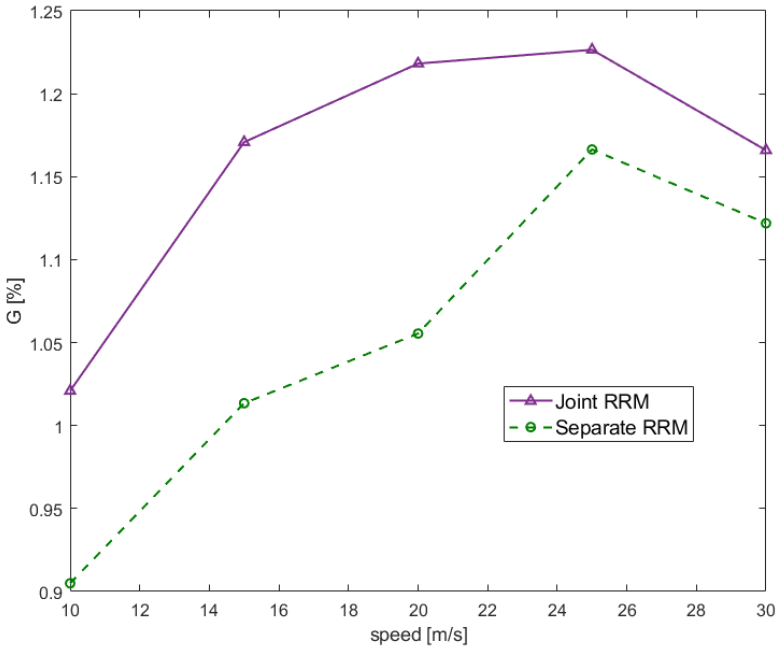

Figure 5.16: Dynamic heuristic. Throughput gain with varying UAV speed [P5].

RRM strategy envisaged for the network. In other words, the UAB trajectory is RRM-dependent.

Results achieved in this activity see a few changes in the simulator parameter settings. The height of the UAB sees its default value equal to 140 m, the transmit power $P_{\text{tx,UAB}}$ is 9 dBm, and the antenna aperture has a default angle of 120 degrees.

Figure 5.16 shows the throughput gain achieved as a function of UAB speed. Here, the lowest curve represents the outcome achieved through the first separate RRM solution mentioned in Sec. 5.1.4. On the opposite, the upper curve is obtained by implementing a joint RRM decision between aerial and terrestrial network, as mentioned before. As expected, the second case provides better performance results in terms of throughput gain, G. In fact, in this solution, RBs are scheduled with the joint RRM comparing the different downlink channel conditions. Moreover, both curves show the same behaviour when varying the UAB speed. As its value increases, performance results increase accordingly. This happens because the UAB is able to reach UUs in a faster way. However, when the speed becomes higher, the UAB is not able to satisfy the user application requirements, as it flies away before the video is fully downloaded. For this reason, a maximum in the curves is present and a tradeoff value for speed has to be set.

The comparison between the two curves shows that the maximum does not

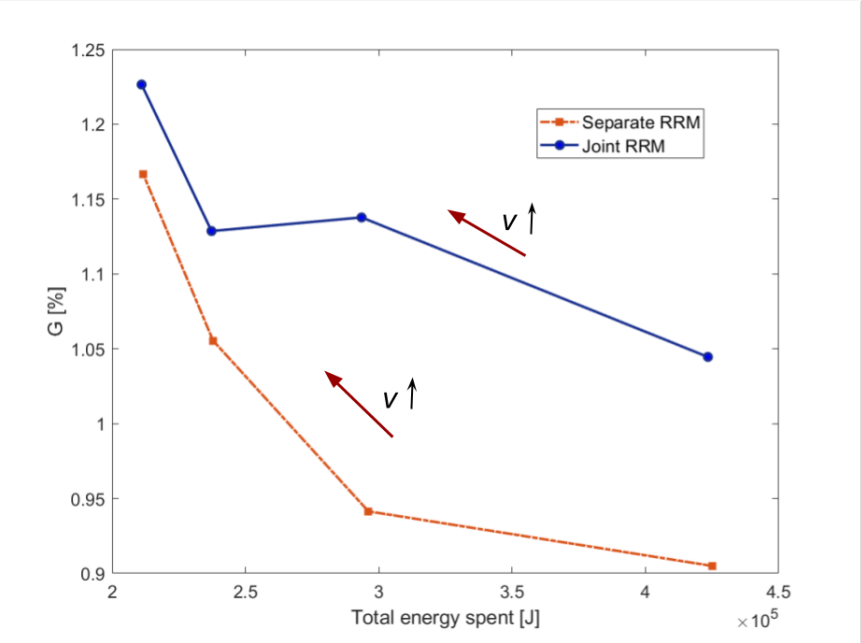

Figure 5.17: Dynamic heuristic. Throughput gain varying energy consumed [P5].

change with the RRM strategy used. Whatever the value of UAV speed, joint RRM provides a significant improvement in gain with respect to separate RRM. Moreover, it is worth noting that comparing these results with others above, the gain is usually larger. Hence, the choice of the new cost function significantly increases the performance improvement achieved by one UAB in the service area.

Figure 5.17 shows the outcome performance while enlightening the influence of energy consumed. The total energy spent is computed as the previously mentioned E_i. The two parameter values c_1 and c_2 featuring the drone's mechanical characteristics are set as $c_1 = 9.26 \cdot 10^{-4}$ and $c_2 = 2250$, as in [B29]. Authors state that the minimum energy spent is obtained for a drone speed of 30 m/s, and the same behaviour applies in this scenario. Therefore, with this speed not only the energy consumption is less, but also the network improves in terms of throughput gain. Thus, higher speeds for the UAB are preferable with respect to low velocity of 10-15 m/s.

In Fig. 5.18 the performance gain is shown with respect to another parameter, M, that is the average number of UUs present inside a cluster. This value is dependent on the total number of clusters, K, chosen as input for the clusterization algorithm. The curve related to a separate RRM is more dependent on this parameter, where for a larger number of users inside each cluster, the throughput gain increases (variations in G below 0.01% are considered as negligible for statistical reasons). Therefore, for this case it is more advantageous to drive the

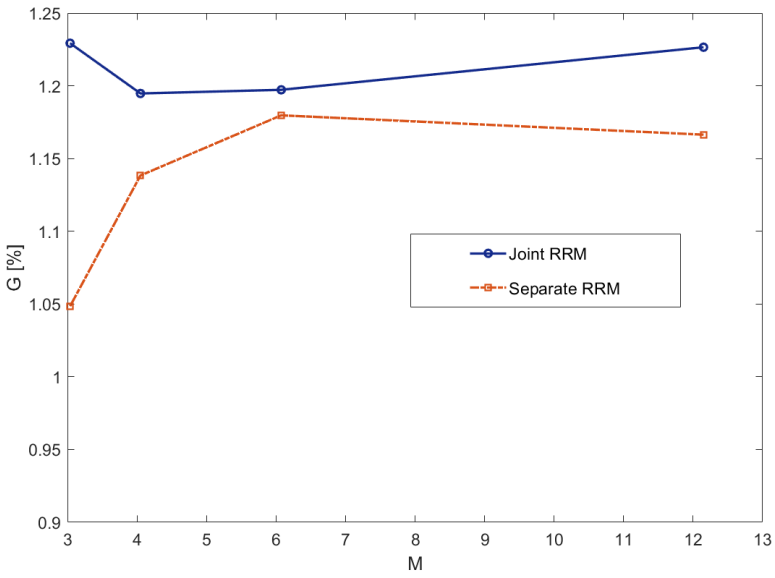

Figure 5.18: Dynamic heuristic. Throughput gain while varying M [P5].

UABs through bigger clusters. However, for what concerns the aforementioned joint RRM, the performance gain obtained is almost equal for different values of M. Once again, the clusterization algorithm appears to be robust. In fact, the difference in performance gain while changing parameter M is small: the slight modifications are probably due to the high randomness present in the scenario.

Finally, the analysis focuses in understanding the different effects of every factor in the proposed cost function. The mass distribution obtained for each factor F_i is shown in Fig. 5.19. Clearly, some factors have a distribution that is quite different than the others. As a result, the role of each factor is rather unique. One possibility to overcome this problem would consist in using different exponents, ϕ_i, applied to the different factors F_i. This might provide some degrees of freedom to be properly used for tuning system performance depending on the specific needs.

However, one can infer from Fig. 5.19 that the most impacting factor between the five is F_S, i.e. the ST factor. Its values are mostly close to 0, making it drive the product to smaller costs. On the contrary, F_δ has values closer to 1, thus affecting less the overall cost. The other factors behave in a similar way, having then comparable weighs.

Figure 5.20 shows the mass distribution of the obtained costs to compare for the best centroid selection, during a simulation run.

The cost function applied here has been still generated according to a heuristic approach, and no one ensures that a better way to define its expression does not exist. Five factors driving the cost function have been identified based on the drone

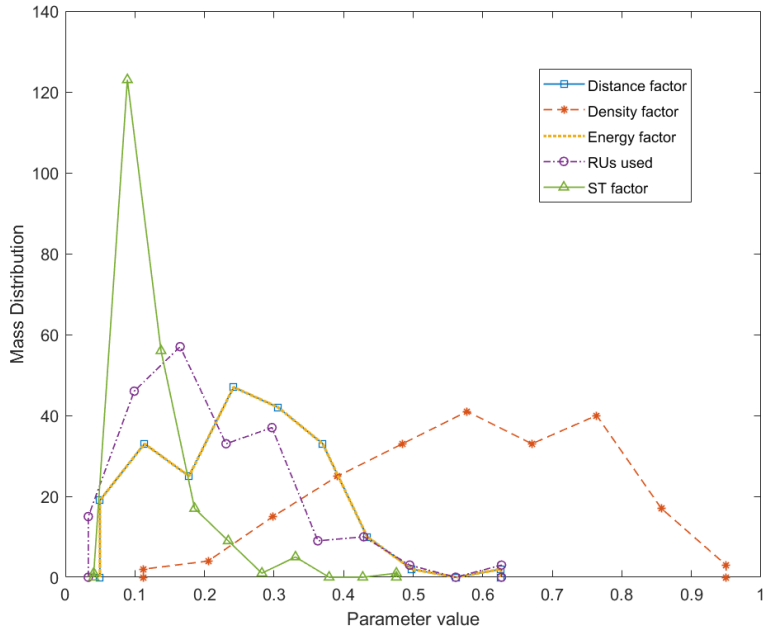

Figure 5.19: Dynamic heuristic. Probability mass distribution of the different factors in the cost function [P5].

hardware and mechanics, as energy and distance, and the final scope to improve performance, as ST, user density and RBs availability. These results are encouraging, since the distribution of the different factors combined in such expression, might bring to interesting conclusions on how to better shape the cost function (e.g. introducing different exponents) for the diverse use cases.

5.2 Optimization framework

Given the previous analyses, in this Section the problem of UAB trajectory design is investigated from a different perspective. Through a few appropriate assumptions partly validated from previous achievements, service optimization through mathematical modelling and linear programming tools are introduced. To fulfill this purpose, the UAB trajectory design is forced to maximise an objective function that accounts for the maximisation of the number of served ground users. In particular, the above introduced scenario is transformed and re-adapted to extract the true optimal network performance given a selected metric. This work has been proposed in [P3].

Differently from the majority of research activities devising complex and mainly non-linear problems able to only obtain supotimal results, this study transforms the

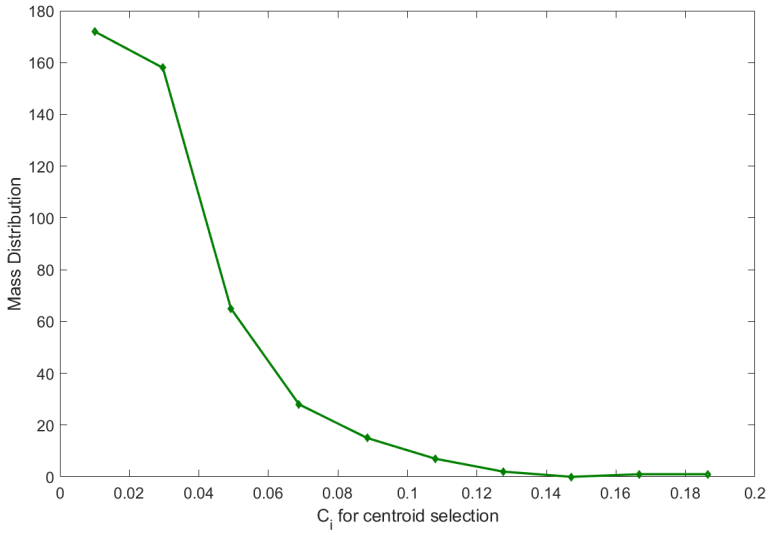

Figure 5.20: Dynamic heuristic. Probability mass distribution of obtained C_i [P5].

network model in a Integer Linear Programming (ILP), which provides an optimal solution through known and appropriate solvers. Furthermore, novelty elements w.r.t. the state of the art in this analysis relies in the consideration of more realistic users requirements. Users i) have to download an entire high throughput video to be considered as served (this requires proper consideration of the time evolution of the service provided); ii) start requesting the service in a random instant; iii) must be served within a given amount of time. The optimisation problem also accounts for constraints on the number of radio resources available at the UAB, the battery duration, different UAB speeds and the data rate that the UAB can provide. Equally as before, a user is assumed to be served or satisfied, only as long as the entire video requested is downloaded. The problem analyzed is a generalization of the Orienteering Problem (OP) [B39], and thus it is NP-hard. However, because of computation complexity resulting in very high simulation times (in terms of several hours or even few days), a more affordable solution is also considered in the Rolling Horizon (RH) approach. In this case, results given are suboptimal, but a comparison with the general ILP for small input istances is provided. This comparison allows the reader to have an idea of the resulting gap between the optimal linear model and a ILP-based heuristic solutions.

5.2.1 Integer Linear Program Modelling

Literature research has quite recently started to study the problem from a operational research or machine learning point of view, thus optimizing mathematically

the UAB placement or path. In particular, similar activities that can be cited are [B30], which considers the placement of UABs with criterion of optimising the energy efficiency of the UABs network, [B31] and [B32], which optimize the trajectory for maximising the minimum user rate. In contrast with these works, the activity presented here has the objective of maximising the number of served users, when assuming each one has to download an entire video. Therefore, the UAB may have to reach and cover the same user multiple times, in order to complete the service. This approach makes the model more complex while ensuring an appropriate QoS. Furthermore, a more realistic random activation and expiration of the service requests is introduced, while the above cited works assume users are active for the entire flight. It is important to cite also the work [B7], since it proposed a method to reconstruct a radio map of the considered environment through UAVs. Through the proposed approach, it is possible to let an UAV fly offline in order to reconstruct and store in its memory the radio map. A similar result would be achieved via RaL simulations, as discussed in Sec. 4.2. Based on these techniques, it would be possible for the UAB to know the channel UAB-user for any user in the considered area, provided that the user position is known. Assumption taken in the following are then solid, making the model robust.

In the recent years, an increasing number of studies regarding drone routing optimisation appeared in the literature, as UAVs can be employed in the commercial sector, for geocoding, in surveillance systems, etc. To cite a few, drone routing optimisation can be found in last mile delivery problems [B40], [B41], [B42] and [B43], in flying over a set of mission-points applications [B44], or in filming sport actions [B45]. All these works assume that all customers/points of interest need to be visited and the main goal is to minimise the routing costs. This differs from the problem analysed in this thesis, where the goal is to maximise the number of served users conditioned to link throughput and data demand. In addition, differently from the model proposed here, speed is usually assumed to be constant.

If one considers as a goal the maximisation of served users, the studied problem is closely related to, and actually generalizes, the OP [B39]. This OP is a routing path problem, defined on a directed graph, whose goal is to determine which vertices or 2D coordinates to visit (at most once) and in which order, so as to maximise the total collected score of the visited vertices, while satisfying a maximum tour duration constraint. In contrast with usual operational research problems, in this model the UAB can serve a user by flying "close" to it, thanks to the AtG model.

In summary, in this study the UAB can fly at different speeds, visit the users multiple times, and does not need to reach the exact location of the user in order to serve it. These specific features lead us to model the problem by means of a

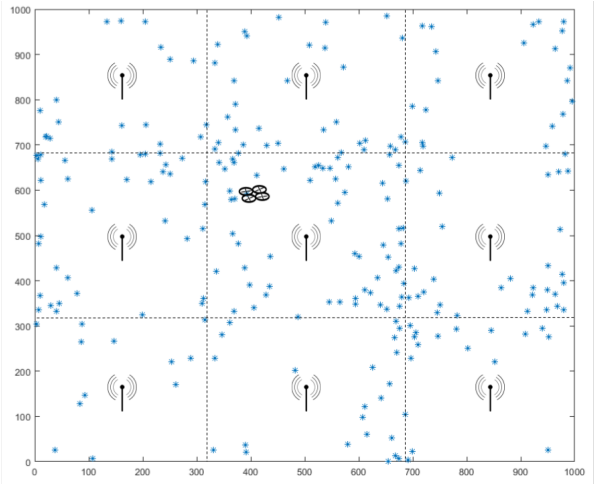

Figure 5.21: The ILP network scenario [P3].

space-time graph, which is not used in the previous related works.

5.2.2 ILP adapted network model

In this section, one scenario denoted as *normal-day* case is considered. Here, the UAB is assumed to provide service to users that cannot be served adequately by TBSs positioned in a grid layout. A square area with side L_{a} serves as the service area. Then, the normal-day scenario takes as reference the daily operation accounted previously for the heuristic approach: even if the terrestrial network does not take part in the optimization problem, when the UAB service starts, users will be reasonably distributed mainly at cell edges (see snapshots from the heuristic in Sec. 5.1). Indeed, users in these positions are the most susceptible to bad channel quality and interference generated by nearby TBSs. Figure 5.21 is a pictorial representation of the scenario considered for the ILP. Since in this problem there is no TBS mathematical modelling because of extremely high problem complexity, the separate RRM case (discussed above in Sec. 5.1.4) is considered. Hence, it is assumed that the UAB disposes of RBs orthogonal to those of TBSs, and all users can be served without interference from them. Then, the UAB needs to serve the UUs only, and the set of UUs is denoted as $\mathcal{U}$ in the following.

The UAB is initially parked in its Home TBS, from which it starts flying at a fixed altitude from the ground. It can recharge its battery when at Home, and, thus, the UAB must come back to Home before the battery expires. The battery lifetime has a duration of B_a seconds.

Each user $u \in \mathcal{U}$ is characterized by three parameters: i) the demand, D_u, that is the number of bits the user wants to download from the network, ii) the

activation time, a_u, that is the instant in which the demand is generated; iii) the expiration time, e_u, that is the maximum amount of time user u can wait before the service is satisfied completely. So, the deadline for completion of data download is at instant $a_u + e_u$ for user $u \in \mathcal{U}$. Each UU generates only one data demand during service time, and a_u is assumed to be randomly and uniformly distributed.

After an assignment of radio resources by the TBSs, $\mathcal{U}$ and its size, $|\mathcal{U}|$, are assumed to be known. The UAB can now start serving the UUs. The Active Unsatisfied Users (AU) are those UEs which are active (not expired yet), while UUs become Served Users (SUs) when the full amount of data requested has been downloaded.

The UAB knows UU positions and demands, as well as activation and expiration times, for a time horizon, denoted as T_h, where $T_\mathrm{h} \geq B$. With this information, the UAB can run an optimization algorithm to find a trajectory such that i) as many UUs as possible are served within their expiration time, ii) the UAB is able to come back to Home before the battery expires.

The link to inspect, being the AtG channel between the UAB and the user, is already described in 4.1. The data rate is evaluated again through the Shannon capacity (see Eq. 5.4). As mentioned before, it is assumed that the UAB has an a-priori knowledge of the coverage map.

To properly construct an ILP that provides an optimal result, a discretization of space, time and speed is required. Furthermore, to model the problem mathematically, a logical *space-time* directed graph is introduced. Space is discretized in steps of Δx m, which corresponds to possible flight segments for the UAB path. The new flight segment will then depend on the selected direction, to be picked from a given set $\mathcal{D}_o$ of possible directions. The 2D points denoting the start and end of a flight segment are called *turning points* (TPs), because they denote a possible change of direction. As an example, in Figure 6.6, the UAB can only fly along segments of a squared grid, and it can move in one of the four directions: North, South, East or West. As one can imagine, the smaller the value of Δx the more flexible a trajectory may be. However, a small Δx enlarges the solution space of the ILP, which increases accordingly the computational time. Let v_max be the maximum speed of the UAB. For convenience, a time step lasting ΔT [s] discretize the time axis so that it is the minimum time needed by the UAB to traverse a segment, i.e., $\Delta T = \Delta x / v_\mathrm{max}$. In addition to the maximum speed, the UAB can fly along a segment at a speed v [m/s] taking discrete values in the range $[v_\mathrm{min}, v_\mathrm{max}]$. More precisely, v is chosen so that the time for moving along a segment is a multiple of ΔT. Let $\mathcal{C}$ be the set of TPs in the considered area (the TP corresponding to H is duplicated, for convenience, as the UAB departs from H and returns to H), and $\mathcal{T}$

the set of time instants in the considered time horizon, T_{h}.

Now, the directed space-time graph to model the ILP can be denoted as $\mathcal{G} = (\mathcal{V}, \mathcal{A})$, where the set of vertices $\mathcal{V}$ contains a vertex v_{ct} for each TP $c \in \mathcal{C}$ and time instant $t \in \mathcal{T}$, plus two artificial vertices: a source σ and a sink τ. The set of arcs $\mathcal{A}$ contains: (i) artificial starting arcs from σ to the vertices $v_{H\,t}$, representing the departure time instants of the UAB from H, (ii) artificial ending arcs from the vertices $v_{H\,t}$ to τ, representing the arrival time instants of the UAB at H, and (iii) travel arcs $(v_{ct}, v_{c't'})$ representing the movement of the UAB from TP c at time instant t towards TP c' at time instant t' by using one of the selected speeds. Let $s(a)$ be the time instant of the starting vertex and $e(a)$ the time instant of the ending vertex of arc $a \in \mathcal{A}$. Moreover, let $\delta^{+}_{(v_{ct})}$ represent the set of outgoing arcs and $\delta^{-}_{(v_{ct})}$ the set of ingoing arcs, from/to vertex $v_{ct} \in \mathcal{V}$.

Notice that unsatisfied users $u \in \mathcal{U}$ are generally not placed exactly in TPs, and it must be determined which UUs can be served by the UAB when it moves between two TPs. Through the radio map and by knowing the position of all UUs, the UAB is able to estimate the data rate it can provide to the users when it is in a certain TP. Since each arc $a = (v_{ct}, v_{c't'})$ is travelled for a time duration $l_a = t' - t$, by knowing the data rate, it is possible to derive how many bits are received by each covered user in the period l_a. Let $r_{uc(a)}$ represent the data rate [bit/s] that the UAB can provide to unsatisfied user $u \in \mathcal{U}$ while moving from TP $c(a)$ (starting vertex of arc a) along arc $a \in \mathcal{A}$; $r_{uc(a)}$ can be computed through Eq. (5.4), where P_{rx} represents the power that the user u receives from the UAB when the latter is in position $c(a)$, i.e. in the starting vertex of arc a.

Notice that, depending on the user demand D_u ($u \in \mathcal{U}$), and on the R available RBs, the UAB might need to traverse several arcs before completely serving the user u. Only if the demand is completely satisfied, the user is counted as served. In order to declare a user as served, its activation and expiration times have to be taken into account. Since the UAB cannot provide capacity to users that are expired or not active, $r_{uc(a)} = 0$ is set for all arcs $a = (v_{ct}, v_{c't'}) \in \mathcal{A}$ such that $t < a_u$ (i.e., the user u is not active yet) or $t > a_u + e_u$ (i.e., the user deadline has already expired).

The considered problem is an extension of the well-known NP-hard OP [B39]. In particular, the problem becomes an OP when i) all the UUs have demand $D_u = 1$, $u \in \mathcal{U}$ (i.e. a user can be served by the UAB in a single travel), and no limits on the available radio resources are imposed, ii) each UU is located in a TP, iii) for each $u \in \mathcal{U}$, $r_{uc(a)} \neq 0$ for only one arc $a \in \mathcal{A}$ (i.e. each UU can be served only by traversing a specific arc), iv) the expiration time of all UUs coincides with the battery duration ($e_u = B$, $u \in \mathcal{U}$), v) all users are active at the beginning of the

time horizon ($a_u = 0$, $u \in \mathcal{U}$), and vi) the UAB has only one allowed speed.

As mentioned previously, the ILP formulation proposed in this thesis is based on the defined space-time graph $\mathcal{G} = (\mathcal{V}, \mathcal{A})$. Two types of binary variables taking into account the served users and the traversed arcs are introduced:

$$y_u = \begin{cases} 1 & \text{if user } u \in \mathcal{U} \text{ is served} \\ 0 & \text{otherwise} \end{cases}$$

$$x_a = \begin{cases} 1 & \text{if arc } a \in \mathcal{A} \text{ is chosen in the UAB trajectory} \\ 0 & \text{otherwise} \end{cases}$$

In addition, to account for a limited number, R, of RBs, the integer variable, w_{au}, representing the number of RBs assigned to user $u \in \mathcal{U}$ along arc $a \in \mathcal{A}$ is also introduced. Hence, the ILP is described as follows.

ILP Formulation:

$$\max \sum_{u \in U} p_u \, y_u \tag{5.13}$$

s.t.:

$$\sum_{a \in \mathcal{A}: s(a) \geq a_u,\ e(a) \leq a_u + e_u} r_{uc(a)} l_a w_{au} \geq d_u y_u \quad \forall\, u \in \mathcal{U} \tag{5.14}$$

$$\sum_{a \in \delta^+_{(\sigma)}} x_a = 1 \tag{5.15}$$

$$\sum_{a \in \delta^-_{(v_{ct})}} x_a = \sum_{a \in \delta^+_{(v_{ct})}} x_a \quad \forall\, v_{ct} \in \mathcal{V} \setminus \{\sigma, \tau\} \tag{5.16}$$

$$x_a \leq \sum_{a' \in \delta^-_{(\tau)}: e(a') - s(a) \leq B} x_{a'} \quad \forall\, a \in \delta^+_{(\sigma)} \tag{5.17}$$

$$\sum_{u \in \mathcal{U}} w_{au} \leq R x_a \quad \forall\, a \in \mathcal{A} \tag{5.18}$$

$$y_u \in \{0, 1\} \quad \forall\, u \in \mathcal{U} \tag{5.19}$$

$$x_a \in \{0, 1\} \quad \forall\, a \in \mathcal{A} \tag{5.20}$$

$$w_{au} \in \{0, .., R\} \quad \forall\, a \in \mathcal{A}, u \in \mathcal{U} \tag{5.21}$$

The objective function (5.13) aims at maximising the number of served users based on their priorities. The constraints (5.14) are the ones imposing the user u to be completely satisfied only fulfilling the demand D_u entirely within the activation and expiration times, and by using the available radio resources. Constraints (5.15) and (5.16) force the selection of a feasible path for the UAB from the source to the sink of $\mathcal{G}$, i.e., the UAB starts from and goes back to H. Constraints (5.17) guarantee that the path ends at τ before expiration of the UAB battery, i.e. the

UAB is able to return to H. In particular, an arc from σ must be selected such that the time difference between the arrival time at τ and the departure time from σ is smaller or equal to the battery duration. Let us note that the formulation depends on T_{h} through $\mathcal{T}$, since vertices of $\mathcal{V}$ are defined for every time instant in $\mathcal{T}$. Constraints (5.18) ensure that no more than R radio resources are assigned simultaneously to users in each time slot, i.e. in each arc $a \in \mathcal{A}$ (note that more resources can be provided to the same user). Finally, constraints (5.19) and (5.20) assure that the variables are binary, and (5.21) ensure the variables w_{au} assume positive integer values between zero and R.

Please note also that, by adding the constraints on limited number of radio resources available (5.18) and (5.21), the algorithm is implicitly optimizing the allocation mechanism via the variable w_{au}. Constraints (5.18) emphasizes the role of the scheduling variable w_{au}, which gives along arc $a \in \mathcal{A}$ more or less resources to user $u \in \mathcal{U}$ for fulfilling its demand, going through the objective function (5.13). Thus, the reader can notice an attempt on (separate) RRM optimization, too.

There are two major issues related to the solution of this model. The first one is that, in real networks, users become active based on which users the TBSs are not able to satisfy. Consequently, information on the activation and expiration instants of the users becomes available in real-time and not a priori. Therefore, not all input data required by the ILP model are really known before starting the flight. The second issue is the size of the space-time graph both in terms of memory needed to store it and for the complexity it implies, which depends on the number of variables and constraints of the ILP model. These issues motivate the development of a heuristic algorithm, still based on the ILP model. Despite these issues, however, the optimal solution of the ILP model can be used as an upper bound to evaluate the performance of realistic algorithms pursuing the optimal performance.

To overcome both issues of the ILP model, the RH heuristic algorithm is developed. It consists in splitting the time axis in N time windows $[T_s^{(n)}, T_e^{(n)}]$ $(n = 1, \ldots, N)$ of duration W, and repeatedly solving for each one a slightly modified version of the ILP model. Thus, in the RH algorithm, the space-time graph is rebuilt for every time window, by considering a time horizon T_{h} equal to W. The constraints that impose the UAB to come back to H at the end of W are removed. This implies that not only vertices corresponding to H are connected to τ, but also vertices corresponding to other TPs, provided that the associated time instant equals the end of the time window $T_e^{(n)}$: this allows the UAB to arrive, at the end of the time window, to a TP different from H. However, to ensure that enough battery energy is left for the UAB to come back to H, only arcs that satisfy

this condition are inserted in the graph. More precisely, in a generic iteration n, the graph $\mathcal{G}_n \subseteq \mathcal{G}$ is built as follows. The source vertex σ of $\mathcal{G}_n$ is only connected to the vertex corresponding to the arrival time instant $T_e^{(n-1)}$ at the TP that was the destination of the UAB in iteration $n-1$, and becomes the starting TP in iteration n ($T_e^{(n-1)} = T_s^{(n)}$). Vertices having time instant $T_e^{(n)}$ are connected to τ. Only vertices whose time instant belongs to $[T_s^{(n)}, T_e^{(n)}]$ are considered, but some of these vertices must be removed to satisfy the battery duration constraint. Let $\bar{B}$ be the residual battery duration: in $\mathcal{G}_n$ there will be no additional vertex v_{ct} (and associated arcs) if it is not possible for the UAB to come back from v_{ct} to H within $\bar{B}$ (i.e. there is no vertex $v_{c't'}$ corresponding to H, such that the time distance from v_{ct} to $v_{c't'}$ is larger or equal to $\bar{B}$). This ensures that the battery duration of the UAB is always enough to reach H.

At iteration $n = 1$, the starting TP is set equal to H, and graph $\mathcal{G}_1$ is built. In this iteration, the source vertex is connected to any vertex representing departure time instants from H. The initial time window $[T_s^{(1)}, T_e^{(1)}]$ is conventionally set to $[0, W]$. The modified ILP is solved on $\mathcal{G}_1$, and the UAB reaches a destination TP denoted as $\overline{TP}$. In the following time window, with $T_s^{(2)} = T_e^{(1)}$ and $T_e^{(2)} = T_s^{(2)} + W$, $\overline{TP}$ is the new starting TP. The procedure is repeated until the UAB goes back to H.

The advantage of this approach is twofold: on one hand, at every iteration, it is possible to dynamically rebuild the space-time graph that has reduced size, leading to a much faster solving time; on the other hand, prior knowledge of the activation and expiration times, and user demands, is only required for the current time window. Therefore, this algorithm better tackles real-life aspects of the considered application.

The set of parameters that are modified with respect to the scenario of previous activities and Table 5.1 are reported here in Table 5.4. To assess the performance of the ILP on this UAV-aided network scenario two metrics are analysed, namely, i) the fraction of served users (that is N_{SU}/U_{tot}, being N_{SU} the number of SUs and U_{tot} the total number of UUs), and ii) the computing time, denoted as T2S (Time to Solve) in seconds. The computing platform used to assess performance metrics is based on a Intel i7-4770S processor with 8GB of RAM. To solve each ILP model during the RH algorithm execution CPLEX v. 12.7.1 was used. Results shown in the following have been averaged over 50 scenarios, where the location of users is fixed but the activation/expiration instants and their demands are randomized, if not stated otherwise.

The UU locations are obtained as outcome of the LTE/5G-like network simulator of [P2] and Sec. 5.1. The Home location coincides with the central TBS.

Table 5.4: Network and Radio Parameters.

Parameter	**Notation**	**Value**
UAB transmit Power	$P_{\text{tx,UAB}}$	8 mW
AtG parameter	β_{atg}	9.6117
AtG parameter	α_{atg}	0.1581
Wavelength	λ_{env}	12 cm
Carrier Frequency	f_{c}	2600 MHz
Area Side	L_{a}	1000 m
Space Step	Δx	100 m
Time Step	ΔT	5 s
UAB Altitude	h	100 m
Number of UUs	U_{tot}	200
Expiration Time	$e_u = E$	$\{60, 120\}$ s for all u
Battery	B	T_{h}
Activation Time	a_u	Uniform[0; $T_{\text{h}}/2$] s
Demand	D_u	Uniform[2; 200] Mbit

A first analysis compares the optimal solution obtained through the ILP in 2hrs of computing time, and RH. Figure 5.22, shows S/O, where O is the offered traffic, given by $\sum_{u \in U} D_u/T_{\text{h}}$. Different values of E are considered with $W = 30$ s for the RH case. As expected, the normalized sum throughput increases with the offered traffic, and an increase of E results in larger sum throughput. Clearly, the solutions obtained by the ILP model are better than those of the RH, but this comes at the cost of significantly longer computing times. Hence, a trade-off between computation time and solution quality forces one to study in more details the RH algorithm by knowing that a 10% gap with respect to the optimal solution is present. One can observe that the RH heuristic obtains a fair trade-off between solution quality and computing time, making it an algorithm that can be used in practical settings.

Now, the results obtained when a different numbers of resources, R, are available at the UAB are compared. Possible values for R ranges from 10 to 50, which are reasonable quantities if one considers that, in the frequency domain, a 20 MHz bandwidth available in an LTE system allows more than 100 theoretical RBs (180kHz each). Results of RH heuristic are shown in Figs. 5.23 by varying the number R of RBs available at the UAB. The outcomes are obtained via RH in terms of fraction of SUs, with E=60 s and E=120 s, respectively. T_{h} is usually

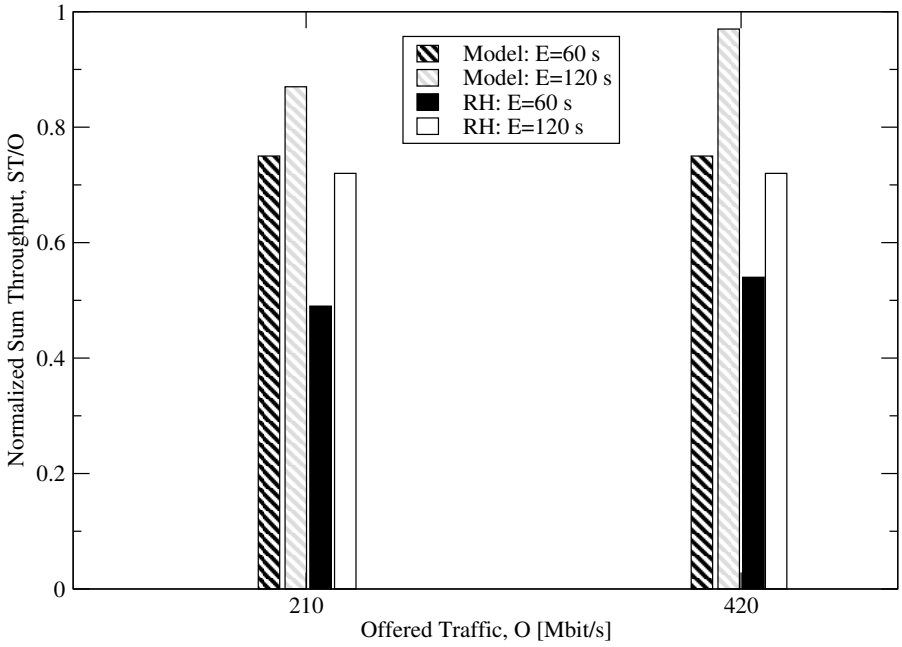

Figure 5.22: Comparison between the model and RH.

fixed to T_{h}=240 s. As expected, the two plots show an increasing performance when using a higher number of resources R. By having R=50 the drone is able to serve more users than the case of R=10. Moreover, both Figures 5.23a and 5.23b show clearly that the fraction of served users increases with W, especially with E=120 s. In fact, the RH algorithm can better optimise the UAB path and the scheduled resources when the network knowledge a priori is wider, since it is able to optimise together the chosen path and the scheduled resources for a longer window. However, when W becomes larger than 25 s, the number of served users *saturates* or even slightly decreases. Although in principle a larger W implies a better knowledge about the future, it also allows the UAB to move farther, possibly letting it reach the borders where the number of users that can be served in the following window is limited. Figure 5.23a shows this trend already from windows of W=15 s and R=10. This happens because for a smaller value of E it becomes more complex to plan an appropriate trajectory that allows the UAB reach the expiring user in time. Also, shorter activation times make the general performance decrease. Moreover, by comparing the same figures another expected trend can be extracted: a larger value of E allows the UAB to serve more users. As one may expect, a higher expiration time of users gives the UAB a better chance to reach them within the allowed time. As long as W increases, the UAB is able to detect an almost expiring UE sufficiently before it disappears.

Figure 5.24 shows the T2S obtained when setting T_{h} = 120 s and E = 60 s.

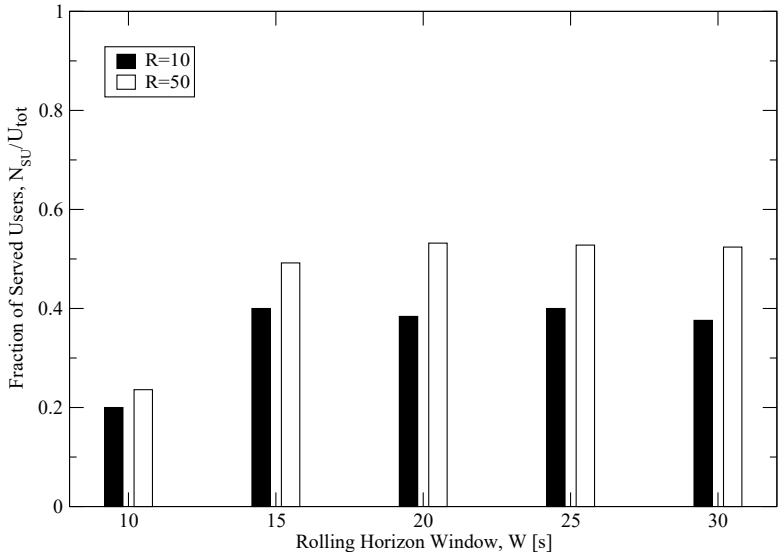

(a) Fraction of SUs for $E = 60$ s.

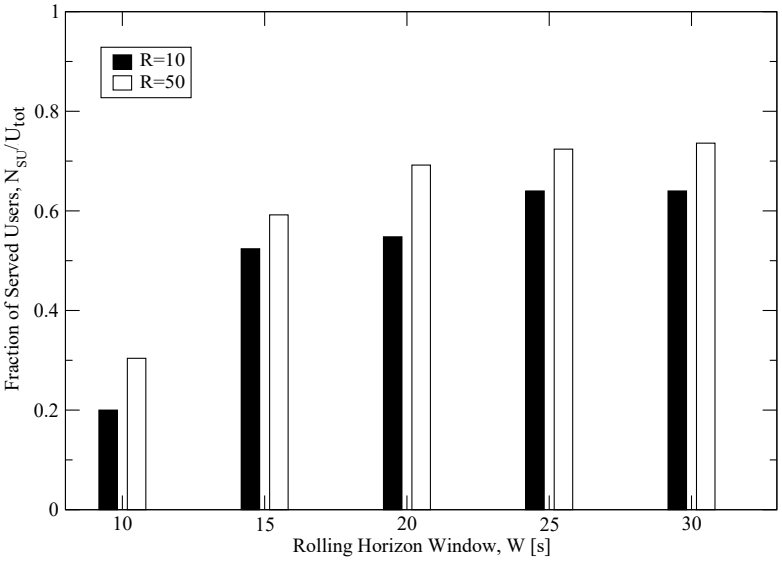

(b) Fraction of SUs for $E = 120$ s.

Figure 5.23: RH. Fraction of Served Users for $T_{\mathrm{h}} = 120$ s, $R = 10, 50$ and varying W.

The T2S diagrams present an exponential increase. This is mainly due to the radio resources factor in the optimization problem, w_{au}, that is an integer value that depends on the number of users (fixed in simulations) and on the number of arcs, which increases with W. This causes the exponential increase of the T2S when getting W larger. However, the behaviour of T2S with $W > 20$ and $R = 10$ is unexpected. This is probably related to the stringent constraint on a larger input instance.

Please note that, in order to maximise the number of users satisfied, the con-

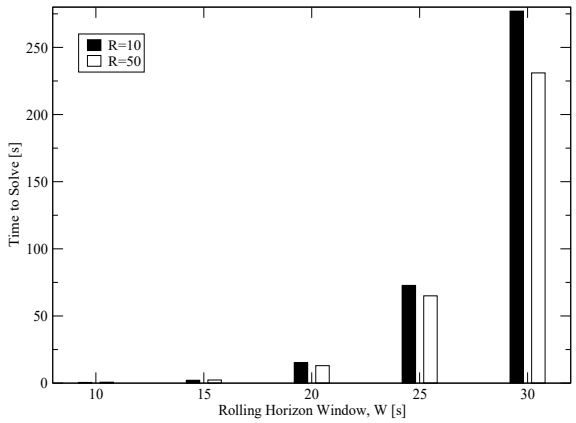

Figure 5.24: RH. Time To Solve for $T_{\mathrm{h}} = 120$ s, $E = 60$, $R = 10, 50$ and varying W.

straint on a limited number of radio resources available forces the algorithm to implicitly optimise the allocation mechanism via the variable w_{au}. In fact, as shown before, the improved performance at the increase of R is the result of an optimised scheduling for users until RBs depletion. However, if R is small, the resource assignment may require a longer computation time, as shown in Fig. 5.24.

Table 5.5: RH. Impact of service priority for $W = 35$ s, $R = 50$.

	$p_u = 1$	$p_u = 2$
Server Users	24%	29%
Not Served Users	26%	21%

Finally, Table 5.5 shows the effect of different priorities given to users. Users priorities, p_u= 1 or 2 are randomly assigned to users (with probability 50% each). Table 5.5 reports the percentage of UUs satisfied or not with the respective priorities for a sample scenario having W=35 s. Though the time window is relatively low, an initial impact of priority is shown: 29% of UUs, from a total of 50% having high priority, are satisfied. In contrast, from the remaining 50% of UUs with low priority, 24% is satisfied. As an effect, the percentage of users remaining unsatisfied is higher for users having low priority.

The comparison between the ILP and RH solutions in terms of computing time, number of served users and sum throughput, shows that the RH algorithm can be considered a good trade-off. Indeed, through the RH approach, it is possible to get, in less than 10 seconds, about 80% of the sum throughput provided by the ILP model in 2 hours over a commercial computing platform.

Chapter 6

UAVs impact on the 3GPP Standard

The practicality of providing connection to users really like an *extended arm* of a BS, makes UABs unveil endless opportunities for new use case scenarios. This unfolds the possibility of employing them in many novel applications, where the cost and efficiency of their use outperform other solutions. Other than new applications for 5G and B5G, UAV-aided systems may introduce significant impacts also on the network procedures involved.

In this Chapter, a number of these applications and protocol procedures are investigated. Firstly, a well-known mechanism like handover (or handoff) will be studied when occurring at the UAB side, and secondly, communications with vehicles and the IoT world are analyzed in two possible use cases. These are diverse application examples which may benefit from the features and scalability of UABs, being therefore an added value to improve the system KPIs. As for the network architecture and channel modelling, the reader can refer to Chapters 3 and 4, respectively.

6.1 Handover

As first, one of the aspects that have a relevant impact on network performance when a UAB is involved, is the handover (or handoff) procedure, as already discussed in [B46]. An handover happens when switching of a service or session between network nodes. The problem from a command and control view point and software defined networking perspective was investigated in [B47]. Furthermore, Authors in [B48] studied the integration of UAVs as aerial users into current and future cellular networks, with an insight on handover costs.

To be specific, here the result of an handover (and later defined Ground-to-Air (GtA) handover) procedure is investigated [P10] for the heterogeneous system introduced in Chapter 5. Thus, the network is composed of both terrestrial infrastructure (i.e. TBSs) and aerial platforms (i.e UABs), and the users requesting service are moving ground nodes who may potentially be served by a TBS or a UAB. For obvious reasons, the handover process is studied to be compliant to 5G and B5G networks. From a high level view, the proposed model requires the consideration of the following three aspects: i) input traffic and its evolution, ii) mobility of both UEs and UABs, iii) radio resource management between the two network tiers.

As done for the activities presented in Chapter 5, the focus lies on the provision of high throughput services to ground UEs having non stringent delay constraints, who are high in numbers and freely move in the considered service area. This work is motivated by the fact that emergency situations (as is a global pandemic) necessitate not only of high quality service but also of seamless operation, especially for efficient smart-working and data gathering.

To keep homogeneous activities, the reference scenario and access networks of the current work are the ones first described in Sec. 5.1. The TBSs shape the first tier of the network, where $|\mathcal{B}|$ TBSs form the set $\mathcal{B}$, and a number $|\mathcal{A}|$ of UABs shape the second tier of the network, forming the set $\mathcal{A}$. These BSs offer their service to users $u \in \mathcal{U}$ making request.

From a high level view, the system shares command and control and data keeping the rationale of [P5, P6] and the analysis reported in Sec. 5.1.4, where a joint network design of the UAB trajectories and RRM is discussed. Concerning network technical procedures, it is possible to refer to 3GPP documentation for the New Radio (NR) and 5G standard. A 5G-like simulator is built on purpose in a MATLAB environment [P10], and new scenario and network parameters are defined in Table 6.1.

As previously mentioned, UABs services are mostly applicable as an on-demand fashion, thanks to their ability to fly just as the need arises. Because of this and their limited speed, services requiring a stringent latency or high reliability cannot realistically benefit from UABs' operation. For this reason, users $u \in \mathcal{U}$ are asking to download a file of size D_u within the maximum waiting time, ΔT_{w}, and a minimum level of throughput, $R_{\min}$. Moreover, a dynamic environment is assumed where users move at a random speed, v_u. Users move according to the random walk model, where a new direction (and a new point in the 2D area) is selected uniformly and randomly such that the user follows a straight line until the new coordinate. If not specified otherwise, the parameter setting corresponds to the

Table 6.1: Scenario and network parameters for Handover heuristic [P10].

Parameter Definition	**Notation**	**Value**
Carrier frequency	f_c	3.5 GHz
Bandwidth	B_w	100 MHz
Spectral efficiency	ξ	20 b/s/Hz
Subcarrier spacing	Δf	30 kHz
Transmit power of TBSs	$P_{tx,TBS}$	36 dBm
Antenna gain of TBSs	$G_{tx,MBS}$	12 dB
Transmit power of UABs	$P_{tx,UAB}$	25 dBm

one shown in Table 5.1.

In this context, it is recalled that the number of UABs present serves the ground users that could not be served efficiently by the TBSs. To trigger the request of UABs' services, it may happen one of the following:

- the number of radio resources assigned by the serving TBS is not sufficient to reach the minimum throughput,
- the TBS-UE link has low SNR $\gamma_{u,b}$, $\gamma_{u,b} < \gamma_{\min}$,
- a switch between serving BSs is requested by the network orchestrator for the joint RRM, via the control plane (more details on this procedure are given later).

UABs within the network fly along dynamic trajectories adjusted based on user positions and needs, which are devised following the minimum cost-cluster principle introduced in [P1, P6] and reported in Sec. 5.1. Following the discussion in [P5] and Sec. 5.1.4, the cost function is set as Eq. (6.1). This determines the cluster having the lowest cost and the next centroid to reach for the interested UAB.

$$C_i = \frac{d_i}{d_{\text{th}}} \cdot \frac{\delta_{\min}}{\delta_i} \cdot \frac{S_{\min}^{(\text{cl})}}{S_i^{(\text{cl})}} \tag{6.1}$$

where the fraction $\frac{d_i}{d_{\text{th}}}$ is the flight distance to the i-th centroid, $\frac{\delta_{\min}}{\delta_i}$ represents the user density (i.e. mean distance of users inside a cluster to their centroid) within the cluster. d_i and δ_i represents the distance of the i-th centroid to the drone and the number of users inside, respectively. d_{th} and $\delta_{\min}$ are normalizing factors with the maximum value of distances and minimum of densities, respectively. Then, the fraction $\frac{S_{\min}^{(\text{cl})}}{S_i^{(\text{cl})}}$ consider the estimated sum throughput obtained in centroid i,

$S_i^{(\mathrm{cl})}$. $S_{\min}^{(\mathrm{cl})}$ is the minimum throughput achievable in the current set of identified clusters. As it can be noted, the cost function is slightly different from the one present in [P5], and follows the discussion related to most relevant cost factors by keeping only the most meaningful ones. This approach determines UABs $a \in \mathcal{A}$ trajectories made of straight segments of different lengths, which are are travelled at constant speed v_a, and altitude h_a from the ground. These values are kept equal for all UABs for simplicity, and therefore it holds $v_a = v, \quad h_a = h \quad \forall a \in \mathcal{A}$. The choice on these two parameters significantly impacts the final network performance. Therefore, the network performance is assessed tuning their values, along with the antenna aperture angle of the UAV. Still, the main focus of this activity lies on the GtA handover algorithm given the position of UAB $a \in \mathcal{A}$ at instant t. The details on the GtA procedure are given in the following.

6.1.1 Handover Procedure

In order to swap from one BS to another, the UE needs to perform an handover. As for 3GPP standardization, the NR performs load balancing through handover and redirection mechanisms upon RRC release command. These are sent by the BS that is currently serving the device (hereby denoted as *serving BS*) to the UE. The network can perform handover within the same RAT (Radio Access Technology) and/or CN (Core Network), or it can involve a change of the two [B38]. As known, the aim of handover procedures is to ensure a connected-state mobility so that connectivity is retained without interruptions and, if any, degradation is negligible as the device moves within the network. The passage from a previously serving cell to a new one has to be as seamless as possible. For achieving it, the device needs to continuously search for new cells both on the current carrier (intra-frequency measurements) and on different carrier frequencies (inter-frequency measurements) it has knowledge of. The mobility of the UEs in RRC_CONNECTED state is controlled by the network (network-controlled mobility). In fact, the device does not make any decisions of its own when it comes to handover. Therefore, the network takes a decision as to whether or not the device is to handover to a new cell. For simplicity, the considered measurements are taken in terms of SNR as evaluation of BS-UE and UAB-UE links, without reproducing all the control signaling involved in the process. Despite this, the handover decision is based on the well-known hysteresis margin, as for real networks.

In more details, the algorithm adopted in performing handover is shown in Algorithm 4. Notations slightly differs from previously, as this algorithm has new variables involved and a specific focus on BSs. First of all, a neighbor base station

Algorithm 4: Handover procedure (single time instant)

Input: User $\{P_u\}_{u=1}^{N_u}$ and TBSs $\{P_b\}_{b=1}^{N_B}$ positions;
SNR of currently serving cell $\{\gamma_u^{(\text{serv})}\}_{u=1}^{N_u}$, H;
Neighbors table $\{\mathbf{M_u}\}_{u=1}^{N_u}$ for each user u;
Output: Next serving cell;
// Repeat this procedure at every time instant;
for $u = 1$ *to* N_u **do**
  Initialize SNR list $\gamma_\mathbf{B}$ for neighboring cells;
  for *each neighbour* $B_i \in \mathbf{M_u}$ **do**
    compute $\gamma_{B_i}^{(u)}$ *// value in dB*;
    append $\gamma_{B_i}^{(u)}$ to $\gamma_\mathbf{B}$
  end
  $\gamma_{\text{best}} \leftarrow \max(\gamma_\mathbf{B})$;
  if $\gamma_{\text{best}} > \gamma_u^{(\text{serv})} + H$ **then**
    // B_i changes;
    $B_i \leftarrow \arg\max_B(\gamma_\mathbf{B})$;
    $\gamma_u^{(\text{serv})} \leftarrow \gamma_{\text{best}}$
  else
    // B_i does not change;
    $B_i \leftarrow B_i^{(\text{serv})}$
  end
  return: B_i;
end

table has been created, with a list of six neighbors per BS. Secondly, for every user and each neighbor included in the list, the SNR is computed. Then, the higher SNR between the neighbors, γ_{best}, is compared to the SNR of the link of the serving BS, $\gamma_u^{(\text{serv})}$ (i.e., where the UE is camping). A hysteresis value H is added at this point, expressed in dB, in order to avoid the well-knwon *ping pong* effect. If the equation is not satisfied the users will keep camping on the current serving cell. On the contrary, the cell offering the best SNR becomes the serving one.

$$\gamma_{B_i}^{(u)} > \gamma_u^{(\text{serv})} + H \tag{6.2}$$

In case of multiple UABs, $\gamma_{B_i}^{(u)}$ can be the SNR registered for B_i being either a TBS or a UAB. The same is true for $\gamma_u^{(\text{serv})}$. Therefore, one from four options may occur: i) Handover from one TBS to another TBS ii) Handover from one TBS to a UAB iii) Handover from one UAB to another UAB iv) Handover from one UAB to a TBS In this work, the focus lies mainly on the second case, since it is the most relevant

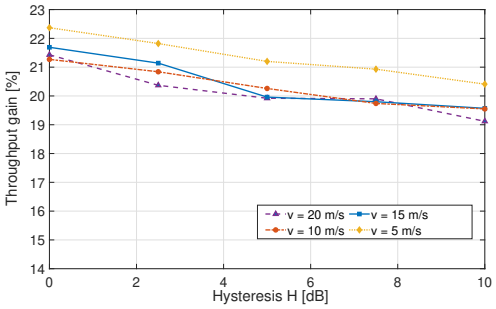

(a) Throughput gain varying speed.

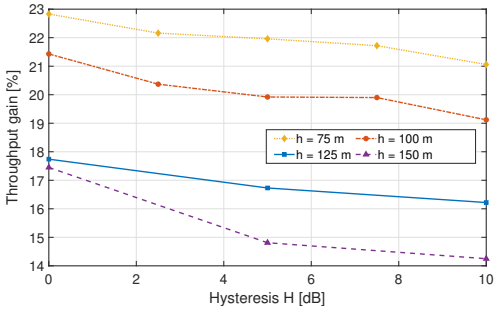

(b) Throughput gain varying altitude.

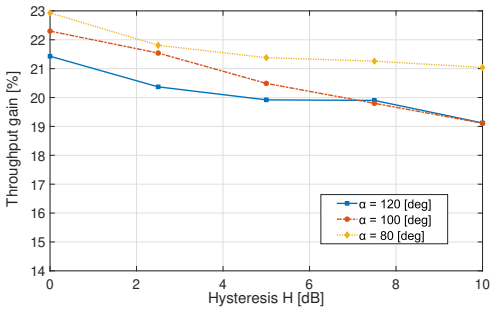

(c) Throughput gain varying aperture angle.

Figure 6.1: Performance results given handover procedures in different hysteresis level [P10].

in highlighting impacts, challenges and trade-offs of UAV-aided networking. This is motivated by the fact that an analysis on the number of handovers, denoted GtA, can extract the usage of UABs in future wireless networks. Algorithm 4 shows the procedure followed to determine in a time instant if one handover has to take place or not. From Algorithm 4, the total number of handovers of the different types can be retrieved. In fact, it is only required to identify which kind of base station (i.e. TBS or UAB) are both B_i and $B_i^{(\text{serv})}$.

6.1.2 GtA Handover Remarks

The numerical results reported here are obtained through a dynamic simulator, first described in Sec. 5.1, and properly updated. The mean throughput gain, G, achieved over a service time T_h, is computed following Eq. (5.7).

In order to account for an average number of handovers occurred throughout the entire service time T_h, rather than the total number of handovers, the following is studied:

$$O_m = \frac{1}{U_{tot}} \sum_{i=1}^{U_{tot}} \frac{1}{T_h} \sum_{t=1}^{T_h} \mathbb{1}\left(B_i(t) \neq B_i^{(\text{serv})}(t)\right) \tag{6.3}$$

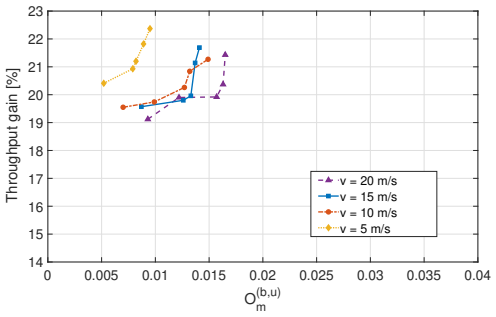

(a) Throughput gain varying speed.

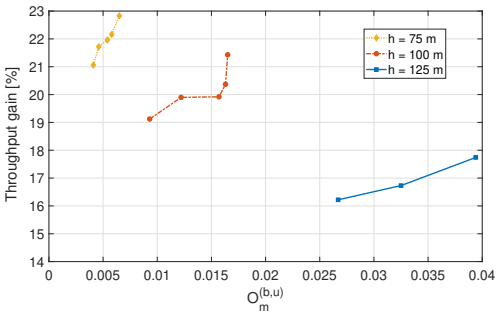

(b) Throughput gain varying height.

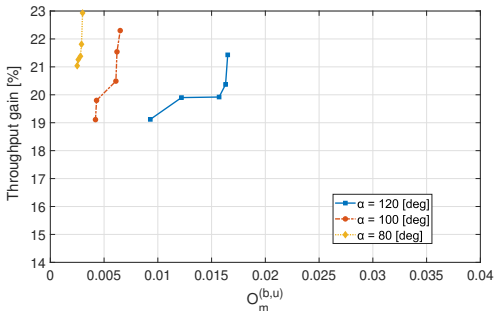

(c) Throughput gain varying aperture angle.

Figure 6.2: Performance results for different mean handover number and $H = 5$ [P10].

and, once it is specified to specifically account for GtA handovers:

$$O_m^{(b,a)} = \frac{1}{U_{tot}} \sum_{i=1}^{U_{tot}} \frac{1}{T_h} \sum_{t=1}^{T_h} \mathbb{1}\Big(B_i(t) \neq B_i^{(\text{serv})}(t), \; B_i(t) \in \mathcal{A}, B_i^{(\text{serv})}(t) \in \mathcal{B} \Big) \tag{6.4}$$

In Eq. (6.4) $\mathbb{1}$ is the indicator function, and $B_i(t)$ and $B_i^{(\text{serv})}(t)$ are the next and currently serving base station, respectively, as stated in Algorithm 4. In this way, the number of GtA handovers are counted and averaged over time and the total number of users. If not set to change, in Figs. 6.1 and 6.2 the default values are $h = 100$ m, $v = 20$ m/s, $\alpha = 120$ degrees.

Figures 6.1 represent the level of throughput gain achieved for different hysteresis H values. As expected, for all curves the gain G is decreasing when incrementing the value of H. In fact, an increased hysteresis level avoids a sudden switching of a link that could undergo the ping pong effect. Moreover, due to the random movement of users, a smaller value for the UAB speed guarantees better results as shown in Fig. 6.1a. In particular, speeds of 10 m/s and above have a similar performance in average, and results improve with a speed as lower as 5 m/s. Furthermore, there

is a monotonic increase in system throughput with a decreasing in UAB height and antenna aperture angle, as represented in Figs. 6.1b, 6.1c. This is probably due to the presence of multiple UABs. In fact, if the number of BSs present in the service area is increased, each single one has a better service to underlying users if the transmitting antenna gain is higher and, consequently, the non-interfering resources are higher in number because the UAB footprint is smaller (see Sec. 5.1.4).

In summary, these results show that, to improve network performance, the system should make UABs: i) fly low, ii) fly slowly, iii) have antenna systems not too directive. Please note, these results are quite different with respect to previous works [P5, P4]. In fact, this proves that, other than a quite different scenario, the GtA handover has a noticeable impact on the overall network performance (e.g., sum throughput) with respect to previous works and changes the system parameters (as UAB height, speed, antenna system) trade-off previously known. Therefore, from a network operator perspective, the consideration of these network procedures is relevant and should not be neglected.

Figures 6.2 show the network performance in terms of throughput gain, G, when the hysteresis level H is fixed, $H = 5$, and the average number of handovers, $O_m^{(b,a)}$, from a TBS to a UAB is in the abscissa. From a high level view, there is an expected monotonic decrease of the different curves of throughput versus the number of handovers, having them placed on the *secondary diagonal* of the plane. In fact, this is what Figs. 6.2 show. There is compliance between the two sets of plots in Figs. 6.2 and 6.1, because an increase of the hysteresis level corresponds to a decrease in the number of applied handovers. Thus, one can see the throughput decreasing when increasing both the hysteresis level and the average number of GtA handovers. Furthermore, it is interesting to note that some are step-curves, meaning that only certain values of the parameters under investigation (e.g. speed, height, aperture angle) change significantly the value of $O_m^{(b,a)}$. Please note, however, that a larger $O_m^{(b,a)}$ reflects a larger number of ground users served by a UAB rather than a TBS. This fact, in some cases, increases the value of G thanks to the augmented service quality the UAB can offer to users (as already discussed thoroughly, thanks to its vicinity and the most likely LoS links).

This work has proposed a UAV-aided network model on where to consider deeply the possible problematic or advantages introduced by an handover procedure. In fact, a ground user may need to perform handover between an aerial base and a terrestrial one or vice-versa (from which, the term of GtA handover), or between bases of the same type. The analysis on how much and with which parameters more GtA handovers occur helps MNOs planning.

6.2 UAVs communication with Vehicles

The transport system is one of the fields expecting the greatest changes in the next decades. Human-driven cars and trucks will be progressively replaced by Connected and Autonomous Vehicles (CAVs), promising safer mobility, more efficient traffic management, significant pollution reduction, and the availability of new services for passengers.

Focusing on connectivity, for several years IEEE 802.11p and the related standards had been the main solution for the vehicular environment [B49]. Starting from 2016, however, 3GPP has introduced the concept of Cellular-Vehicle-to-Anything (C-V2X), which specifically addresses this sector within LTE, 5G, and beyond [B50, B51, B52]. In C-V2X, long and short-range communications are parts of the same framework, with the promise of a single chip-set, a native involvement of vulnerable users, and a long term support from the entire cellular ecosystem. Regarding the applications envisaged for the vehicular scenarios, often denoted as use cases, a large list has been presented for what are called the Day-1 or Day-1.5, which are in principle supported by both IEEE 802.11p and the first versions of C-V2X and are based on the unidirectional distribution of information to improve context awareness; emergency vehicle warning, stationary vehicle warning, and roadworks warning are just a few examples [B53, B54, B55]. Recently, 3GPP has started a discussion about advanced use cases, where vehicles do not only share basic information about their status through small packets, but also exchange large messages and interact in order to coordinate their actions. Such applications have challenging requirements in terms of wireless capabilities that are hardly guaranteed by current standards [B56]. One relevant example is extended sensing [B57]; by allowing a collective perception of the environment, it implies the need for data rates that range between 10 Mbps to 1 Gbps within a limited range [B56].

Although connected vehicles are often associated with the capability of short-range wireless communications, it is clear that it will take time before all cars are equipped and that the long-range connection guaranteed by cellular base stations must be viewed as a valuable option at least during this transitory. However, providing an ubiquitous and reliable coverage to vehicles is particularly challenging with TBSs, since the density and distribution of vehicles is significantly variable in both time and space, in ways that are not always easy to predict.

In a scenario where the penetration of cars equipped with wireless communication devices is far from 100% and the requirements tend to be challenging for a cellular network not specifically planned for the vehicular scenario, the use of an UAB, carrying a mobile base station, could be helpful to fill the gap of short-range

connections and address unpredictable traffic distribution in space and time. UABs are vehicles themselves, with the peculiarity of much less constraints in both mobility patterns and mechanical design. Trajectories can be accurately planned for one or even joint purposes, and the UAVs can be different in size and computational power depending on the tasks they have to pursue.

In this work, C-V2X users are moving in an urban area and request to be served by the network. To this purpose, a number of TBSs are deployed in the area and one UAB is launched to support the TBSs in the service provision.

Equipping vehicles with wireless communication devices to implement advanced services on the road has been studied for decades and standards today appear mature for large scale deployment [B58]. However, given their critical impact on road safety and the need that the various car-manufacturers agree to common technologies, still a small percentage of vehicles is presently connected, normally relying on long-range cellular coverage and providing services that are limited to entertainment [B59, B60] or vehicle tracking [B61].

It is anyway generally believed that CAVs will come to market in the next few years and this represents an enormous opportunity for all companies directly or indirectly involved. In this context, the cellular ecosystem started to think about protocols and services for LTE and 5G specifically devoted to the vehicular environment. Beginning even before first definitions inside the standards in 2016, much effort has thusfar being devoted to C-V2X [B62]. Many activities actually focus on short-range communications [B63], which is expected to minimize the delay and guarantee a high spatial reuse, but it is clear that long-range communications will always play a relevant role, especially until the percentage of equipped vehicles will be limited [B64]. When dealing with long-range communications, however, it appears very challenging to combine a fixed deployment of base stations with stringent requirements of a significantly variable and possibly huge data traffic, which is presumable for vehicles that might be sparse or very dense in different parts of a city or at different times of day [B65].

The use of UAVs to support vehicular communications has recently raised significant attention as an efficient, flexible, and limited cost solution when the deployed infrastructure is not sufficient or in case of particular events. The majority of works investigate the use of UAVs to improve routing in vehicular networks. For example, in [B66] a novel reactive algorithm exploiting UAVs as relays is suggested when the capacity or coverage becomes insufficient. In [B67], drones are used with store and carry capabilities when disconnections occur due to a low density of vehicles. Also in [B68], routing is addressed, with the use of game theory to predict disconnected segments where UAVs should be moved.

A broader view about using UAVs in vehicular scenarios is provided in [B69, B70]. In [B69], various possible applications are discussed, including flying accident report agents, flying Road Side Units (RSUs), flying speed cameras, flying police eyes, and flying dynamic traffic signals. In addition, some simulations are reported assuming a number of UAVs statically deployed as RSUs to improve the coverage of hazardous areas where accidents occur with some probability. A list of issues and advantages deriving from the use of drones in the vehicular scenario is instead provided in [B70].

Testbeds with few devices have been also implemented in [B71]. Experiments with two UAVs and three vehicles forming a platoon are conducted, where the drones are exploited to monitor the surrounding territory where the convoy is moving. In that case, IEEE 802.11a and ZigBee are adopted for data and control messages, respectively. Preliminary results demonstrate the feasibility to use drones to cooperate with vehicles. In the majority of cases, IEEE 802.11p or another WiFi-related technology is assumed and in none of the mentioned works the cellular standards are explicitly addressed. Furthermore, most results refer to generic applications and the focus is on routing or coverage aspects. Finally, only in a few cases the movements and trajectory of UAVs are investigated. Differently, this thesis considers a system where an aerial and terrestrial component cooperate to provide the desired quality of service of the extended sensing application, by taking into account all network related aspects.

A rectangular area with a set $\mathcal{B}$ of BSs is considered, where in each site are placed four directional TBSs (see Figure 6.3). The service provider designated a UAB to support the network on-demand. The UAB starts its flight from one of the TBS sites, then, its dynamic trajectory is computed. The path planning follows the general design studied so far for an heterogeneous system (see Sec. 5.1).

In the considered scenario, a number of vehicles move according to traffic traces reproduced using the micro-traffic simulator VISSIM [B72], which reproduces in detail the movements of vehicles taking into account the real road map, physical laws and the road rules.

Among all vehicles $v \in \mathcal{V}$ vehicles, a portion P_v of them is active (i.e. requesting for service) and equipped with C-V2X devices. Further, the application requirements are set to be coherent with the 3GPP documentation [B56] on the extended sensing use case, which defines a range of data rates between 10 Mbps to 1 Gbps. The focus of this activity is on the downlink only, by setting requirements of either 25 Mb/s or 50 Mb/s. This choice has been made because the downlink becomes a bottleneck for the network when the same sensing information collected from one vehicle has to be forwarded in broadcast to all the interested neighbors.

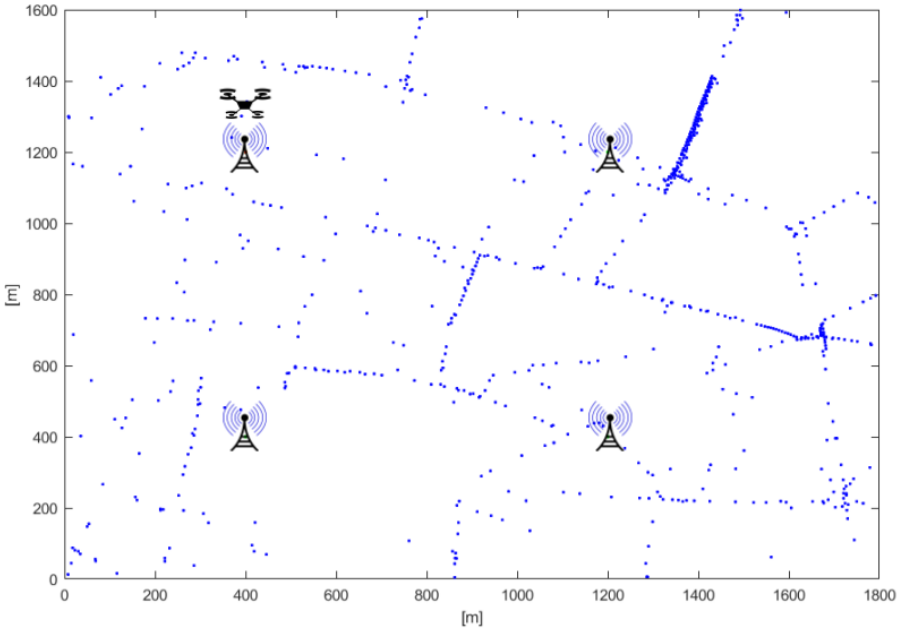

Figure 6.3: Reference scenario for C-V2X services: dots represent vehicles in a given simulation snapshot [P7].

As far as the radio interface is concerned, an LTE scenario is considered (via using OFDMA for downlink, as per Table 5.2) where vehicles are using C-V2X technology. If different from the settings in Table 5.1, Table 6.2 shows the parameters related to this C-V2X scenario. Both the TBSs and the UAB operate within the same carrier of 2600 MHz and have the same RBs availability. Propagation in both terrestrial and aerial tiers is computed as detailed in Chapter 4.

The terrestrial and aerial components compute the SNR and SIR of the different links to take decisions on RRM. In order to achieve a satisfactory quality of service, SNR and SIR for the single vehicle u have to overcome a minimum threshold of $\gamma_{\text{min}} = 10$ dB and $gamma^{\text{I}}_{\text{min}} = 2$ dB, respectively.

As before, the intervention of one UAB is due to an insufficient service quality from the terrestrial network, resulting in a low number of served vehicles. Therefore, the system model, channel modelling, RRM and trajectory design follows the algorithm and findings of [P6, P5], reported in Sec. 4.1 and 5.1.

The RRM is performed by a high level entity that jointly supervises both the TBSs and UAB (namely, the MANO as introduced in Ch. 3). For any vehicle that can be served by both the TBSs and the UAB, the one providing the highest throughput is chosen, and Algorithm 5 is reported for simplicity (taken from Algorithm 3).

At first, the values of SNR and SIR of a vehicle towards its closest TBS are computed; the same computation is repeated for the link of the vehicle with the

Algorithm 5: Radio resource scheduling applied to C-V2X applications [P7].

Data: UAB and TBSs positions, vehicle positions and data-rate demand, channel modelling (Sec.4.1), $\gamma_{\min}$, $\gamma^{\mathrm{I}}_{\min}$, TBSs and UAV resource pool capacity

Result: Set of served and set of unserved vehicles

for *each RRM interval* **do**
  for *each vehicle u in the scenario* **do**
    compute SNR and SIR of u to closest TBS, $\gamma_{u,b}$ and $\gamma^{\mathrm{I}}_{u,b}$;
    compute SNR and SIR of u to the UAV if in the coverage range, $\gamma_{u,a}$ and $\gamma^{\mathrm{I}}_{u,a}$;
    if $\gamma_{u,a} > \gamma_{min}$ *AND* $\gamma^{\mathrm{I}}_{u,a} > \gamma^{\mathrm{I}}_{min}$ *AND RBs required* $<$ *pool capacity* **then**
      if $\gamma_{u,b} > \gamma_{u,a}$ *AND* $\gamma^{\mathrm{I}}_{u,b} > \gamma^{\mathrm{I}}_{min}$ **then**
        $\gamma_u = \gamma_{u,b}$ and $\gamma^{\mathrm{I}}_u = \gamma^{\mathrm{I}}_{u,b}$ (u is served by the TBS);
      else
        $\gamma_u = \gamma_{u,a}$ and $\gamma^{\mathrm{I}}_u = \gamma^{\mathrm{I}}_{u,a}$ (u is served by the UAB);
      end
    else
      if $\gamma_{u,b} > \gamma_{min}$ *AND* $\gamma^{\mathrm{I}}_{u,b} > \gamma^{\mathrm{I}}_{min}$ *AND RBs required* $<$ *pool capacity* **then**
        $\gamma_u = \gamma_{u,b}$ and $\gamma^{\mathrm{I}}_u = \gamma^{\mathrm{I}}_{u,b}$ (u is served by the TBS);
      else
        u is not served;
      end
    end
  end
  compute Round Robin algorithm for scheduling at the TBSs;
  compute Round Robin and Proportional Fair algorithm for scheduling at the UAB;
end

Table 6.2: Mobile network parameters adapted to C-V2X application consideration [P7].

Parameter	**Notation**	**Value**
Rectangular service area	A	1.8×1.6 m^2
Average number of vehicles in the scenario	$\lvert\mathcal{V}\rvert$	600
Number of TBSs in the area	$\lvert\mathcal{B}\rvert$	16
TBSs equivalent radiated power	$EIRP_{\text{tx,TBS}}$	43 dBm
UAV transmit power	$P_{\text{tx,UAB}}$	20 dBm
Single carrier UAV and TBS	$f_{\text{c,TBS}} = f_{\text{c,UAB}}$	2600 MHz
Bandwidth of TBSs	B_w	[5–20] MHz
UAB speed	s	20 m/s
UAB altitude	h	120 m
UAB antenna aperture angle	α	120 deg

UAB. If both values of SNR and SIR are above the corresponding threshold, the interested base station checks if the vehicle request does not exceed the RBs remaining capacity. Then, when these three requirements are satisfied, a vehicle can be considered served. If the vehicle is also in the coverage range of the UAB, it will be served by the station providing the higher SNR value between the TBS and the UAB. In this way, the UAB both serves vehicles unsatisfied by the terrestrial network, and improves the QoS of the others. Via the interference avoidance, the co-channel interference that the UAB can cause to the vehicles served by a TBS can be neglected and it does not influence the TBS normal operation.

As part of the applications related to previous studies, the design of the UAB trajectory follows a number of rules to ensure an efficient operation, and is determined by approaches of [P1, P5], and re-adapted to the vehicular scenario. In particular, the path planning was defined according to a number of factors: the position of vehicles, their application requirements, the traffic density and the sum throughput estimation based on the resource pool capacity. Therefore, Algorithm 2 already presented the procedure applied for the UAB trajectory. Also, the cluster cardinality $|\mathcal{K}|$ has been properly adapted to the scenario; the hierarchical UP-GMC algorithm selects a number $|\mathcal{K}| = P_v \cdot 100$ (e.g., 10 clusters for 10% of active vehicles, 20 clusters for 20%, etc.).

Now, to pursue system efficiency, the cost function design should include parameters such as the UAB energy consumption, its RB availability and the number of users that could be served in one spot. For these reasons, the travel distance,

the estimation of network throughput and the density of vehicles are the factors affecting the cost function, which is defined as

$$C_i = \frac{d_i}{d_{\text{th}}} \cdot \frac{\delta_{\min}}{\delta_i} \cdot \frac{S_{\min}^{(\text{cl})}}{S_i^{(\text{cl})}} \tag{6.5}$$

where the parameters have been already defined for Eq. (6.1). The rationale behind the cost function is to jointly give priority to a region near to where the UAB is present, to a cluster with a large number of vehicles, and to enhance throughput.

Results are presented with two different KPIs, being the throughput gain, G, (see Eq. 5.7) and the actual percentage of vehicles served either by the terrestrial or aerial network. Then, the system is tested under the application requirements of 25 and 50 Mb/s of data rate, in compliance with extended sensing. Figure 6.4 shows the gain, G, while increasing the percentage of active vehicles, P_v. A number of curves were introduced having different bandwidth values, which means a RB pool was changing in size. The bandwidth dedicated to the vehicular service is of 5, 10, 15 or 20 MHz. Figure 6.4a,b refer to 25 Mb/s and 50 Mb/s, respectively.

In each curve of Figure 6.4 the gain, G, has a decreasing trend while increasing the number of active vehicles in the scenario. This can be easily explained by the fact that the TBSs are using a higher number of RBs as the traffic demand increased; due to the common resource pool, the UAB has consequently a lower number of RBs still left available. The network response to an increased offered traffic, sees the bandwidth (i.e., RB pool capacity) reserved for vehicular applications increase, and the UAB capability decrease. A larger system bandwidth allows the UAB to keep the gain close to 10%, yet serving a higher number of active vehicles. Therefore, the overall bandwidth should be kept larger if willing to keep the UAB service sustainable. Moreover, the values of the gain G in Figure 6.4a differ from the corresponding ones in Figure 6.4b. In the former plot, the values of G for the 10% of active vehicles range from a 20% to almost 120%, whereas half of such values can be observed in the latter. This can be explained in terms of availability of resources, too. In Figure 6.4b the application demand from vehicles is doubled w.r.t. Figure 6.4a, requiring then double the number of resources from TBSs and the UAV to serve each vehicle. This means that, not only the TBSs employ more resources subtracting them from the UAV pool, but also a lower number of vehicles will be served (see also Figure 5.18). Furthermore, note that, when considering the transitory in which a few of the travelling vehicles are equipped with C-V2X devices, these results are relevant. In fact, a single UAB is capable of providing up to 100% gain with the proposed approach, even with reuse factor of one. When a larger number of vehicles is equipped with C-V2X services, the probability that

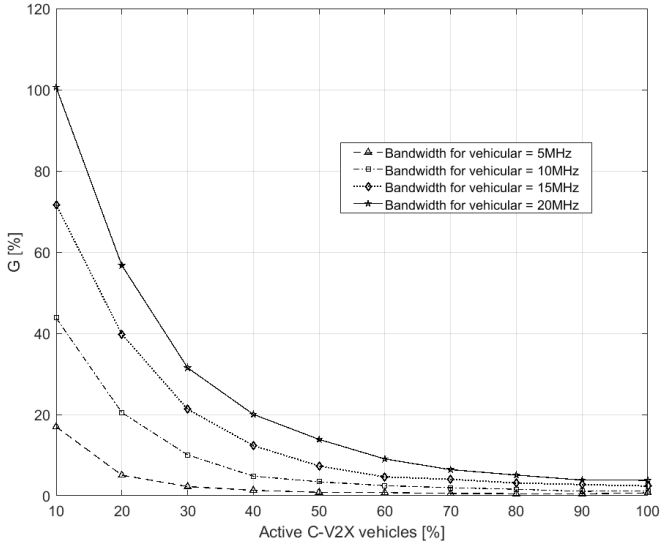

(a) Traffic demand for C-V2X services set to 25 Mb/s.

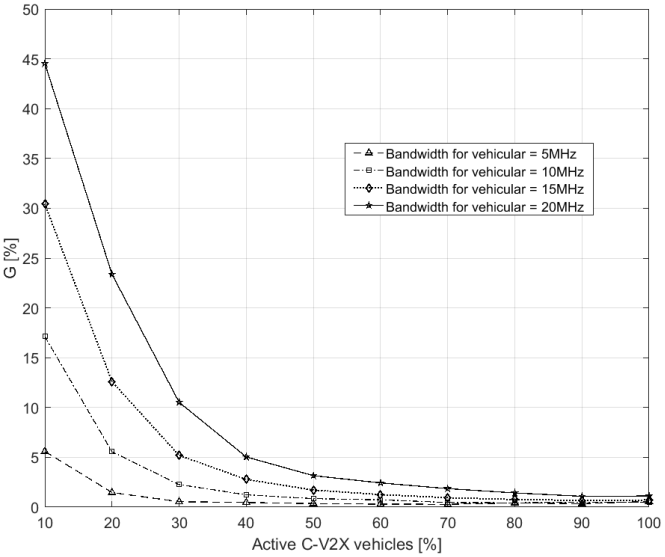

(b) Traffic demand for C-V2X services set to 50 Mb/s.

Figure 6.4: Obtained gain for different bands while varying the number of active C-V2X vehicles, $|\mathcal{V}| \cdot P_v$, in the network [P7].

two vehicles are close enough to each other and can share useful nearby information with the short range dedicated communication in the 5.9 GHz band increases. For this reason, it is still acceptable that the gain in network throughput offered by the drone remains at 5% to 2% (i.e., in absolute numbers, it is in the order of hundreds of Mb/s).

For the second set, Figure 6.5 shows the number of vehicles served by the entire network while increasing the number of active users. Two plots are shown when the traffic demand has 25 Mb/s (Figure 6.5a) and 50 Mb/s (Figure 6.5b) throughput requirement. Different curves for three different bandwidth sizes of 5, 10 and 20 MHz are shown. For each dedicated band, two curves differentiate the network behaviour with or without the presence of one UAB. A similar trend can be seen for both Figure 6.5a,b: when the number of vehicles asking the network service increases, it becomes more probable that TBSs or the UAB have not enough RBs to serve them. If the percentage of satisfied vehicles does not reach 100%, this is due either to SNR or SIR under the respective thresholds. As happened with the gain, G, the larger is the number of active vehicles, the larger is the probability that RBs available are not sufficient. The UAB, in average, becomes especially effective when the active vehicles are below 50%. Being interested in supporting the network in the initial phase when few vehicles are able to communicate, these results are promising. In particular, with a bandwidth size as large as 20 MHz, the advantage of including one UAB reusing the same RBs as TBSs proves to be an interesting choice even at a later stage. As expected, the different needs of resources in the two cases make the network serve 68% of vehicles in Figure 6.5a and 50% of vehicles in Figure 6.5b in the best case (i.e., 20 MHz band) when 100% of them is active. For developing the novel concept of UABs working alonside the terrestrial network to serve vehicles by using the C-V2X technology, a number of key concepts have been introduced. To this aim, this work: (1) defines vehicular applications requirements compliant to 3GPP documents; (2) applies an RRM technique that ensures network efficiency; and (3) adapts the trajectory design to the specific vehicular use case. Simulation results show that, in particular for the initial phase in which few vehicles are equipped with C-V2X devices and should interface with the LTE network, the proposed system model is promising. A single UAB increases the number of satisfied users of up to 10%. The scenario becomes critical when the number of vehicles asking for service is significantly larger w.r.t. RBs availability and interference avoidance does not allow the UAB to leverage on a sufficient number of resources. Nonetheless, in the considered scenario, if the bandwidth reserved for vehicular applications is above 10 MHz and the throughput requirement is not much larger than 25 Mb/s, one UAB can efficiently enhance

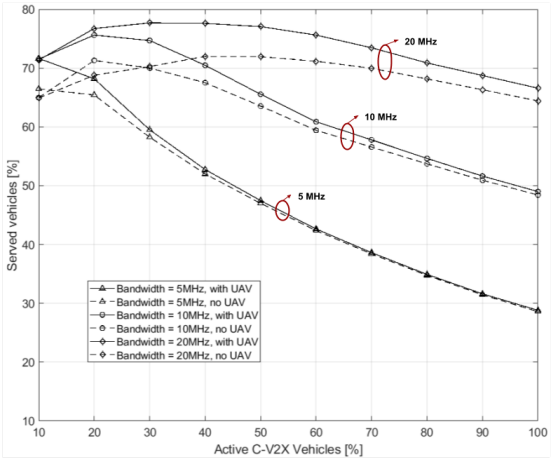

(a) Traffic demand for C-V2X services set to 25 Mb/s.

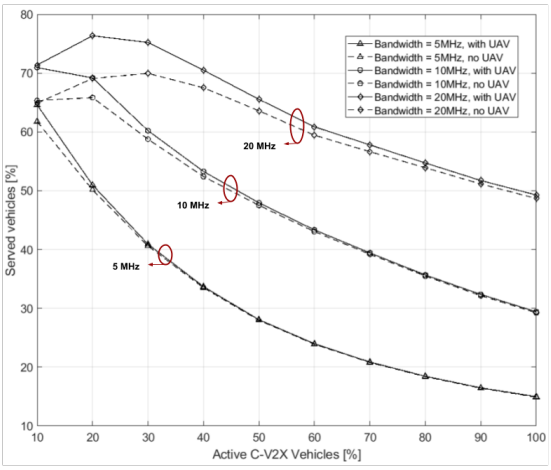

(b) Traffic demand for C-V2X services set to 50 Mb/s.

Figure 6.5: Percentage of served vehicles for different bandwidths and varying the number of active C-V2X vehicles, $|\mathcal{V}| \cdot P_v$, in the network [P7].

network performance even when 100% of vehicles are active. When this is not the case, for example when small bandwidths such as 5 to 10 MHz are analyzed and the number of active vehicles grows above 50%, it happens that the resource availability at the UAB becomes rather scarce (being it shared with TBSs) to cope with the traffic demand. Thus, the UAB should be employed when the bandwidth and resources are enough to sustain the local RBs reuse proposed by this approach.

As a final remark, UAVs employed with C-V2X capabilities can be considered as vehicles themselves employing short-range communications. In this way, especially for extended sensing applications, one may envision communications from a vehicle to the UAB to another vehicle in the dedicated 5.9 GHz band, then back to the network (if needed) through LTE.

6.3 UAV-Aided NB-IoT Networks

Statistical reports[1] demonstrate the steady increase of the number of the machine-type connectivity links happening every year, and predict the further increase of its pace. However, not only an increase of the IoT device numbers and their traffic represents a major challenge for the future. Another key challenge still to be addressed is the increase of the requirements for communication performance - the demand - imposed by the various applications and use cases (including, e.g., autonomous vehicles, Industry 4.0, and wearables). Both these trends call for a new paradigm to networks design. One possibility will be to apply densification, that dramatically increases the number of TBSs deployed. However, this will inquire substantial investments and will introduce extra energy consumption, which is already huge[2].

As discussed thoroughly, one possible alternative is to use mobile BSs, denoted in the thesis as UABs, providing service where and when needed to cope with peaks of traffic demand. UABs are particularly interesting since they are not tied to roads, not affected by traffic congestion and can feature good connectivity with both, on-ground users, and TBSs (i.e., backhaul), thanks to the large probability of being in LoS.

Differently from the other applications discussed in this thesis, the work intro-

[1] See, e.g., https://www.statista.com/statistics/802690/worldwide-connected-devices-by-access-technology/ or https://www.ericsson.com/en/mobility-report/reports/november-2019/iot-connections-outlook .

[2] https://www.gsma.com/futurenetworks/wiki/energy-efficiency-2/, https://www.ericsson.com/en/blog/2019/9/energy-consumption-5g-nr, https://www.mdpi.com/2071-1050/10/7/2494/pdf.

duced in this section involves highly predictable and usually fixed in given positions UEs, being machine-type nodes of the IoT world.

Being the IoT devices, which are usually programmed to monitor or collect data, static, their position does not change in time. Hence, their location is known, or can be made known easily through learning or discovery. Moreover, the traffic they generate can usually be predicted (e.g, due to its periodic nature). The knowledge of these two basic inputs allows the UAB to make decisions in advance on the trajectory to follow to serve as many IoT devices as possible.

One of the key mobile technologies that will be used in the coming years with the advent of 5G is Narrowband IoT (NB-IoT). NB-IoT takes the same numerology as 4G (and, possibly, 5G), and therefore perfectly fits with a UAB implementing Evolved/Next Generation Node B (eNB/gNB) functionalities. However, the NB-IoT technology, adapted specifically for the IoT requirements, substantially differs from conventional LTE.

For this reason, this activity studies the network performance of a UAB flying over groups of NB-IoT nodes, taking into account the access mechanism, the time frame structure and the resource allocation schemes as they are specified by 3GPP. In particular, the network performance is tested on the following parameters:

- NB-IoT frame structure in the uplink (UL),
- Transmitted packet size,
- NB-IoT nodes density and distribution,
- UAB speed while completing its trajectory.

Differently from the many literature works reported in Chapter 2, this activity conforms to specific protocol constraints, practicalities and signalling structure as it is in 3GPP standards.

Furthermore, the impact of nodes having a given activation time (randomly distributed) and a given expiration time, that imposes a maximum delay within which they have to be served, are considered. On the contrary, the above cited works assume users are active for the entire flight and no activation and expiration times are addressed.

6.3.1 NB-IoT overview

The initial version of NB-IoT technology addressing the needs of the massive machine-type communication (mMTC) applications has been standardized by 3GPP as a part of release 13 in 2016 with new functionalities introduced in the subsequent

releases. The NB-IoT technical solution originates from the LTE technology, which has been substantially simplified and re-worked to reduce the overheads, minimize complexity, cost and consumption, and maximize the possible communication link length. The NB-IoT technology features substantial flexibility allowing to deploy the NB-IoT cell by rolling a software update on top of an already existing LTE cell. An NB-IoT cell may be deployed standalone in a dedicated frequency band, use the LTE guard bands or even operate in-band with LTE or LTE-M.

The conventional media access procedure of a NB-IoT User Equipment (UE) operation is composed of a number of steps. First, a UE scans the channels for the synchronization signals. Once synchronized to the cell base station (i.e., the eNB), the UE obtains first the Master and then a set of Secondary Information Blocks (MIB and SIBs, respectively), containing all the relevant information about the network, the cell, and its resource allocations. To connect to the cell, the UE has to go through the procedure of random access (RA), the initial phase of which is the transmission of an access preamble during one of the periodic random access windows. In this activity, the UE randomly selects the preamble to be used. Following the transmission of the random access preamble, the resources for the UL and downlink (DL) transmissions are scheduled by the cell eNB with data integrity insured through the Hybrid Automatic Repeat Request (HARQ) processes.

Before Release 15 introducing time division duplex (TDD) operation mode, the frequency division duplex (FDD) mode was the only option for NB-IoT. In this activity the latter is considered, since it is the primary mode used in most commercial networks and enables the maximum performance. The FDD mode implies different frequency bands to be used for UL and DL transmissions. In UL resource grid the subcarrier spacing of either 15 or 3.75 kHz are possible, providing either 12 or 48 possible subcarriers within a 180 kHz resource block. The 15 kHz spacing allows transmission of either single and multicarrier (over up to 12 carriers) signals, while only single-carrier transmissions are possible for 3.75 kHz grid. In DL the 15 kHz resource grid is used. Importantly, to increase the maximum communication range, the eNB may configure several coverage extension classes featuring different number of packet/symbols repetitions, and may even specify the number of repetitions to be used in UL and DL (can reach 2048 in DL and 128 in UL) by a specific UE.

Only two channels are defined in the UL, the narrowband physical random access channel (NPRACH) and the narrowband physical uplink shared channel (NPUSCH). The NPRACH is used to trigger the RA procedure. It is composed of a contiguous set of either 12, 24, 36, or 48 subcarriers with 3.75 kHz spacing, which are repeated with a predefined periodicity, that may take several discrete values

between 40 ms and 2560 ms. The RA procedure starts with the transmission of a preamble, with a duration of either 5.6 ms or 6.4 ms (Format 0 and 1, respectively) depending on the size of the cell, and can be repeated up to 128 times to improve coverage. A preamble is composed of four symbol groups, each transmitted on a different subcarrier. The initial subcarrier is chosen randomly, while the following ones are determined according to a specific sequence depending on the first one. Two UEs selecting the same initial subcarrier will thus collide for the entire sequence. A special mechanism can help resolving the collisions and thus the access probability of a node can be approximated as Eq. (6.6):

$$P_{\text{acc}} = e^{-\frac{U}{N_{\text{RU}}}} \tag{6.6}$$

where U is the number of nodes entering RA and N_{RU} are the total available subcarriers.

In case of standalone deployment the NPUSCH occupies all the UL resources left available after the allocation of the NPRACH. NPUSCH is used for UL data and UL control information. Only Binary or Quadrature Phase-Shift Keying (BPSK or QPSK) modulations are used, and the code rate is 1/3 for data transmission and 1/16 for HARQ Acknowledgement (ACK). The eNB decides how many resources to allocate to the UEs depending on the amount of data to be sent, the modulation-coding scheme (MCS) used and the number of repetitions needed to correctly receive the data. The minimum resource block which can be allocated, referred to as a resource unit (RU), depends on the UE capabilities and the configured numerology. Specifically, in the case of 3.75 kHz subcarrier spacing and single-tone operation, the RU is 32 ms long. In the case of multi-tone-enabled UE and 15 kHz spacing, an RU can be composed of 12 subcarriers and 2 time slots featuring QPSK modulation and have the total cumulative duration of 1 ms. The number of the RUs (ranging from one to ten) to be allocated depends on the size of the transport block size (up to 1000 bits in Rel. 13) and the MCS chosen to meet the required success probability. In addition, the eNB specifies the desired number of repetitions.

Without the loss of generality, in what follows 3.75 kHz subcarrier spacing is assumed with 48 carriers allocated for RACH. Furthermore, since the UAB is expected to be close and in, primarily, line-of-sight conditions, only single coverage class with one repetition is implied. This implication also allows to minimize the potential interference experienced by the TBS, and to simplify the design and reduce the consumption of the eNB on the UAV. Furthermore, it is implied that the NPUSCH setting for MCS is defined by $I_{\text{TBS}} = I_{\text{MCS}} = 6$ and the size of the sensor data is either 500 or 1000 bits. Table 6.3 shows the packet size (or

Transport Block Size as for NB-IoT terminology) in bits for the selected scheme for the different possible number of RUs (for clarity, only the selected cases are reported).

Table 6.3: NB-IoT UL Transport Block Size in bits [P9].

RUs number	2	4	5	6	8	10
Max. packet size for $I_{\text{MCS}} = 6$ [bits]	176	392	504	600	808	1000

6.3.2 Reference NB-IoT Scenario

The service area is an urban environment, where IoT devices are deployed at smart traffic junctions, in city parks, at waste collection points, in the parking lots, or into buildings, to name just a few examples. Thus, in this realistic scenario IoT devices are clustered and each group is characterized by close vicinity and distributed in different areas of a city.

A realistic modelling of this scenario follows a Poisson Cluster Process, namely the Thomas cluster process (TCP) [B73], as conventionally done in the literature (see, e.g., [B74]). The TCP is a stationary and isotropic Poisson cluster process generated by a set of offspring points independently and identically distributed (i.i.d.) around each point of a parent Poisson Point Process (PPP) [B73]. In particular, the locations of parent points are modeled as a homogenous PPP, with intensity λ_{p}, around which offspring points are distributed according to a symmetric normal distribution with variance σ^2 and mean value n. therefore, the intensity of the offspring points is $\lambda = \lambda_{\text{p}} \cdot n$. In the scenario, both parent and offspring points represent the IoT nodes, without any difference in the type and role of the physical device. However, as it will be clarified later, parent points will be used as reference 2D points to define the UAB trajectory.

A square area of size L x L m^2 is considered, where parent points and offspring points are deployed according to the description above. A snapshot of the simulated scenario is depicted in Fig. 6.6. A single UAB is considered to save expenses. It starts its flight from a fixed position, denoted as Home, and coincident with one of the parent points. It has then to come back there at the end of the trajectory. In this way, it can recharge or change its battery for the next flight. Note that, in this study, the processes of take-off and landing are not simulated. Moreover, the consumption of the UAB is not modelled, but the capacity of the UAB battery is

assumed sufficient to enable a full round trip over any trajectory in the area under consideration. This is reasonable, since the total flight times considered do not exceed half an hour. The UAB is assumed to fly at a constant altitude from the ground of 100 m (not violating the regulations in EU - [B75]).

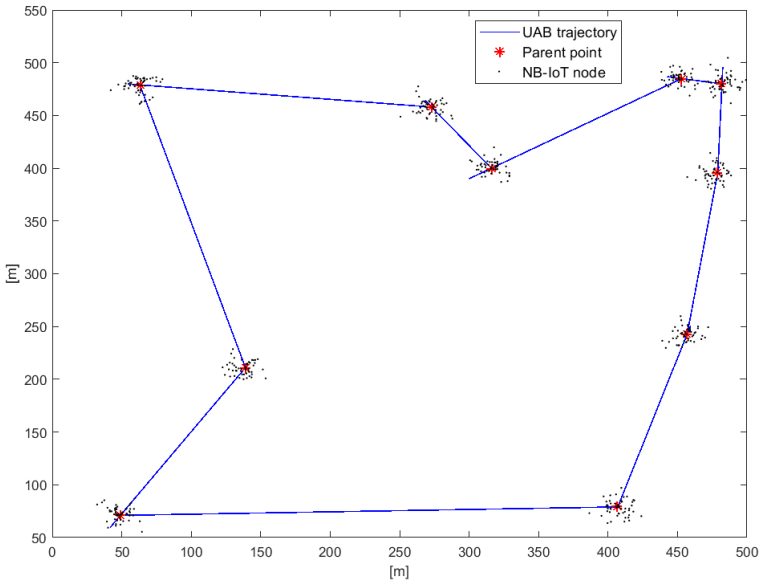

Figure 6.6: NB-IoT. Node deployment illustration and TSP example [P9].

Each user u is characterized by three parameters related to traffic demand: i) the size of data demand, D_u, that is the number of bits the user wants to send in uplink, ii) the activation time, a_u, that is the instant in which the demand is generated; iii) the expiration time, e_u, that is the maximum amount of time user u can wait before the service is satisfied completely. So, the deadline for completion of data download is at instant $a_u + e_u$ for user u. Also, each node generates only one packet to transmit and a_u is assumed to be randomly and uniformly distributed.

Once more, the propagation model affects the UAB-ground node link as the probabilistic model for drones in urban environment provided in [B5] and reported in Sec. 4.1. An additional penetration loss, η_{iot}, is added to PL computation to account for indoor nodes monitoring or basement applications.

If the received power is above the receiver sensitivity Pr_{min}, then the node is in connectivity range of the UAB. At this moment, it can attempt to access the channel through the NB-IoT NPRACH (see Sec. 6.3.1), so that, if succeeded, it may be given resources to transmit its data. The number of resources assigned determines the packet size that the device is able to transmit in the assigned time slot (see Sec. 6.3.1 and Table 6.3 for scheduling details). Note that, since the IoT

nodes are the devices more limited in their available resources (especially including the maximum transmit power), i) the connectivity range is defined by the uplink, ii) the downlink control communication is error-less.

In this activity, the UAB is flying over clusters of ground nodes following a predefined path. Given the cluster-based nature of devices distribution, a simple approach for the UAB trajectory design has been used. Since the UAB has to serve clusters of fixed nodes, the locations of the parent points is to be considered also as reference points to model a Traveling Salesman Problem (TSP) [B76]. The TSP addresses the task to find, for a finite set of points whose pairwise distances are known, the shortest route connecting all points. Therefore, to reduce both energy consumption and service delays, the UAB trajectory follows the TSP solution for cluster reference points. Despite the fact users have activation and expiration times, their high number in the area allows the TSP to be an effective method (see Sec. 6.3.3). An example is depicted in Fig. 6.6.

Table 6.4: NB-IoT Radio and Network Parameters [P9].

Parameter	**Notation**	**Value**
UL transmit power	P_{tx}	14 dBm
Antennas loss	A_L	2.5 dBi
Penetration loss	η_{iot}	40 dB
Noise power	P_{N}	30 10^{-17} W
Receiver sensitivity	$P_{\text{rx,min}}$	-121 dBm
Channel bandwidth	B_{c}	180 KHz
Subcarrier spacing	Δf	3.75 kHz
Available subcarriers	N_{RU}	48
Carrier frequency	$f_{\text{c,UAB}}$	1747.5 MHz
RU duration	-	32 ms
MCS index	I_{MCS}	6
Activation Time	a_u	Uniform[0; 120] s
Expiration Time	e_u	10 s for all u

As one can easily see, the performance of the considered network depends both on the UAB mobility pattern and the UAB NB-IoT cell configuration.

6.3.3 NB-IoT Final Remarks

In the simulations performed, the radio and network parameters are set as summarized in Table 6.4. The simulations are performed for a UAB altitude of 100 m in an area with side $L = 500$ m. Therefore, due to the finite area size, a number N_u of IoT devices is present in each simulation. The numerical results are obtained by averaging over 1000 iterations, characterised by different nodes distributions and values of N_u. The simulations were carried out in a MATLAB environment using a specifically-developed script for nodes deployment. Then, a NB-IoT simulator was developed in a Java environment, including the IBM CPLEX v. 12.7.1 framework to solve the TSP.

The performance is evaluated in terms of the number of served users, to which the UAB has assigned enough radio resources for the full transmission of their data, and network throughput, S_{N}, defined as:

$$S_{\mathrm{N}} = \sum_{u=1}^{N_u} S_u \tag{6.7}$$

where S_u is the u-th user throughput, given by: $S_u = D_u/T_u$, where T_u is the service delay.

To study the performance of the proposed UAV-aided NB-IoT network, the percentage of served NB-IoT nodes is analyzed in different cases, by varying:

- the density of parent points, λ_{p},
- the mean number of nodes in one cluster, n.

The value of σ^2 is fixed to 100 m. In addition, results by varying the NPRACH periodicity are shown, which affects the number of occasions a node may try requesting access to the UAB. Note that, this in turns affects the NPUSCH duration. Frequent NPRACH occurrences lead to shorter NPUSCH, thus reduce resources available for UL user data transfer.

Figure 6.7 reveals the effect of the nodes distribution on the cumulative throughput of the network. The demand of each node is either 500 or 1000 bit, and the UAB speed is fixed at 20 m/s. Two sets of curves can be easily distinguished: 1) with dashed lines, and 2) without dashed lines. The former set is obtained with 1000 bit of node demand, and the latter with 500 bit. Interestingly, curves in the same set show a similar behaviour, that is an increased network throughput as the average number of nodes increases, and a maximum for the same value of NPUSCH duration (320 ms and 160 ms). One can deduce that, despite the diverse distribution of nodes, there is one value for the NPUSCH duration (or, equally, timing

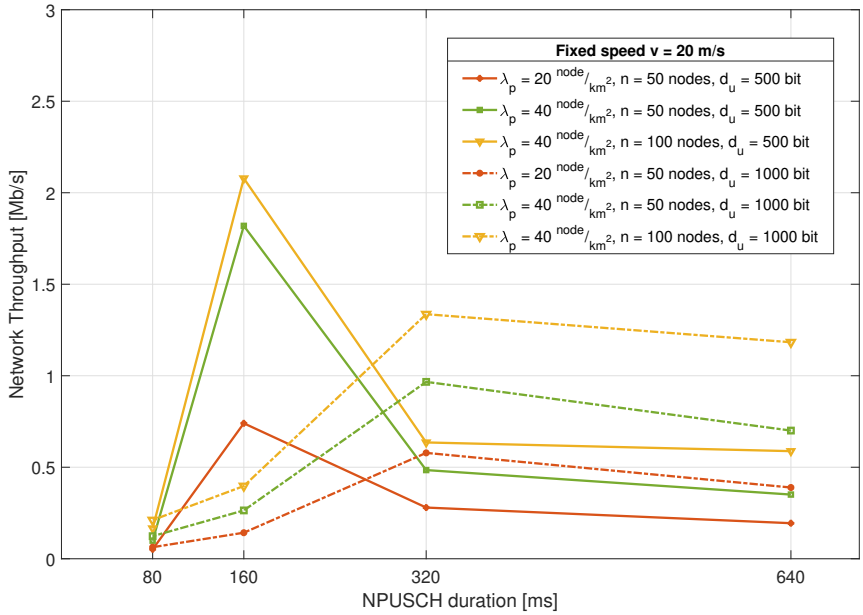

Figure 6.7: NB-IoT. Effect of nodes distribution on network throughput [P9].

of NPRACH occurrences) that is optimal for the specific user demand. Moreover, it has to be noted that the position of this maximum differs from 500 to 1000 bit demand because the number of resources to be assigned changes.

From Table 6.3 one can infer that 5 RUs are needed in the first case, and 10 in the second. Then, if one RU lasts 32 ms, 160 ms perfectly fit 500 bit, while 320 ms the case of 1000 bit. Then, for both sets, the maximum lays in the value of NPUSCH duration guaranteeing to each node no additional overhead (i.e., extra NPRACH occurrences) nor additional delays.

Figures 6.8a and 6.8b show the percentage of served nodes while varying their distribution and the UAB speed. Node's demand is fixed at 500 bit. Again in these plots, there is often a maximum at 160 ms. This shows that, given the number of nodes in the service area, an optimal choice on the timing of NPRACH occurrences has to be planned. When designing an NB-IoT network with UABs, a good trade-off between the access occasions, availability of RUs in the NPUSCH and the number of active devices is to be considered. Furthermore, these curves show that the UAB speed strongly impacts the system performance. If the average number of nodes is low, the trajectory is shorter and a lower speed (e.g. 10 m/s) increases the node's chance to connect to the UAB and transmit its packet. On the other hand, if the number of nodes increases, a higher speed (e.g. 20 m/s) allows to visit and serve more nodes in the given expiration time. Note that the percentage of served nodes is in almost all considered cases above 90%. Therefore, one can deduce that a TSP trajectory may be a good solution to achieve both an

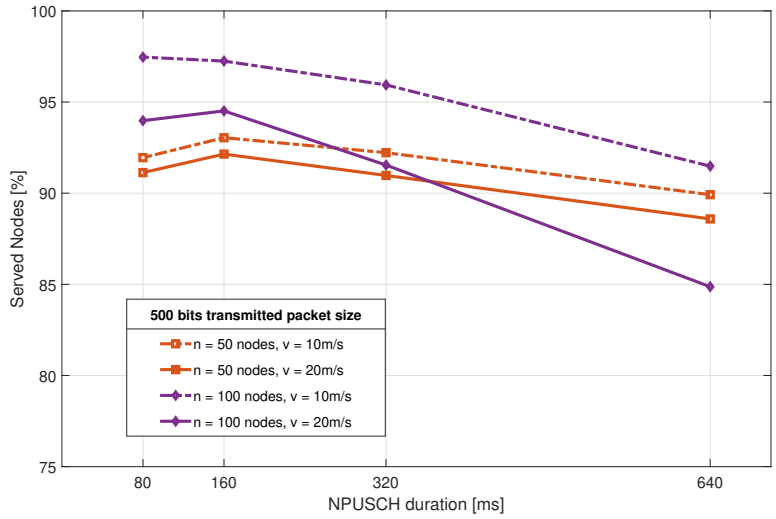

(a) $\lambda_p = 20$.

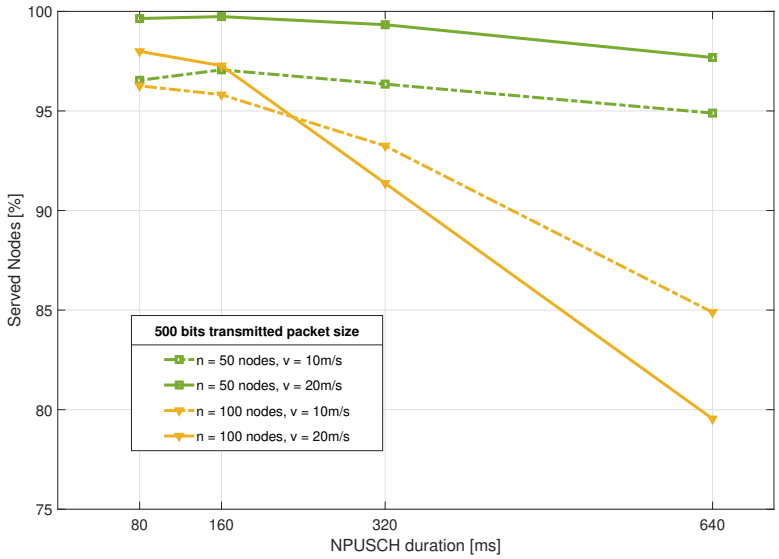

(b) $\lambda_p = 40$.

Figure 6.8: NB-IoT. Variation of nodes distribution vs the number of nodes served [P9].

acceptable performance and algorithm simplicity.

To summarize, this IoT scenario shows that UAB and network parameters should be properly tuned depending on the scenario, and that in the considered case even a well-known TSP approach provides a good balance between achieved performance and algorithm simplicity.

This activity shows an insight of the NPRACH periodicity and user demand impact, where results still demonstrate that the use of UABs in the IoT scenario is promising.

Chapter 7

Conclusions

The main scope of this thesis is to validate and thoroughly discuss the many aspects and possible future roles of UAV-aided mobile radio networks for B5G. To this aim, novel network nodes, denoted as UABs acting as flying BSs, are introduced in a new heterogeneous network paradigm. Terrestrial and aerial network components represent thus two integrated tiers that need to jointly cooperate to improve both the system coverage and capacity and to sustain network costs. Trajectory design schemes and algorithms have been proposed in two different frameworks, for a scalable heuristic and optimal planning. All these together resulted in good performance improvement. Along with path planning, an accurate AtG propagation model has been considered, and a proper architecture for the system management has been proposed.

The efficiency, flexibility, scalability and convenience of these additional UAB nodes have been investigated throughout the thesis.

Efficiency lies in a proper trajectory design, that allows the UABs to be directed where is needed for the due time. If a TBS suffers temporarily from overload for excessive demand or in the event of maintenance or an unusual blackout (for example a disaster event), UABs can fly in the interested area and provide service during the required time interval. Furthermore, it may happen that, for TBS deployment difficulties (e.g. terrain conformance, low population density, and so on), some cell borders are not covered sufficiently. Even in this case, UABs can be deployed when the demand arise, like a TBS extended arm. Efficiency has been investigated in all its facets in Chapter 5.

Scalability and flexibility come when dealing with different scenarios and use cases. For their inherent features of being able to fly on-demand, UABs can be adapted on purpose for the specific case, as discussed in Chapter 6.

Convenience is tightly combined with both efficiency, scalability, plus low CAPEX

and possibly OPEX costs. This concept has been considered in the architecture of Chapter 3, which has been validated throughout the thesis.

From each different activity, a number of key concepts can be extracted as lessons learned. To start with, clusterization algorithms allow a UAB to target multiple users instead of one at a time, increasing significantly the network throughput. Then, it is shown that the UAB can re-use the spectrum resource, therefore saving expenses, while achieving a noticeable performance improvement with respect to a system architecture without UABs. In this case, a good trade-off on the UAB altitude or coverage range must be achieved. Moreover, when the UAB is dynamically driven by a cost function, a database storing PL samples would both allow to i) estimate the achievable sum throughput, ii) adjust the UAB route accordingly. Another important factor that improves the network performance to a relevant extent is the joint RRM. Through this technique, aerial and terrestrial tiers can identify the users and agree on who will serve them best.

In conclusion, for each scenario investigated in the activities of this thesis, UAB nodes have proven to enhance network connectivity and capacity. Therefore, UAV-aided wireless networking has the potential to play a significant if not crucial role in future B5G mobile systems. The throughput gain introduced by a single node of this kind can be of few percent based on the deployment choice, and proportionally increases with multiple UABs. Even if it appears modest, in absolute terms, when referring to a capacity of hundreds of Gbps or more, it becomes a relevant improvement from the MNO perspective.

Acknowledgments

During these years, I must say I have been learning a lot. I could appreciate the quality improvement, one by one, of the activities carried out throughout my PhD studies. For this achievement, I would also like to acknowledge a number of people. First, I would like to thank my Supervisor, Professor Roberto Verdone, who has envisioned the "big picture" and inspired this work. He has always found the time to guide me through the evolution of these studies and has helped me grow in my professional and soft skills. I would also like to thank my Co-Supervisor, Professor Chiara Buratti, that gave me the opportunity to broaden my research field to different topics as well as different work methodologies. This final result was also possible thanks to their constant supervision and care.

Thoughts of gratitude go to my friends and colleagues for the frequent "brainstorming sessions": Gianluca, Luca, Lucia, Francesca, Giacomo, Elisabetta, Max, Matteo, Giampaolo, Riccardo, Marco, Francesco, Andrea, Chiara(x2), and many others.

A special appreciation goes to my boyfriend (and former colleague), Federico, who was there to help me embed the slightest detail that could improve these works' presentation. Many thanks to my dearest friends, who even let me continue to update my thesis during the pandemic-caused periodical call. To name a few, Sara, my language expert, Pietro, Luca(x2), Matteo, Beatrice(x2), Silvia, Veronica, Paul, Degio, Monta. Last but not least, I wish to thank my family, always supporting my choices.

Bologna - April 13, 2021

Bibliography

[B1] CISCO. "CISCO Visual Networking Index: Global Mobile Data Traffic Forecast Update 2016-2021". In: *C. V. Forecast* (Sept. 2017).

[B2] Recommendation ITU-R M.2083. "IMT Vision, Framework and overall objectives of the future development of IMT for 2020 and beyond". In: (Sept. 2015).

[B3] H. Gonzalez-Jorge, J. Martinez-Sanchez, M. Bueno, et al. "Unmanned aerial systems for civil applications: A review". In: *Drones* 1.1 (2017), p. 2.

[B4] Q. Feng, J. McGeehan, E. K. Tameh, and A. R. Nix. "Path loss models for air-to-ground radio channels in urban environments". In: *2006 IEEE 63rd Vehicular Technology Conference*. Vol. 6. IEEE. 2006, pp. 2901–2905.

[B5] A. Al-Hourani, S. Kandeepan, and A. Jamalipour. "Modeling air-to-ground path loss for low altitude platforms in urban environments". In: *2014 IEEE Global Communications Conference*. IEEE. 2014.

[B6] A. Al-Hourani, S. Kandeepan, and S. Lardner. "Optimal LAP altitude for maximum coverage". In: *IEEE Wireless Communications Letters* 3.6 (2014), pp. 569–572.

[B7] J. Chen, U. Yatnalli, and D. Gesbert. "Learning radio maps for UAV-aided wireless networks: A segmented regression approach". In: *Communications (ICC), 2017 IEEE International Conference on*. IEEE. 2017, pp. 1–6.

[B8] J. Chen and D. Gesbert. "Optimal positioning of flying relays for wireless networks: A LOS map approach". In: *Communications (ICC), 2017 IEEE International Conference on*. IEEE. 2017, pp. 1–6.

[B9] E. Yanmaz. "Connectivity versus area coverage in unmanned aerial vehicle networks". In: *2012 IEEE International Conference on Communications (ICC)*. IEEE. 2012, pp. 719–723.

[B10] I. Bor-Yaliniz and H. Yanikomeroglu. "The new frontier in RAN heterogeneity: Multi-tier drone-cells". In: *IEEE Communications Magazine* 54.11 (2016), pp. 48–55.

[B11] M. Mozaffari, W. Saad, M. Bennis, and M. Debbah. "Optimal Transport Theory for Cell Association in UAV-Enabled Cellular Networks". In: *IEEE Communications Letters* (2017).

[B12] B. Galkin, J. Kibilda, and L. A. DaSilva. "Deployment of UAV-mounted access points according to spatial user locations in two-tier cellular networks". In: *Wireless Days (WD), 2016*. IEEE. 2016, pp. 1–6.

[B13] M. Mozaffari, W. Saad, M. Bennis, and M. Debbah. "Drone small cells in the clouds: Design, deployment and performance analysis". In: *2015 IEEE Global Communications Conference (GLOBECOM)*. IEEE. 2015, pp. 1–6.

[B14] V. Sharma, M. Bennis, and R. Kumar. "UAV-Assisted Heterogeneous Networks for Capacity Enhancement". In: *IEEE Communications Letters* 20.6 (2016), pp. 1207–1210.

[B15] Y. Li and L. Cai. "UAV-Assisted Dynamic Coverage in a Heterogeneous Cellular System". In: *IEEE Network* 31.4 (July 2017), pp. 56–61.

[B16] P. Yang, X. Cao, C. Yin, Z. Xiao, X. Xi, and D. Wu. "Proactive Drone-Cell Deployment: Overload Relief for a Cellular Network Under Flash Crowd Traffic". In: *IEEE Transactions on Intelligent Transportation Systems* 18.10 (Oct. 2017), pp. 2877–2892.

[B17] A. Merwaday and I. Guvenc. "UAV assisted heterogeneous networks for public safety communications". In: *Wireless Communications and Networking Conference Workshops (WCNCW), 2015 IEEE*. IEEE. 2015, pp. 329–334.

[B18] M. Deruyck, J. Wyckmans, L. Martens, and W. Joseph. "Emergency ad-hoc networks by using drone mounted base stations for a disaster scenario". In: *2016 IEEE 12th International Conference on Wireless and Mobile Computing, Networking and Communications (WiMob)*. IEEE. 2016, pp. 1–7.

[B19] C. Giannini, A. A. Shaaban, C. Buratti, and R. Verdone. "Delay Tolerant Networking for smart city through drones". In: *2016 International Symposium on Wireless Communication Systems (ISWCS)*. Sept. 2016, pp. 603–607.

[B20] M. Mozaffari, W. Saad, M. Bennis, and M. Debbah. "Mobile Unmanned Aerial Vehicles (UAVs) for Energy-Efficient Internet of Things Communications". In: *IEEE Transactions on Wireless Communications* 16.11 (Nov. 2017), pp. 7574–7589.

[B21] M. Mozaffari, W. Saad, M. Bennis, and M. Debbah. "Efficient Deployment of Multiple Unmanned Aerial Vehicles for Optimal Wireless Coverage". In: *IEEE Communications Letters* 20.8 (2016), pp. 1647–1650.

[B22] P. Ladosz, H. Oh, and W.-H. Chen. "Optimal positioning of communication relay unmanned aerial vehicles in urban environments". In: *2016 International Conference on Unmanned Aircraft Systems (ICUAS)*. IEEE. 2016, pp. 1140–1147.

[B23] M. Mozaffari, W. Saad, M. Bennis, and M. Debbah. "Mobile Internet of Things: Can UAVs Provide an Energy-Efficient Mobile Architecture?" In: *2016 IEEE Global Communications Conference (GLOBECOM)*. 2016, pp. 1–6.

[B24] V. V. C. Ravi and H. S. Dhillon. "Downlink coverage probability in a finite network of unmanned aerial vehicle (UAV) base stations". In: *Signal Processing Advances in Wireless Communications (SPAWC), 2016 IEEE 17th International Workshop on*. IEEE. 2016, pp. 1–5.

[B25] M. N. Soorki, M. Mozaffari, W. Saad, M. H. Manshaei, and H. Saidi. "Resource allocation for machine-to-machine communications with unmanned aerial vehicles". In: *Globecom Workshops (GC Wkshps), 2016 IEEE*. IEEE. 2016, pp. 1–6.

[B26] J. Baek, S. I. Han, and Y. Han. "User scheduling for non-orthogonal transmission in UAV-assisted relay network". In: *2017 IEEE 28th Annual International Symposium on Personal, Indoor, and Mobile Radio Communications (PIMRC)*. Oct. 2017, pp. 1–5.

[B27] S. Koulali, E. Sabir, T. Taleb, and M. Azizi. "A green strategic activity scheduling for UAV networks: A sub-modular game perspective". In: *IEEE Communications Magazine* 54.5 (2016), pp. 58–64.

[B28] J. Lyu, Y. Zeng, R. Zhang, and T. J. Lim. "Placement Optimization of UAV-Mounted Mobile Base Stations". In: *IEEE Communications Letters* 21.3 (Mar. 2017), pp. 604–607.

[B29] Y. Zeng and R. Zhang. "Energy-efficient UAV communication with trajectory optimization". In: *IEEE Transactions on Wireless Communications* 16.6 (2017), pp. 3747–3760.

[B30] J. Lu, S. Wan, X. Chen, Z. Chen, P. Fan, and K. B. Letaief. "Beyond Empirical Models: Pattern Formation Driven Placement of UAV Base Stations". In: *IEEE Transactions on Wireless Communications* 17.6 (June 2018), pp. 3641–3655.

[B31] Q. Wu, Y. Zeng, and R. Zhang. "Joint Trajectory and Communication Design for Multi-UAV Enabled Wireless Networks". In: *IEEE Trans. Wireless Commun.* 17.3 (2018), pp. 2109–2121.

[B32] Q. Wu and R. Zhang. "Common throughput maximization in UAV-enabled OFDMA systems with delay consideration". In: *IEEE Transactions on Communications* 66.12 (2018), pp. 6614–6627.

[B33] 3GPP TS 36.777 V1.0.0. "Enhanced LTE support for aerial vehicles". In: (2017). URL: ftp://www.3gpp.org/specs/archive/36%5C_series/36.777.

[B34] ETSI GS NFV-EVE 005 V1.1.1. "Network Functions Virtualisation (NFV); Ecosystem; Report on SDN Usage in NFV Architectural Framework". In: (2015).

[B35] J. S. Lu, E. M. Vitucci, V. Degli-Esposti, F. Fuschini, M. Barbiroli, J. A. Blaha, and H. L. Bertoni. "A discrete environment-driven GPU-based Ray Launching algorithm". In: *IEEE Transactions on Antennas and Propagation* 67.2 (2018), pp. 1180–1192.

[B36] M. J. Arpaio, E. M. Vitucci, M. Barbiroli, V. Degli-Esposti, D. Masotti, and F. Fuschini. "Narrowband Characteristics of Air-to-Ground Propagation for UAV Assisted Networks in Urban Environments By Means of Fast Ray-Launching Simulations". In: *2020 IEEE 91st Vehicular Technology Conference (VTC2020-Spring)*. IEEE. 2020, pp. 1–5.

[B37] 3GPP TS 36.106 V16.0.0. "Evolved Universal Terrestrial Radio Access (E-UTRA); FDD Repeater radio transmission and reception". In: (2020).

[B38] 3GPP TS 38.300 V16.3.0. "NR; NR and NG-RAN Overall Description; Stage 2". In: (2020).

[B39] P. Vansteenwegen, W. Souffriau, and D. V. Oudheusden. "The orienteering problem: A survey". In: *European Journal of Operational Research* 209.1 (2011), pp. 1–10.

[B40] C. Murray and A. Chu. "The flying sidekick traveling salesman problem: Optimization of drone-assisted parcel delivery". In: *Transportation Research Part C: Emerging Technologies* 54 (2015), pp. 86–109.

[B41] N. Agatz, P. Bouman, and M. Schmidt. "Optimization Approaches for the Traveling Salesman Problem with Drone". In: *ERIM Report Series Research in Management* ERS-2015-011-LIS (2016).

[B42] P. Bouman, N. Agatz, and M. Schmidt. "Dynamic Programming Approaches for the Traveling Salesman Problem with Drone". In: *ERIM Report Series Research in Management* ERS-2017-011-LIS (2017).

[B43] J. Carlsson and S. Song. "Coordinated logistics with a truck and a drone". In: *Management Science* (to appear).

[B44] F. Furini, C. Persiani, and P. Toth. "The Time Dependent Traveling Salesman Planning Problem in Controlled Airspace". In: *Transportation Research Part B: Methodological* 90 (2016), pp. 38–55.

[B45] F. Guerriero, R. Surace, V. Loscri, and E. Natalizio. "A multi-objective approach for unmanned aerial vehicle routing problem with soft time windows constraints". In: *Applied Mathematical Modelling* 38.3 (2014), pp. 839–852.

[B46] L. Gupta, R. Jain, and G. Vaszkun. "Survey of important issues in UAV communication networks". In: *IEEE Communications Surveys & Tutorials* 18.2 (2015), pp. 1123–1152.

[B47] V. Sharma, F. Song, I. You, and H.-C. Chao. "Efficient management and fast handovers in software defined wireless networks using UAVs". In: *IEEE Network* 31.6 (2017), pp. 78–85.

[B48] M. M. Azari, F. Rosas, and S. Pollin. "Cellular connectivity for UAVs: Network modeling, performance analysis, and design guidelines". In: *IEEE Transactions on Wireless Communications* 18.7 (2019), pp. 3366–3381.

[B49] A. Festag. "Standards for vehicular communication—from IEEE 802.11p to 5G". In: *e & i Elektrotechnik und Informationstechnik* 132.7 (2015), pp. 409–416.

[B50] H. Seo, K. D. Lee, S. Yasukawa, Y. Peng, and P. Sartori. "LTE evolution for vehicle-to-everything services". In: *IEEE Communications Magazine* 54.6 (June 2016), pp. 22–28.

[B51] S. h. Sun, J. l. Hu, Y. Peng, X. m. Pan, L. Zhao, and J. y. Fang. "Support for vehicle-to-everything services based on LTE". In: *IEEE Wireless Communications* 23.3 (June 2016), pp. 4–8.

[B52] A. Bazzi, B. M. Masini, A. Zanella, and I. Thibault. "On the Performance of IEEE 802.11p and LTE-V2V for the Cooperative Awareness of Connected Vehicles". In: *IEEE Transactions on Vehicular Technology* 66.11 (Nov. 2017), pp. 10419–10432.

[B53] "Vehicle Safety Communications Project, Task 3 Final Report, Identify Intelligent vehicle Safety Applications Enabled by DSRC". In: *NHTSA DOT HS 809 859* (Mar. 2005).

[B54] "Intelligent Transport Systems (ITS); Vehicular communications; Basic set of applications; Definitions". In: *ETSI TR 102.638 V1.1.1* (June 2009).

[B55] "Technical Specification Group Radio Access Network; Study on LTE-based V2X services". In: *3GPP TR 36.885 V14.0.0* (July 2016).

[B56] "Technical Specification Group Radio Access Network; Study on enhancement of 3GPP support for 5G V2X services". In: *3GPP TR 36.886 V16.1.1* (2018).

[B57] H. Gunther, O. Trauer, and L. Wolf. "The potential of collective perception in vehicular ad-hoc networks". In: *2015 14th International Conference on ITS Telecommunications (ITST)*. Dec. 2015, pp. 1–5.

[B58] B. M. Masini, A. Bazzi, and A. Zanella. "A Survey on the Roadmap to Mandate on Board Connectivity and Enable V2V-Based Vehicular Sensor Networks". In: *Sensors* 18.7 (2018).

[B59] E. Costa-Montenegro, F. Quinoy-Garcia, F. J. Gonzalez-castano, and F. Gil-Castineira. "Vehicular Entertainment Systems: Mobile Application Enhancement in Networked Infrastructures". In: *IEEE Vehicular Technology Magazine* 7.3 (Sept. 2012), pp. 73–79.

[B60] A. M. Vegni and V. Loscrí. "A Survey on Vehicular Social Networks". In: *IEEE Communications Surveys Tutorials* 17.4 (Fourthquarter 2015), pp. 2397–2419.

[B61] R. Du, C. Chen, B. Yang, N. Lu, X. Guan, and X. Shen. "Effective Urban Traffic Monitoring by Vehicular Sensor Networks". In: *IEEE Transactions on Vehicular Technology* 64.1 (Jan. 2015), pp. 273–286.

[B62] G. Araniti, C. Campolo, M. Condoluci, A. Iera, and A. Molinaro. "LTE for vehicular networking: a survey". In: *IEEE Communications Magazine* 51.5 (May 2013), pp. 148–157.

[B63] A. Bazzi, G. Cecchini, A. Zanella, and B. M. Masini. "Study of the Impact of PHY and MAC Parameters in 3GPP C-V2V Mode 4". In: *IEEE Access* 6 (2018), pp. 71685–71698.

[B64] C. Campolo, A. Molinaro, A. Iera, and F. Menichella. "5G Network Slicing for Vehicle-to-Everything Services". In: *IEEE Wireless Communications* 24.6 (Dec. 2017), pp. 38–45.

[B65] K. Zheng, Q. Zheng, P. Chatzimisios, W. Xiang, and Y. Zhou. "Heterogeneous Vehicular Networking: A Survey on Architecture, Challenges, and Solutions". In: *IEEE Communications Surveys Tutorials* 17.4 (Fourthquarter 2015), pp. 2377–2396.

[B66] O. S. Oubbati, A. Lakas, F. Zhou, M. Güneş, N. Lagraa, and M. B. Yagoubi. "Intelligent UAV-assisted routing protocol for urban VANETs". In: *Computer Communications* 107 (2017), pp. 93–111.

[B67] W. Fawaz, R. Atallah, C. Assi, and M. Khabbaz. "Unmanned Aerial Vehicles as Store-Carry-Forward Nodes for Vehicular Networks". In: *IEEE Access* 5 (2017), pp. 23710–23718.

[B68] H. Sedjelmaci, M. A. Messous, S. M. Senouci, and I. H. Brahmi. "Toward a lightweight and efficient UAV-aided VANET". In: *Transactions on Emerging Telecommunications Technologies* 0.0 (2018). e3520 ETT-18-0228.R1, e3520.

[B69] H. Menouar, I. Guvenc, K. Akkaya, A. S. Uluagac, A. Kadri, and A. Tuncer. "UAV-Enabled Intelligent Transportation Systems for the Smart City: Applications and Challenges". In: *IEEE Communications Magazine* 55.3 (Mar. 2017), pp. 22–28.

[B70] W. Shi, H. Zhou, J. Li, W. Xu, N. Zhang, and X. Shen. "Drone Assisted Vehicular Networks: Architecture, Challenges and Opportunities". In: *IEEE Network* 32.3 (May 2018), pp. 130–137.

[B71] Y. Zhou, N. Cheng, N. Lu, and X. S. Shen. "Multi-UAV-Aided Networks: Aerial-Ground Cooperative Vehicular Networking Architecture". In: *IEEE Vehicular Technology Magazine* 10.4 (Dec. 2015), pp. 36–44.

[B72] A. Bazzi, B. M. Masini, A. Zanella, and G. Pasolini. "IEEE 802.11 p for cellular offloading in vehicular sensor networks". In: *Computer Communications* 60 (2015), pp. 97–108.

[B73] M. Haenggi. *Stochastic Geometry for Wireless Networksk*. U.K.: Cambridge Univ. Press, 2012.

[B74] C. Saha, M. Afshang, and H. S. Dhillon. "3GPP-Inspired HetNet Model Using Poisson Cluster Process: Sum-Product Functionals and Downlink Coverage". In: *IEEE Trans. Commun.* 66.5 (May 2018), pp. 2219–2234.

[B75] URL: `https://uavcoach.com/drone-laws/`.

[B76] G. Dantzig, R. Fulkerson, and S. Johnson. “Solution of a large-scale traveling-salesman problem”. In: *J. Operations Research Soc. of Amer.* 2.4 (1954), pp. 393–410.

Publications

[P1] M. Deruyck, A. Marri, **S. Mignardi**, L. Martens, W. Joseph, and R. Verdone. "Performance evaluation of the dynamic trajectory design for an unmanned aerial base station in a single frequency network". In: *2017 IEEE 28th Annual International Symposium on Personal, Indoor, and Mobile Radio Communications (PIMRC)*. IEEE. 2017, pp. 1–7.

[P2] **S. Mignardi** and R. Verdone. "On the performance improvement of a cellular network supported by an unmanned aerial base station". In: *2017 29th International Teletraffic Congress (ITC 29)*. Vol. 2. IEEE. 2017, pp. 7–12.

[P3] **S. Mignardi**, C. Buratti, V. Cacchiani, and R. Verdone. "Path Optimization for Unmanned Aerial Base Stations with Limited Radio Resources". In: *2018 IEEE 29th Annual International Symposium on Personal, Indoor and Mobile Radio Communications (PIMRC)*. IEEE. 2018, pp. 328–332.

[P4] **S. Mignardi**, C. Buratti, and R. Verdone. "On the impact of radio channel over REM-aware UAV-aided mobile networks". In: *WSA 2018; 22nd International ITG Workshop on Smart Antennas*. VDE/IEEE. 2018, pp. 1–6.

[P5] **S. Mignardi** and R. Verdone. "Joint path and radio resource management for UAVs supporting mobile radio networks". In: *2018 17th Annual Mediterranean Ad Hoc Networking Workshop (Med-Hoc-Net)*. IEEE. 2018, pp. 1–7.

[P6] R. Verdone and **S. Mignardi**. "Joint aerial-terrestrial resource management in uav-aided mobile radio networks". In: *IEEE Network* 32.5 (2018), pp. 70–75.

[P7] **S. Mignardi**, C. Buratti, A. Bazzi, and R. Verdone. "Trajectories and resource management of flying base stations for C-V2X". In: *Sensors* 19.4 (2019), p. 811.

[P8] **S. Mignardi**, M. J. Arpaio, C. Buratti, E. M. Vitucci, F. Fuschini, and R. Verdone. "Performance Evaluation of UAV-Aided Mobile Networks by Means of Ray Launching Generated REMs". In: *2020 29th International Telecommunication Networks and Applications Conference (ITNAC)*. Accepted.

[P9] **S. Mignardi**, K. Mikhaylov, V. Cacchiani, R. Verdone, and C. Buratti. "Unmanned Aerial Base Stations for NB-IoT: Trajectory Design and Performance Analysis". In: *2020 IEEE 31st Annual International Symposium on Personal, Indoor and Mobile Radio Communications*. IEEE, pp. 1–6.

[P10] **S. Mignardi**, P. M. Pulcinella, and R. Verdone. "The Role of Ground-to-Air Handovers in B5G UAV-Aided Mobile Networks". In: *2021 EEE Consumer Communications And Networking Conference (CCNC)*. Accepted.